In our response, referee comments are marked in bold, our responses and original text in plain text, and altered text in the paper in *italic.* Additionally we highlight altered text in the tracked changes pdf as requested.

Response to reviewer 1 (Steve Ghan)

Major comment: Uncertainty in autoconversion is likely to be major source of uncertainty in both present day radiation and in ERFaci. The manuscript notes the model presently lacks the feedback of aerosol effects on precipitation back onto the aerosols themselves. This feedback can be important in driving the transition from stratiform cloud to pockets of open celled convection. Moreover, the study does not consider the sensitivity to the representation of autoconversion itself, in particular the dependence of the autoconversion rate on droplet number. I would like to see more discussion of the impacts of these limitations on the conclusions of the study.

The following paragraph has been added to the conclusion section immediately before line 864 in the original submission (line 877 in the revised article):

"One important source of ERF_ACI uncertainty we did not include in our study is the autoconversion rate of cloud drops into rain drops (Michibata et al., 2015, Malavelle et al., 2017 and Toll et al., 2017). Were we to include the autoconversion rate as an additional source of uncertainty the credible range of aerosol ERFs would be larger. If the autoconversion rate were an important cause of uncertainty in both ToA flux and aerosol ERF, the constraint on ERF uncertainty would likely be stronger. However, if autoconversion were to affect ToA flux and aerosol ERF in different ways or to different extents then including this additional source of uncertainty may amplify the equifinality problem by introducing another important degree of freedom. The additional uncertainty from autoconversion could be constrained to a large extent using collocated observations of changes in liquid water path, cloud fraction and aerosol concentrations. We expect such observations of cloud-aerosol relationships will be particularly useful for constraining a model's ability to represent transitions between cloud regimes and we plan to test their efficacy as constraints in the next phase of our research."

Minor comment 1: Lines 71-72: uncertainty.

Fixed.

Minor comment 2: Lines 390-396. The validation of the emulators is never presented. How accurately did the emulators reproduce the simulated fields?

Fixed.

Revised text:
"Once emulators were validated, *by ensuring that at least 75% of the validation simulations produced output within the relatively small emulator uncertainty bounds,* new emulators conditioned on output from the 191 perturbed parameter simulations (with better space-filling properties) were created by combining the validation simulations with the original set of simulations."

Minor comment 3: Lines 458-462. Won't the variance for the combined uncertainty be greater if there are no interactions? If independent don't the variances add? Couldn't negatively correlated interactions decrease the uncertainty from the neutral case, and possible produce less uncertainty than with either set of parameters?

Yes, if there were no interactions or compensating effects between the aerosol and atmospheric parameters, the combined uncertainty would be much larger because the uncertainties would be additive. Also, it is feasible that multiple negatively correlated interactions could reduce the uncertainty in either the aerosol-only or atmospheric-only samples when the sets of parameters are combined, as Steve suggests. However, in our case the compensating effects between the groups of parameters are strong enough to prevent the individual uncertainties from being additive, but not strong enough to reduce the uncertainties in either individual sample.

Minor comment 4: Line 704. Make it clear this is global mean. How does this accuracy constraint compare with the accuracy of the emulator?

Fixed.

Revised text:

"Figure 12 shows the effect of constraining the modelled present-day *global, annual mean* RSR to within…"

Revised text:
"We also neglect uncertainty caused by unknown model structural errors (Goldstein et al., 2004, Sexton et al., 2012 and Stier et al., 2013), observation representativeness errors (Schutgens et al., 2017) and the emulators themselves (Oakley and O'Hagan, 2004) *which are of the same order of magnitude as the observational uncertainty.*"

Minor comment 5: Lines 714-716. Why focus on the lower bound and not the range?

We focus on the lower credible interval value because there is substantial debate within the climate forcing community about the validity of the strongest aerosol ERF values and this result contributes to that debate. However, because the credible range is also of interest, we have revised the text.

Revised text:

"The effect of applying the RSR observational constraint is to rule out 1850-2008 aerosol ERF values lower than around -2.4 Wm^{-2}, which represents around 15% of the original aerosol ERF range *(-2.7, -0.7 Wm^{-2}). However, the 95% credible range is only reduced by around 10% because the distribution of aerosol ERFs in the constrained sample is skewed towards weaker forcings and the upper bound of the credible interval (-0.6 Wm^{-2}) is larger (Table A4).*"

Minor comment 6: Lines 756. than the in the. Line 778. equifinality needs to be defined with a reference provided. Section 3.5.4. Explain why this particular region is chose.

Fixed.

Revised text:

"because cloud droplet activation is more sensitive to Sig_W in the present-day atmosphere than *[the]* in the aerosol-limited pre-industrial atmosphere."

We now introduce equifinality, with appropriate citations, when compensating errors are first discussed on line 921 (line 894 of original submission).

Revised text:

"However, despite a very large reduction in plausible parameter space, the effectiveness of the observational constraint is modest because it is hampered by compensating effects between multiple uncertain parameters, *which results in multiple equally plausible solutions (sometimes referred to as `equifinality'; Beven and Freer, 2001, Lee et al., 2016)."*

Revised text:

"Therefore we now use satellite observations of the North Pacific (region R1; latitude 32N-54N; longitude 125W-144E; *the largest regional contribution to global mean aerosol ERF)".*

Minor comment 6: Lines 876-877. Please expand on this. Do Johnson et al. explore aerosol optical depth as a constraint?

Fixed.

Revised text:

"using multiple observable quantities *(e.g. aerosol optical depth and aerosol concentrations)* in Johnson et al. (2018)."

Response to reviewer 2 (Anonymous reviewer)

<u>Main Point 1</u>: The abstract focuses on percentages of variance explained, but this seems to be entirely dependent on the choice of parameters.

Indeed. The results from any study depend on the assumptions made. Interested readers will presumably ask the same question, then we trust they will make their own judgement about the completeness of the study by reading the paper. The perturbed parameter ensemble presented here was designed to include perturbations to all processes known to be important for global mean aerosol ERF. The choice of parameters included in the experimental design was informed by expert analyses, including multiple existing perturbed parameter ensembles and our one-at-a-time-screening experiments. We find it difficult to add further detail on the completeness issue in the abstract. However, we have added text to the body of the article.

Additional text:

"Our results may change slightly with the inclusion of additional parameters. However, we went through a thorough parameter screening and prioritisation process so we consider the parametric uncertainty to be close to an upper limit. Furthermore, with many possible opportunities for parameter compensation, additional parameters only very gradually increase the overall uncertainty."

<u>Main Point 2</u>: the expert elicitation mentioned in passing in the conclusions is interesting, but needs its own section in the results first.

We describe the use of the expert-elicited pdfs in section 2.3. Furthermore, the expert elicitation process is described in detail elsewhere (e.g. Lee et al, 2012, Yoshioka et al., 2018 and Sexton et al., 2018). The latter two article were not available at the time of review. These articles focus on design aspects of our perturbed parameter ensembles. Therefore, we feel that including a more detailed description of the elicitation process here would duplicate what is presented in these papers (and specifically Yoshioka et al., 2018).

<u>Main Point 3</u>: I'd be interested in a TOA constraint based on minimizing the root mean square spatial difference from observations, not just the mean TOA.

We agree that there are multiple ways to use observations to constrain the aerosol ERF uncertainty and the suggested strategy could provide additional constraint. Constraining the RMSE is akin to constraining the ToA flux in multiple regions. We will follow up on this suggestion in our future research and have revised the text accordingly.

Revised text:

"The aerosol ERF uncertainty decreases when we constrain global mean ToA RSR (-2.37 to -0.59 Wm^{-2}) and when we constrain both North Pacific and global RSR (-2.30 to -0.56 Wm^{-2}). *These results suggest that additional constraint of aerosol ERF uncertainty could be achieved using multiple regional ToA flux observations."*

Main Point 4: I think perhaps TOA flux should be first section in the manuscript.

We feel that this is a matter of style. Our priority is the reduction of uncertainty in aerosol ERF and its components. Therefore, we quantify the uncertainty and identify the key causes of uncertainty in these terms first. The paper then progresses to an analysis of one observable quantity that may help to constrain the model. Furthermore, the main result of the article is the importance of both aerosol and physical atmosphere parameters as causes of aerosol ERF uncertainty. The existing order of the results section allows us to make these points clearly, whereas the suggested change of order of analyses would obscure what we consider to be the most important results.

Main Point 5: I'm not sure how the authors go to regional, that might take a bit more discussion. Is it an entirely different emulator. I think it might be good to show an emulator figure to explain the method a bit more.

We agree that the transition into regional analyses was abrupt and lacked the important enunciation of the fact that distinct emulators are used for global and regional analyses.

Revised text:

"Emulators of regional-mean aerosol ERFs and its components were created so that the key causes of variance in each region could be identified (Fig. 11)."

Specific comment 1: Page 1, L14: This does not seem like much of a change. Also: seems like a large value.

The reviewer is correct that this is a stronger value of forcing than is commonly cited in the literature. However, our values are lower credible bounds on aerosol ERF given our dense sampling of model uncertainty. Such bounded estimates of forcing cannot be achieved using ensembles of well-tuned climate models where individual model uncertainty is neglected (as outlined in Section 1 and in Johnson et al. (2018)). The change in the credible lower bound on aerosol ERF from -2.65 to -2.37 Wm^{-2} is only around 10% of the original lower bound. The change is indeed not substantial, but does serve to illustrate the challenge of reducing uncertainty in complex models. Furthermore, observational constraint of the lower credible bound (regardless of magnitude) adds to the debate within the climate forcing community about the plausibility of the strongest aerosol ERFs.

Specific comment 2: Page 1, L12: is this 60% of the 60% aerosol uncertainty for 4 parameters?

We appreciate the confusion.

Revised text:

"Four atmospheric and aerosol parameters account for around 80% of the uncertainty in short-wave ToA flux (mostly parameters that directly scale cloud reflectivity, cloud water content or cloud droplet concentrations), and these parameters also account for around 60% of the aerosol ERF uncertainty."

Specific comment 3: Page 1, L15: isn't the TOA flux 2 orders of magnitude larger than 2wm-2 ERF (~240 Wm-2)?

Fixed.

Revised text:
"the ToA flux is *two orders* of magnitude larger than the aerosol ERF"

"These results counter the belief that observations of ToA reflected short-wave radiation should not constrain the aerosol ERF (because RSR values are *two orders* of magnitude larger than the aerosol ERF)"

Specific comment 4: Page 6, L181: if the choice of parameters is arbitrary, then the fractions I think in the abstract are arbitrary. Please clarify: I assume some parameters were thrown out, are you sure you have a comprehensive set and another choice of parameters will give the same percentage change?

The choice of parameters is not arbitrary. In fact the aim of this paragraph is to explain that the list of parameters was chosen based on expert elicitation – so we think it is as comprehensive as can be achieved based on expert knowledge. Expert elicitation is widely used to make such assessments in many fields. To make this point somewhat clearer, we have included the word 'domain' in the phrase 'model domain experts' and added a sentence at the end of the paragraph: *"Our results may change slightly with the inclusion of additional parameters. However, we went through a thorough parameter screening and prioritisation process so we consider the parametric uncertainty to be close to an upper limit. Furthermore, with many possible opportunities for parameter compensation, additional parameters only very gradually increase the overall uncertainty.".* While we acknowledge that different results would be obtained with a different set of parameters, we consider our set of parameters to sufficiently complete that the results are useful. There is no prior work that enables any estimate of the relative importance of aerosol and atmospheric parameters, so our paper is at least a first step, and the methodology is sufficiently well explained that readers can reach their own judgement.

Revised text:
"model *domain* experts"

Additional text:
"Our results may change slightly with the inclusion of additional parameters. However, we went through a thorough parameter screening and prioritisation process so we consider the parametric uncertainty to be close to an upper limit. Furthermore, with many possible opportunities for parameter compensation, additional parameters only very gradually increase the overall uncertainty."

Specific comment 5: Page 12, L376: autoconversion is more important but overstated? This is confusing. Please rephrase.

Fixed. Note that an incorrect reference was used in the initial submission and has now been changed.

Revised text:

"The cloud liquid water path response to aerosols in low, warm clouds is weaker in HadGEM than in other global climate models (Ghan et al., 2016). Therefore, autoconversion may *seem* more important in other models, but will likely be overstated (*Toll et al., 2017*). This process should be considered in future uncertainty analysis studies once shared model structural errors are addressed and the process uncertainty better quantified."

Additional text (Section 4):
"One important source of ERF_ACI uncertainty we did not include in our study is the autoconversion rate of cloud drops into rain drops (Michibata et al., 2015, Mallavelle et al., 2017 and Toll et al., 2017). Were we to include the autoconversion rate as an additional source of uncertainty the credible range of aerosol ERFs would be larger. If the autoconversion rate were an important cause of uncertainty in both ToA flux and aerosol ERF, the constraint on ERF uncertainty would likely be stronger. However, if autoconversion were to affect ToA flux and aerosol ERF in different ways or to different extents then including this additional source of uncertainty may amplify the equifinality problem by introducing another important degree of freedom. The additional uncertainty from autoconversion could be constrained to a large extent using collocated observations of changes in liquid water path, cloud fraction and aerosol concentrations. We expect such observations of cloud-aerosol relationships will be particularly useful for constraining a model's ability to represent transitions between cloud regimes and we plan to test their efficacy as constraints in the next phase of our research."

Specific comment 6: Page 12, L383: is ERF the total? I.e. ari and ACI? Can you separate them?

Fixed.

Revised text:
"(ToA flux, aerosol ERF and its components)"

Specific comment 7: Page 13, L406: there is an emulator for each gridbox for TOA flux? Maybe a figure is necessary.

We have changed the key sentence to specify that the analyses were applied at all levels for ToA flux as well as forcing terms. We prefer not to add another figure for the ToA flux, but the fraction of uncertainty caused by aerosols and physical atmosphere parameter at the individual gridbox level is shown in Fig 10.

Please note that we have corrected the statement of degraded model resolution.

Revised text:
"Emulation and sensitivity analyses were applied at the individual model gridbox level (degraded to N*48* model resolution) as well as at the regional and global mean level*s for the ToA flux as well as the forcing terms.*"

Specific comment 8: Page 18, L504: how much does this parameter affect TOA flux? Figure 4 just shows the ERF. What would a plot of the actual TOA variance look like?

Fig. 4 shows the causes of variance in aerosol ERF and its components. The equivalent figure showing the fraction of variance in ToA flux is Fig. 7. We have revised the text to better connect the current statements about the aerosol ERF and this parameter to ToA flux which is analysed in section 3.3.

Revised text:
"altering (amongst other things) reflected radiation, tropospheric temperature profiles and cloud amount *(Section 3.3).*"

Specific comment 9: Page 24, L602: this concerns me since I think a different set of parameters will behave differently.

We're unsure what aspect of this sentence concerns the referee. We have included additional text for clarification (Main Comment 1 and Specific Comment 4).

Specific comment 10: Page 25, L617: how were the regions identified? Sigma? Please clarify.

The sentence states the criterion for selecting these regions: "regions of substantial aerosol ERF (stronger than around -2.5 Wm^{-2})". We changed this to be more specific.

Revised text:
"(*ensemble mean* stronger than around -2.5 Wm^{-2})"

Specific comment 11: Page 30, L718: so you have used a total global value. But this can be a result of cancellation of errors. What if you tried to minimize the RMSE v. CERES? Would that give a similar result? Usually the RMSE is better for model evaluation v. Obs.

The RMSE approach suggested by reviewer 2 is equivalent to applying multiple regional observational constraints. We showed that the observed monthly mean regional ToA flux provided little additional constraint on aerosol ERF over and above the global, annual mean ToA flux (Section 3.4). We can expect some modest additional constraint on aerosol ERF uncertainty by extending to more regions, but this is beyond the scope of this paper. We have added text to Section 4.

Additional text:

"*These results suggest that additional constraint of aerosol ERF uncertainty could be achieved using multiple regional ToA flux observations.*"

Specific comment 12: Page 31, L719: figure 12 is a bit confusing with the multiple axes for ERF over the different periods. Maybe divide it differently?

Fixed.

Revised text:
Consequently, the smaller set of model variants also predicts reasonably constrained 1978 and 1850 RSR ranges *(Fig. 12(a))*. However, despite reducing the plausible parameter space by 97% and the RSR range by 98% the impact on the aerosol ERF uncertainty is more modest *(Fig. 12(b) and (c))*.

Revised caption text:
(a) Observationally constrained present-day ToA RSR and the values of 1978 and 1850 ToA RSR and *(b)* 1978-2008 and *(c)* 1850-2008 aerosol ERF values from matching model variants.

Specific comment 13: Page 31, L726: fig 13 is confusing. I take away that the only thing the observations do is constrain rad_mcica_sigma to a narrower range. The discussion is good, but maybe the figure could be simplified.

Yes, the Rad_Mcica_Sigma parameter is constrained. The remainder of Section 3.5.2 contains important insights regarding why this constraint does not feed through to aerosol ERF, when that parameter dominates the uncertainty. This discussion informs the reader why we need to explore the constraint using parameter relationships. Although it's quite complicated, the figure content is all relevant to the discussion in this section.

Specific comment 14: Page 35, L831: where did you analyze the expert elicitation selection? Did I miss something?

This was presented on lines (436 – 439 of original submission; 440-443 of revised article) in section 3.1 where we quantify the effect of the expert elicited pdfs on the aerosol ERF uncertainty. We have cross-referenced Section 3.1 within Section 4, to ensure readers do not overlook this important result.

Revised text:
"can be achieved by applying probability distributions to the parameters based on expert elicitation *(Section 3.1)."*

Specific comment 15: Page 36, L836: how much is that dependent on the parameter set choice?

Fixed.

Additional text:
"Our results may change slightly with the inclusion of additional parameters. However, we went through a thorough parameter screening and prioritisation process so we consider the parametric uncertainty to be close to an upper limit. Furthermore, with many possible opportunities for parameter compensation, additional parameters only very gradually increase the overall uncertainty."

Specific comment 16: Page 36, L840: might be good to mention what fraction are natural aerosol emissions or preindustrial background to compare to previous work. How do these results differ from Carslaw et al 2013?

Fixed.

Revised text (Section 3.2.1):
"Natural aerosol emissions (here, *predominantly* Sea_Spray, DMS and BB_Diam) persist as important sources of industrial-period ERF_{ACI} uncertainty, as in previous studies of several climate models (Wilcox et al., 2015) and the aerosol-only component of a global model (Carslaw et al., 2013). *Here, natural aerosols are responsible for around 63% of the proportion of ERF_{ACI} variance caused by aerosol parameters, compared to 45% of the variance in aerosol-cloud-albedo effect forcing in the absence of rapid atmospheric adjustments (Carslaw et al., 2013).* However, by far the largest source of uncertainty is the Rad_Mcica_Sigma parameter."

Revised text (Section 4, although not exactly where suggested by reviewer 2):
"Therefore, the causes of aerosol ERF uncertainty in recent decades (1978-2008) are model deposition rates (model process parameters) and anthropogenic emissions, whilst the 1850-2008 aerosol ERF is most sensitive to natural aerosol emissions *(which collectively cause around 63% of the aerosol contribution to ERF_{ACI} variance).* The magnitude of global mean aerosol forcing on the decadal timescale depends on the combination of uncertain positive and negative regional forcings (Regayre et al., 2015; Fig. 5)."

Aerosol and physical atmosphere model parameters are both important sources of uncertainty in aerosol ERF

Leighton Regayre[1], Jill Johnson[1], Masaru Yoshioka[1], Kirsty Pringle[1], David Sexton[2], Ben Booth[2], Lindsay Lee[1], Nicolas Bellouin[3], and Kenneth Carslaw[1]

[1]Institute for Climate and Atmospheric Science, School of Earth and Environment, University of Leeds, Leeds, LS2 9JT, UK.
[2]UK Hadley Centre Met Office, Exeter, Fitzroy Road, Exeter, Devon, EX1 3PB, UK.
[3]Department of Meteorology, School of Mathematical & Physical Sciences, Faculty of Science, University of Reading, Reading, RG6 6BB, UK.

Correspondence to: Leighton Regayre (L.A.Regayre@leeds.ac.uk)

1 **Abstract.** Changes in aerosols cause a change in net top-of-the-atmosphere (ToA) short-wave and long-wave radiative fluxes,
2 rapid adjustments in clouds, water vapour and temperature, and cause an effective radiative forcing (ERF) of the planetary
3 energy budget. The diverse sources of model uncertainty and the computational cost of running climate models make it difficult
4 to isolate the main causes of aerosol ERF uncertainty and to understand how observations can be used to constrain it. We explore
5 the aerosol ERF uncertainty by using fast model emulators to generate a very large set of aerosol-climate model variants
6 that span the model uncertainty due to twenty-seven parameters related to atmospheric and aerosol processes. Sensitivity
7 analyses shows that the uncertainty in the ToA flux is dominated (around 80%) by uncertainties in the physical atmosphere
8 model, particularly parameters that affect cloud reflectivity. However, uncertainty in the change in ToA flux caused by aerosol
9 emissions over the industrial period (the aerosol ERF) is controlled by a combination of uncertainties in aerosol (around
10 60%) and physical atmosphere (around 40%) parameters. Four atmospheric and aerosol parameters account for around 80%
11 of the uncertainty in short-wave ToA flux (mostly parameters that directly scale cloud reflectivity, cloud water content or
12 cloud droplet concentrations), and these parameters also account for around 60% of the aerosol ERF uncertainty. The common
13 causes of uncertainty mean that constraining the modelled planetary brightness to tightly match satellite observations changes
14 the lower 95% credible aerosol ERF value from -2.65 $\mathrm{W\,m^{-2}}$ to -2.37 $\mathrm{W\,m^{-2}}$. This suggests the strongest forcings (below
15 around -2.4 $\mathrm{W\,m^{-2}}$) are inconsistent with observations. These results show that, regardless of the fact that the ToA flux is
16 two orders of magnitude larger than the aerosol ERF, the observed flux can constrain the uncertainty in ERF because their
17 values are connected by constrainable process parameters. The key to reducing the aerosol ERF uncertainty further will be to
18 identify observations that can additionally constrain individual parameter ranges and/or combined parameter effects, which can
19 be achieved through sensitivity analysis of perturbed parameter ensembles.

1 Introduction

21 Large aerosol radiative forcing uncertainty has persisted through all Intergovernmental Panel on Climate Change assessment
22 reports since 1996 despite substantial developments in climate model complexity (Flato et al. 2013, Section 9.1.3), numerous

intercomparison projects (Randles et al., 2013; Tsigaridis et al., 2014; Kim et al., 2014; Mann et al., 2014; Pan et al., 2015; Lacagnina et al., 2015; Kipling et al., 2016; Ghan et al., 2016; Koffi et al., 2016), and enormous investments in observing systems (Khain et al., 2000; Lacagnina et al., 2015; Seinfeld et al., 2016; Reddington et al., 2017). Reducing aerosol forcing uncertainty has therefore proven to be one of the most challenging and persistent problems in atmospheric science.

Reduction of uncertainty in aerosol effective radiative forcing (ERF) is an important objective, not least because it would improve climate change projections (Andreae et al., 2005; Myhre et al., 2013; Collins et al., 2013; Tett et al., 2013; Seinfeld et al., 2016). An improved understanding of the causes of uncertainty would also help to prioritise model developments, suggest fruitful analyses across multiple models, and point to potential new observations to constrain the uncertainties. However, the task remains challenging for multiple reasons. For example, aerosol ERF is usually quantified with reference to a period pre-dating the satellite era (usually 1850 or 1750) meaning it is not a directly observable quantity. Satellite-derived observations of present-day aerosol-cloud relationships have the potential to constrain the aerosol ERF uncertainty, but require an improved understanding of aerosol changes over the industrial period (Gryspeerdt et al., 2017). Some of the ERF uncertainty might therefore be irreducible unless pristine present-day environments are shown to be a good proxy for pre-industrial conditions (Carslaw et al., 2013; Hamilton et al., 2014; Carslaw et al., 2017). Furthermore, aerosol ERF depends on many poorly understood interactions of aerosols with components of the physical climate system. Important sources of uncertainty are known to be aerosol emission fluxes (Granier et al., 2011), representations of complex sub-grid processes such as clouds (Haerter et al., 2009; Lohmann and Ferrachat, 2010; Guo et al., 2013; Gettleman et al., 2013; Golaz et al., 2013; Neubauer et al., 2014; Lohmann, 2017), precipitation responses (Tost et al., 2010; Croft et al., 2012; Michibata and Takemura, 2015), aerosol processes (Croft et al., 2012; Textor et al., 2006, 2007; Storelvmo et al., 2009; Kasoar et al., 2016), radiation calculations (Stier et al., 2013; Wilcox et al., 2015) and subsequent feedbacks on atmospheric dynamics (Booth et al., 2012; Bollasina et al., 2013; Kirtman et al., 2013; Villarini and Vecchi, 2013; Allen et al., 2014) and surface temperatures (Golaz et al., 2013).

Our intention here is to constrain aerosol ERF uncertainty by pursuing a 'bottom-up' approach that explores the underlying process uncertainty. This approach provides a set of observationally plausible model variants with which near-term climate simulations could be performed. Although a lower limit to the global mean aerosol ERF might be found using a 'top-down' approach and historical temperature trends (Stevens, 2015), inferences made about the climate system are very sensitive to the simplifying assumptions that are made in top-down approaches (Knutti et al., 2008; Kretzschmar et al., 2017). More importantly, such methods do not provide a model with which to make improved climate projections and they provide no information about regional variations in forcing, which are known to be important drivers of climate variability (Chalmers et al., 2012; Dunstone et al., 2013; Shindell et al., 2013; Kirtman et al., 2013; Bollasina et al., 2013). Therefore, bottom-up methods that quantify aerosol ERF using global climate models whose performance and uncertainty are constrained by observations are required.

Multi-model studies (or model intercomparison projects, MIPs) can provide some information about ERF uncertainty because a set of models with different dynamical cores and physical process parametrisations produces a range of aerosol re-

sponses. However, such opportunistic sampling has three main disadvantages. Firstly, inter-model comparisons often include models with vastly different degrees of complexity (Collins et al., 2013). For example, aerosol indirect effects are not represented in many of the models included in such studies and this artificially inflates multi-model forcing uncertainty (Bellucci et al., 2017). Secondly, multiple members of an inter-model comparison will share key modules and behaviours (Pennell and Reichler, 2010; Collins et al., 2010; Knutti et al., 2013). This leads to compensating effects between groups of models with shared structural errors that causes the multi-model mean to outperform the majority of individual models across a range of climate metrics (Rougier, 2016). Thirdly, a small set of models (perhaps around twenty) cannot possibly sample the effects of dozens of interacting uncertain processes in the individual models (Carslaw et al., 2018). Therefore, inter-model comparisons do not provide statistically representative samples (Sexton et al., 2012; Knutti et al., 2013; Collins et al., 2013), making it difficult to draw inferences about the causes of aerosol ERF uncertainty and the robustness of any observational constraint. Leading experts subjectively assess the uncertainty in aerosol forcing as being larger than that quantified by multi-model studies (Morgan et al., 2006).

A complementary approach to exploring aerosol ERF uncertainty in multiple models is to systematically explore the uncertainty in underlying parameters and processes within a single model. Much progress has been made in understanding the causes of uncertainty in state variables related to aerosol ERF, such as cloud-active aerosol concentrations (Lee et al., 2011, 2012, 2013; Samset et al., 2014; Mann et al., 2014; Shrivastava et al., 2016; Kipling et al., 2016), precipitation (Lebo and Feingold, 2014; Qian et al., 2015; Johnson et al., 2015) and ToA radiative fluxes (Shiogama et al., 2012; Zhou et al., 2013; Randles et al., 2013). Furthermore, important sources of aerosol forcing uncertainty (in the absence of rapid atmospheric adjustments) have been identified (Schulz et al., 2006; Haerter et al., 2009; Lohmann and Ferrachat, 2010; Carslaw et al., 2013; Myhre et al., 2013; Regayre et al., 2014, 2015). However, no study has comprehensively explored aerosol ERF uncertainty in a model that accounts for rapid atmospheric adjustments. Studies that do include rapid adjustments (e.g. Gettleman, 2015) rely on one-at-a-time experiments (where individual parameters or model structures are perturbed in isolation) which do a poor job of sampling the model uncertainty because they neglect important parameter interactions (Pianosi et al., 2016).

Here we present a perturbed parameter ensemble of the HadGEM3-GA4-UKCA global aerosol-chemistry-climate model and use model emulation (Lee et al., 2013) to enable the combined effects of uncertainties in 27 aerosol, cloud and other atmospheric model processes to be quantified. Compared to our previous studies (Carslaw et al., 2013; Regayre et al., 2014, 2015) we take a more holistic approach to exploring model forcing uncertainty here by accounting for both the uncertainty in cloud and other physical atmospheric processes, as well as the uncertainties in the aerosol component of the model. We also explore for the first time the uncertainty in aerosol ERF (including rapid atmospheric adjustments to aerosols), and in the components of ERF from aerosol-radiation interactions (ERF_{ARI}) and aerosol-cloud interactions (ERF_{ACI}). Other attempts to quantify the uncertainty in the ToA radiative flux caused by aerosols (Tett et al., 2013; Shiogama et al., 2012) explored only the current state of the atmosphere and not how it changes over time.

The main questions we address in this paper are: 1) How much of the uncertainty in aerosol ERF is caused by aerosol processes and how much by physical atmosphere processes? The answer is important because it will tell us how the tuning of model processes apparently unrelated to aerosols might inadvertently affect the aerosol ERF that models calculate. 2) What are the processes that cause uncertainty in the aerosol ERF and to what extent do they also affect the observable radiative state of the atmosphere? This is important because aerosol ERF uncertainty will only be effectively constrained by observations if the uncertainty in both the ERF and the observations are driven by the same uncertain processes (Lee et al., 2016). 3) How much does tuning the radiative state of the model (i.e., ruling out implausible model settings) affect the range of aerosol ERFs? The effect of tuning of, for example, ToA radiative flux (Lohmann and Ferrachat, 2010; Mauritsen et al., 2012) on the aerosol ERF is not normally considered. However, we show that many model variants (and parts of uncertain parameter space) can be ruled out using ToA flux observations and that such state variable observations can play an important part in reducing the overall uncertainty in aerosol ERF. The results from this paper inform our more comprehensive effort to constrain aerosol ERF uncertainty using multiple observational quantities (Johnson et al., 2018).

In Section 2 we outline our methodology, then in Section 3.1 we quantify the magnitude of the uncertainty in aerosol ERF, ERF_{ARI} and ERF_{ACI} through comprehensive sampling of model parameter uncertainty. We then analyse the main causes of uncertainty in aerosol ERF over multi-century and multi-decadal periods in Section 3.2 and the causes of ToA radiative flux uncertainty in Section 3.3 using sensitivity analysis techniques (Section 2). We also quantify the relative importance of atmospheric and aerosol parameters as sources of uncertainty in aerosol ERF and ToA radiative flux in Section 3.3. In Section 3.4 we identify the main causes of uncertainty in aerosol ERF and its components within 11 climatically important regions. Following Lohmann and Ferrachat (2010), we then explore how constraint of the model state using present-day ToA flux observations influences the plausible range of aerosol ERF (Sections 3.5.1 and 3.5.4). We show that while the relationships between the important driving parameters and individual parameter ranges are well constrained by ToA flux measurements (Sections 3.5.2 and 3.5.3), the range of credible aerosol ERFs is only moderately (10%) constrained. We investigate the causes of the modest constraint in sections 3.5.2, 3.5.3 and 4.

2   Methods

2.1   Set-up of the HadGEM-UKCA aerosol-climate model

We used the UK Hadley Centre Met Office Unified Model (HadGEM3, 2017) including release version 8.4 of the UK Chemistry and Aerosol (UKCA) model, within which the evolution of particle size distribution and size-resolved chemical composition of aerosols are calculated using the GLObal Model of Aerosol Processes (GLOMAP; Spracklen et al., 2005; Mann et al., 2010). The model has a $1.25° \times 1.875°$ horizontal resolution and 85 vertical hybrid pressure levels. The aerosol size distribution is defined by seven log-normal modes: one soluble nucleation mode as well as soluble and insoluble Aitken, accumulation and coarse modes. The aerosol chemical components are sulphate, sea salt, black carbon, particulate organic carbon and dust.

4

Secondary organic aerosol material is produced from the first stage oxidation products of biogenic monoterpenes under the assumption of zero vapour pressure. After kinetic condensation onto existing aerosols organic aerosols (primary and secondary) are treated as one chemical tracer.

The GLOMAP model resolves new particle formation, particle coagulation, gas-to-particle transfer, cloud processing (aqueous chemistry) and the deposition of gases and aerosols. Sulphate particles form by binary homogeneous nucleation (Vehkamäki et al., 2002) throughout the atmosphere and by organically-mediated nucleation (Metzger et al., 2010) in the boundary layer. The activation of aerosol particles into cloud droplets is calculated using distributions of sub-grid vertical velocities (West et al., 2014) and the removal of cloud droplets by autoconversion into rain drops is calculated by the physical atmosphere model. Aerosol removal by impaction scavenging of falling raindrops (within and below clouds) in the physical atmosphere model depends partly on the collocation of clouds and precipitation (Boutle et al., 2014). Soluble particles grow according to the relative atmospheric humidity using composition dependent hygroscopicity factors (κ) in accordance with 'Köhler theory' (Petters and Kreidenweis, 2007).

Successive versions of the GLOMAP model have been widely evaluated against global measurements of particle number concentration (Spracklen et al., 2010; Reddington et al., 2011), chemical compositions (Spracklen et al., 2011b; Schmidt et al., 2011; Browse et al., 2012) and cloud active aerosol concentrations (Korhonen et al., 2008; Spracklen et al., 2011a; Pringle et al., 2012). The HadGEM models are subject to constant monitoring for ongoing use in numerical weather prediction and have informed successive Coupled Model Inter-comparison Project (CMIP) experiments (Taylor et al., 2012). HadGEM capably represents changes in cloud regime (Nam et al., 2012); one of the requirements for simulating rapid adjustments to aerosol perturbations (Stevens and Feingold, 2009; Zhang et al., 2015). Cloud water responses to aerosols may be too strong in the HadGEM model because the current model version does not represent enhanced drying in polluted clouds (Toll et al., 2017). However, over multiple cloud regimes the cloud water response is not of a sufficient magnitude to be climatically important (Malavelle et al., 2017).

Anthropogenic emission scenarios prepared for the Atmospheric Chemistry and Climate Model Inter-comparison Project (ACCMIP; Lamarque et al., 2010) and prescribed in some of the CMIP Phase 5 experiments (Taylor et al., 2012) are prescribed here. Carbonaceous aerosol emissions from fires were prescribed using a ten year average of 2002 to 2011 monthly mean data from the Global Fire and Emissions Database (GFED3; van der Werf et al., 2010).

Model horizontal winds were relaxed (nudged) towards winds from the European Centre for Medium-Range Weather Forecasts (ECMWF) ERA-Interim reanalysis above around 2 km. Nudging of atmospheric states is used primarily to evaluate output from global models (Telford et al., 2008) or to ensure that pairs of simulations have near-identical atmospheric states, so that aerosol and/or chemistry perturbations can be applied and their effects quantified using single realisations of each simulation. In 'free-running' (non-nudged) simulations radiative fluxes need to be averaged over many decades in order to produce

161 signals stronger than the noise resulting from internal variability (Kooperman et al., 2012). Nudging to horizontal winds above
162 around 2 km forces synoptic-scale dynamical features to be consistent across the ensemble, whilst allowing boundary layer
163 atmospheric adjustments in response to changes in aerosols to be affected by the parameter perturbations.

165 Each simulation was subject to a seven-month spin-up period from a consistent starting simulation, with parameters set to
166 their median values for the first four months. Parameter perturbations were applied during the final three months of the spin-up
167 period, after which a full year of data was produced for each ensemble member. Aerosol ERF is calculated as the difference in
168 net ToA short-wave plus long-wave radiative fluxes between pairs of simulations with identical parameter settings but distinct
169 prescriptions of anthropogenic emissions (1850, 1978 and 2008). The aerosol ERF and its components were calculated based
170 on the method of Ghan (2013).

2.2 Parameter sampling

173 The 27 parameters perturbed in the ensemble, as well as the roles they play in the model, are presented in Table A1. We per-
174 turbed 9 parameters in the physical atmosphere model known to affect the properties and distribution of clouds and humidity
175 within the boundary layer (*atmospheric parameters*; Sexton et al. 2018) in combination with 18 aerosol emission, deposition
176 and process parameters (*aerosol parameters*) known to affect cloud droplet number concentrations (Lee et al., 2013) and/or
177 aerosol cloud-albedo effect forcing (the ERF_{ACI} without accounting for rapid adjustments) at the global (Carslaw et al., 2013;
178 Regayre et al., 2014) and/or regional scale (Regayre et al., 2015). Some parameters have been included in the ensemble because
179 they represent model structural advances with inherent process uncertainty (Yoshioka et al., In prep.).

181 We did not attempt to include an exhaustive set of uncertain parameters in the experimental design. Current supercomputing
182 resources are too valuable to justify an uninformed, exhaustive exploration of model uncertainty. Instead, we used one-at-a-
183 time perturbation screening experiments (not shown) to identify the parameters most likely to influence radiative forcing within
184 the model. The parameters included in the preliminary screening process were identified by model domain experts as the key
185 parameters within individual model schemes (e.g. cloud microphysics) and/or model processes (e.g. cloud droplet activation)
186 with the potential to significantly affect aerosol ERF. Our results may change slightly with the inclusion of additional param-
187 eters. However, we went through a thorough parameter screening and prioritisation process so we consider the parametric
188 uncertainty to be close to an upper limit. Furthermore, with many possible opportunities for parameter compensation, addi-
189 tional parameters only very gradually increase the overall uncertainty.

191 The parameters we perturb here are likely to have readily identifiable counterparts in other climate models. All global cli-
192 mate models have similarities because they describe the same physical processes and although process parametrisations can
193 differ between models they often share common biases when compared to measurements (Knutti et al., 2013). Therefore, our
194 aim to identify the main causes of aerosol ERF uncertainty in the HadGEM model (Section 3) will provide valuable clues for

195 reducing the aerosol ERF uncertainty in other models.

196

2.2.1 Definition of atmospheric parameters

198 **Rad_Mcica_Sigma**: *The fractional standard deviation of the sub-grid cloud condensate as seen by radiation*. This parameter
199 controls the inhomogeneity of cloud condensate within vertically overlapping sub-grid clouds (Räisänen et al., 2004) which
200 is used to calculate cloud radiative fluxes. Higher values of Rad_Mcica_Sigma increase cloud condensate inhomogeneity and
201 hence reduce cloud albedo (because of the non-linear relationship between albedo and cloud condensate; Barker and Räisänen,
202 2005). Atmospheric temperature profiles respond to changes in the cloud radiative fluxes and can induce changes in precipita-
203 tion rates and cloud amount. The effect of perturbing Rad_Mcica_Sigma on reflected radiation is largest in regions of persistent
204 stratocumulus cloud where low-altitude, high-albedo clouds occupy a substantial fraction of each model grid box.

205

206 **C_R_Correl**: *Cloud and rain sub-grid horizontal correlation*. The collocation of clouds and rain within the model is impor-
207 tant because it determines the accretion rate of cloud droplets and aerosols by rain drops. Higher values cause more accretion
208 because regions of high cloud water are closely correlated with regions of high precipitation. Perturbations to this parameter
209 affect cloud radiative properties by altering in-cloud interstitial aerosol concentrations and cloud amount.

210

211 **Niter_BS**: *Number of microphysics iteration substeps*. The microphysical processing of in-cloud interstitial aerosols and
212 cloud droplets is controlled by the cloud microphysics scheme within the physical atmosphere model. The values of this pa-
213 rameter determine the degree of processing within a model timestep. Each iteration of the microphysics scheme allows drops
214 to grow larger before precipitation occurs. Therefore, higher parameter values allow for greater microphysical processing and
215 cause the model to produce less light rain. This affects the amount of liquid water within clouds and alters the amount of cloud
216 which is important for cloud radiative effects.

217

218 **Ent_Fac_Dp**: *Entrainment amplitude scale factor*. This convection scheme parameter controls the shape of the convective
219 mass flux and the sensitivity of convection to relative humidity. Higher values reduce the depth of convection and suppress
220 convective precipitation. This parameter is important for cloud radiative effects for several reasons. First, the retention of cloud
221 water increases cloud amount and short-wave reflectivity. Second, lower altitude clouds have a higher cloud top temperature
222 and attenuate less of the long-wave energy emitted by the Earth's surface. Third, if atmospheric moisture is not precipitated
223 convectively, the increase in relative humidity causes more large-scale, frontal precipitation which affects spatial distributions
224 of aerosols and clouds and hence the aerosol ERF.

225

226 **Amdet_Fac**: *Mixing detrainment rate scale factor*. This parameter controls the rate of humidification of the atmosphere
227 and the shape of the convective heating profile. Amdet_Fac is important for cloud radiative effects for similar reasons to
228 Ent_Fac_Dp. Both parameters affect clouds through their influence on convection but through different mechanisms. Higher

7

229 values of Amdet_Fac increase atmospheric humidity and temperature leading to enhanced convection.

230

231 **Dbsdtbs_Turb_0**: *The cloud erosion rate*. This parameter alters the radiative properties of clouds by altering the rate at

232 which unresolved sub-grid motions mix clear and cloudy air. Higher values cause more rapid mixing of clear, dry air into

233 clouds, thereby reducing cloud liquid water content, autoconversion of cloud droplets to rain drops and cloud amount. The

234 atmospheric lifetimes of aerosols and precursor gases are noticeably affected by this parameter.

235

236 **Mparwtr**: *Maximum value of the function controlling convective parcel maximum condensate*. Convective parcels near the

237 Earth's surface precipitate when the amount of moisture reaches the threshold set by this parameter. Higher values increase

238 cloud amount and lifetime by reducing convective precipitation. As with other convective parameters Mparwtr affects cloud

239 radiative effects and aerosols by altering the spatial distributions of clouds and precipitation.

240

241 **Dec_Thres_Cld**: *The threshold for cloudy boundary layer decoupling*. Boundary layer stability plays an important role in

242 determining the magnitude of cloud radiative effects because a well-mixed, stable boundary layer retains more heat and permits

243 more dynamic activity. This parameter is the threshold at which the boundary layer decouples from the rest of the atmosphere.

244 Hence, higher parameter values lead to a more well-mixed boundary layer, increased cloudiness and longer in-cloud processing

245 times for aerosols.

246

247 **Fac_Qsat**: *Rate of change of convective parcel maximum condensate with altitude*. The maximum amount of moisture a con-

248 vective parcel can hold transitions from the threshold set by the parameter Mparwtr at the surface to a much smaller threshold

249 at high altitudes. Fac_Qsat controls the rate at which this threshold changes with altitude. Fac_Qsat therefore influences cloud

250 radiative effects through similar mechanisms to Mparwtr (higher values suppress precipitation and increase cloud amount and

251 lifetime) but is more important in the upper boundary layer.

252

253 ### 2.2.2 Definition of the aerosol parameters

254 **Ageing**: *Ageing of hydrophobic aerosols*. Carbonaceous aerosols are assumed to be non-hygroscopic when emitted into the

255 atmosphere and cannot act as cloud condensation nuclei until sufficient layers of sulphuric acid and condensible organic mat-

256 ter coat their surface. This parameter is the number of monolayers of soluble material required to convert initially insoluble

257 aerosols into cloud condensation nuclei. Higher values reduce the conversion rate of hydrophobic to hygroscopic aerosols. This

258 parameter is important for aerosol ERF because it affects cloud condensation nuclei and the removal rate of highly-absorbing

259 carbonaceous aerosols from the atmosphere.

260

261 **Cloud_pH**: *pH of cloud droplets*. The pH of cloud droplets is used in the aqueous chemistry module of GLOMAP to cal-

262 culate the conversion of SO_2 into sulphate particles. Cloud droplet pH depends on kinetic and thermodynamic processes that

8

263 are not explicitly simulated. Therefore, we use a globally defined value of cloud droplet pH to control the reaction rate. Un-
264 certainty in this parameter accounts for the simplification in its application. Higher values of this parameter increase sulphate
265 production near SO_2 emission sites and tend to reduce aerosol concentrations in remote regions (through effects on new parti-
266 cle formation). Therefore, the cloud pH parameter affects the spatial distribution of aerosols which is important for aerosol ERF.
267

268 **Carb_BB_Ems**: *Carbonaceous biomass burning emission scale factor*. Higher values of this scale factor increase the
269 amount of carbonaceous aerosols emitted into the atmosphere from large-scale biomass burning. Carbonaceous aerosols are
270 important for aerosol ERF because they absorb solar radiation and the resulting energy redistribution affects boundary layer
271 temperatures and stability and can affect cloud cover (Gnanadesikan et al., 2017).
272

273 **Carb_BB_Diam**: *Carbonaceous biomass burning emission diameter (nm)*. This parameter determines the size of carbona-
274 ceous aerosols at time of emission. Higher values cause fewer, larger carbonaceous aerosols to be emitted for a given value
275 of Carb_BB_Ems. Therefore, the total carbonaceous aerosol particle number is reduced, leading to fewer cloud condensation
276 nuclei and a change in aerosol optical properties.
277

278 **Sea_Spray**: *Sea spray aerosol emission scale factor*. Aerosol ERF is sensitive to emission fluxes of natural aerosols because
279 they strongly influence the pre-industrial background aerosol concentration and the relative magnitude of the change in aerosols
280 over the industrial period. Perturbations to the wind-driven emission fluxes affect aerosol distributions in marine and coastal
281 regions.
282

283 **Anth_SO2**: *Anthropogenic SO_2 emission scale factor*. SO_2 gas forms H_2SO_4 molecules which condense to form sulphate
284 particles. Furthermore, SO_2 condenses onto existing particles increasing their size and solubility. Therefore, scaling anthro-
285 pogenic SO_2 emissions affects aerosol ERF by influencing the concentrations and composition of present-day aerosols.
286

287 **Volc_SO₂**: *Volcanic SO_2 emission scale factor*. Volcanic SO_2 emissions are treated identically to anthropogenic SO_2 emis-
288 sions. However, they are present in both the pre-industrial and present-day atmospheres so exert an influence on aerosol ERF
289 through a similar mechanism as Sea_Spray by altering the pre-industrial aerosol concentration.
290

291 **BVOC_SOA**: *Biogenic secondary aerosol formation from volatile organic compounds scale factor*. Secondary organic
292 aerosols form through multi-stage oxidation reactions of biogenic volatile organic compounds (monoterpenes in this case).
293 This parameter scales the secondary organic aerosol emission flux, with higher values producing larger emissions. Perturbing
294 this parameter changes the aerosol concentration and size distribution in the pre-industrial and present-day atmosphere.
295

296 **DMS**: *Dimethylsulphide surface ocean concentration scale factor*. Perturbing the concentration of DMS in the oceans alters
297 the wind-driven flux of DMS into the atmosphere. DMS is important for aerosol ERF because it is a source of natural aerosols

which affect the pre-industrial aerosol background concentrations. Similar to the Sea_Spray parameter, DMS affects aerosol concentrations in marine and coastal regions. However, marine DMS concentrations increase with ocean temperature so perturbations to this parameter will have the greatest influence on aerosol ERF in warmer months.

Dry_Dep_Acc: *Accumulation mode dry deposition velocity scale factor*. Aerosols are removed from the atmosphere at a velocity calculated using Brownian diffusion, impaction and interception. This calculation in the GLOMAP model depends on wind speeds and surface roughness. High values of this parameter more readily remove accumulation mode aerosols from the atmosphere causing a reduction in cloud condensation nuclei concentrations.

Dry_Dep_SO2: *SO_2 dry deposition velocity scale factor*. This parameter determines the removal of SO_2 gas from air masses that interact with the surface. The removal of SO_2 is important for aerosol ERF because SO_2 is a precursor for sulphate particles and condenses onto existing particles causing them to grow to the larger sizes needed to act as cloud condensation nuclei. Higher values of this parameter increase the removal rate of SO_2 from the atmosphere. This affects aerosol size distributions by simultaneously reducing particle formation rates and the growth rates of existing aerosols.

Kappa_OC: *Köhler coefficient of organic carbon*. Aerosol water uptake efficiency is determined by 'Köhler theory' using size and composition dependent hygroscopicity factors (κ; Petters and Kreidenweis, 2007). Higher values of this parameter increase the water uptake efficiency of the organic material in the particles. Perturbations to this parameter will change the light-scattering efficiency of the particles and the droplet activation process, thereby affecting cloud microphysical processes. In particular, cloud-active aerosol concentrations in the pre-industrial atmosphere are expected to be susceptible to this parameter value (Liu and Wang, 2010).

Sig_W: *Updraft vertical velocity standard deviation*. This parameter controls the width of the probability distribution of sub-grid vertical velocities used to calculate the activation of aerosols into cloud droplets. Higher Sig_W values widen the distribution of updraft velocities. The largest sub-grid updrafts within the distribution have the greatest influence on cloud droplet concentrations because, for any given supersaturation, a larger updraft velocity will cause a greater proportion of relatively small aerosols to activate. Higher values of Sig_W therefore increase cloud droplet concentrations, decrease precipitation efficiency (through reduced autoconversion rates), cloud liquid water content and cloud albedo. Sig_W perturbations have the greatest influence on cloud droplet concentrations in regions of relatively high aerosol concentrations because in such environments droplet activation is updraft-limited rather than aerosol-limited.

Dust: *Dust emission scale factor*. Dust aerosols are large, insoluble particles when emitted, but are treated as hygroscopic once sufficiently aged by the condensation of soluble material onto the particle surface (as defined by the 'ageing' parameter). We perturb dust emissions in our ensemble because they are important for the ERF_{ARI} component of aerosol ERF. Furthermore, dust influences cloud-active aerosol concentrations (Manktelow et al., 2010) and cloud droplet concentrations (Karydis

333 et al., 2017).

334

335 **Rain_Frac**: *Fraction of cloud-covered area in large-scale clouds where scavenging occurs*. Rain and clouds do not correlate
336 perfectly (as discussed in the C_R_Correl definition). Higher values of this parameter allow aerosols to be scavenged by rain
337 drops over a greater fraction of cloudy areas. The value of this parameter is important for aerosol ERF because it affects aerosol
338 atmospheric lifetimes.

339

340 **Cloud_Ice_Thresh**: *Threshold of cloud ice fraction above which nucleation scavenging of aerosol material is suppressed*.
341 The scavenging of aerosol material in dynamic rain systems is controlled partly by the rain formation process - either collision-
342 coalescence process that efficiently removes many aerosol particles in raindrops or the Wegener-Bergeron-Findeisen process
343 in mixed-phase clouds, which leads to less aerosol scavenging and seems to account for the efficient winter-time transport of
344 aerosols to the Arctic (Barrett et al., 2011; Browse et al., 2012). In our previous studies (Regayre et al., 2014, 2015) we de-
345 fined a temperature below which scavenging was suppressed. Here, we instead use the mass fraction of ice to define a threshold
346 above which no nucleation scavenging occurs. Higher values require a greater proportion of ice to be present before scavenging
347 is suppressed. This parameter is important for high latitude aerosol concentrations and cloud radiative effects (Browse et al.,
348 2012; Regayre et al., 2015; Yoshioka et al., In prep.).

349

350 **BC_RI**: *Imaginary part of the black carbon refractive index*. This parameter controls the absorption of radiation as it passes
351 through aerosols containing black carbon. Higher values of the imaginary refractive index cause more energy to be absorbed
352 and re-emitted by black carbon aerosols. The real part of the refractive index is defined according to the imaginary part mean-
353 ing that this parameter also controls the scattering of radiation by black carbon aerosols. Higher values of the real part cause
354 more incoming radiation to be refracted towards the Earth's surface (more forward scattering). Perturbations to BC_RI affect
355 ERF_{ARI} as well as the vertical profile of atmospheric heating and hence convection, cloud amount and cloud radiative effects.
356 Our simulations do not account for effect of depositing light-absorbing carbonaceous aerosols on snow (Bond et al., 2013), nor
357 the air-sea interactions that enhance rapid adjustments in marine regions (Gnanadesikan et al., 2017).

358

359 **OC_RI**: *Imaginary part of the organic carbon refractive index*. The absorption of radiation by organic carbon is controlled
360 by this parameter. Unlike BC_RI, the real part of the organic carbon refractive index is held constant. Therefore, perturba-
361 tions to this parameter have no effect on the refractive properties of organic carbon. Otherwise, OC_RI affects the atmosphere
362 through the same mechanisms as BC_RI.

363

364 One potentially important parameter that we did not perturb is the autoconversion rate of cloud droplets into rain drops (al-
365 though we did perturb Rain_Frac and C_R_Correl which affect aerosol and cloud droplet removal by rain drops). The coupling
366 between the GLOMAP model and the cloud microphysics scheme is currently one-way: cloud droplet concentrations calcu-
367 lated in GLOMAP are used in the autoconversion scheme and thereby affect precipitation rates, cloud liquid water content and

11

albedo. However, precipitation only alters the cloud droplet concentrations in HadGEM and not aerosol concentrations within the GLOMAP model. For aerosol concentrations to be directly altered by the autoconversion process, the coupling would need to be two-way so that cloud droplet concentrations in GLOMAP were consistent with those calculated in the atmospheric model's microphysics scheme.

Other HadGEM simulations showed that over multiple cloud regimes cloud liquid water path is not substantially affected by aerosols through autoconversion (Malavelle et al., 2017), suggesting that neglecting the uncertainty in this process is not important to our results. However, in relatively polluted regions (such as the North Atlantic) cloud liquid water path responses to aerosols in low-altitude clouds (particularly Stratocumulus) are likely to be overestimated in the model because of known structural errors (Toll et al., 2017). The cloud liquid water path response to aerosols in low, warm clouds is weaker in HadGEM than in other global climate models (Ghan et al., 2016). Therefore, autoconversion may seem more important in other models, but will likely be overstated (Toll et al., 2017). This process should be considered in future uncertainty analysis studies once shared model structural errors are addressed and the process uncertainty better quantified.

2.3 Statistical methodology

Maximin Latin Hypercube sampling was used to create a parameter combination design of 162 points with excellent space-filling properties that provide information on model output across the 27-dimensional parameter uncertainty space. A simulation with all parameters set to their median values (from distributions described in table A1) was also included in the ensemble. Emulators were then constructed which describe individual model outputs (ToA flux, aerosol ERF and its components) over the 27-dimensional space of the uncertain parameters. Emulators provide a statistical representation of model output for all points within the multi-dimensional parameter space and have been widely used to analyse climate models (Lee et al., 2013; Carslaw et al., 2013; Tett et al., 2013; Regayre et al., 2014; Hamilton et al., 2014; Regayre et al., 2015; Johnson et al., 2015; Lee et al., 2016) as well as complex models in many other areas of science, including hydrology (Liu and Gupta, 2007), galaxy formation (Rodrigues et al., 2017) and disease transmission (Andrianakis et al., 2017).

In total 217 perturbed parameter simulations were created for each anthropogenic emission period including a set of 54 simulations with parameter combinations that augment the original design and were used to validate the emulators. Twenty-six simulations did not complete an annual cycle in at least one of the anthropogenic emission periods (1850, 1978 and 2008) because the combinations of parameters caused the model to fail. Hence, the ensemble of simulations for each period was made up of the remaining 191 simulations. Once emulators were validated, by ensuring that at least 75% of the validation simulations produced output within the relatively small emulator uncertainty bounds, new emulators conditioned on output from the 191 perturbed parameter simulations (with better space-filling properties) were created by combining the validation simulations with the original set of simulations.

Probability density functions (pdfs; Table A1) were used to represent expert beliefs about parameter uncertainty. We pre-dominantly used trapezoidal distributions (Hetzel, 2012) to represent parameter uncertainty in order to avoid having an overly-centralized multi-variate sample (Yoshioka et al., In prep.).

By combining perturbed parameter ensembles with model emulation and then densely sampling emulator output using the extended-FAST sampling method (Saltelli et al., 1999), we were able to perform sensitivity analyses (Saltelli et al., 1999, 2000; Lee et al., 2012) and decompose the variance in model output into individual components. We used the percentage reduction in variance which would be achieved if a parameter value was known exactly as our main statistic for identifying the causes of uncertainty. Emulation and sensitivity analyses were applied at the individual model gridbox level (degraded to N48 model resolution) as well as at the regional and global mean level for the ToA flux as well as the forcing terms. For the sensitivity analyses, samples of 270000 members were drawn from the emulators at parameter combinations determined by the param-eter pdfs. The sensitivity analysis results are therefore informed by expert knowledge about the model behaviour in relation to the uncertain processes. However, for the constraint of aerosol ERF using ToA flux observations we sampled one million model variants using uniform pdfs. This sampling approach uses the expert-elicited parameter pdfs to determine the ranges of uniform pdfs for sampling but neglects expert prior beliefs about parameter value likelihoods. As such, the effects of applying the observational constraint and expert knowledge can be quantified and compared. Furthermore, the effect of applying the observational constraint on the uncertain parameter space can be more readily assessed when uniform pdfs are used to create the original sample because parameter combinations are more evenly spaced throughout the 27-dimensional parameter space.

Preliminary parameter combination screening tests revealed that values of Ent_Fac_Dp higher than around 1.8 in combi-nation with values of Amdet_Fac higher than around 8.0 caused model simulations to fail. This part of the 27-dimensional parameter space (a corner of a 2D plane) was removed from the ensemble design and analyses. The sampling method used to perform the sensitivity analyses, was adapted to reject samples from the 2D corner of parameter space not included in the de-sign. Rejected combinations of the Ent_Fac_Dp and Amdet_Fac parameters were re-sampled from the restricted 2D parameter space without affecting the sampling frequency across the remaining 25-dimensional parameter space.

3   Results

3.1   Uncertainty in aerosol ERF and its components

Figure 1 shows pdfs of the global mean aerosol ERF (from 1850 to 2008) and its components; ERF_{ARI} and ERF_{ACI}. The 95% credible interval of aerosol ERF used in the sensitivity analysis is -2.18 to -0.71 $W\,m^{-2}$. Most of the uncertainty in aerosol ERF comes from the ERF_{ACI} component, which has a credible interval of -2.20 to -0.61 $W\,m^{-2}$ and captures much of the recognised uncertainty in this forcing term (Myhre et al., 2013; Shindell et al., 2013). We also account for above-cloud aerosols (Ghan, 2013) in our calculation of ERF_{ACI} and ERF_{ARI} which affects the balance between these two components of aerosol

435   ERF (Yoshioka et al., In prep.). This adjustment results in distributions of weaker ERF_{ARI} values and stronger ERF_{ACI} values

436   in our sample compared to (Myhre et al., 2013). We discuss these effects further in Section 3.1.2.
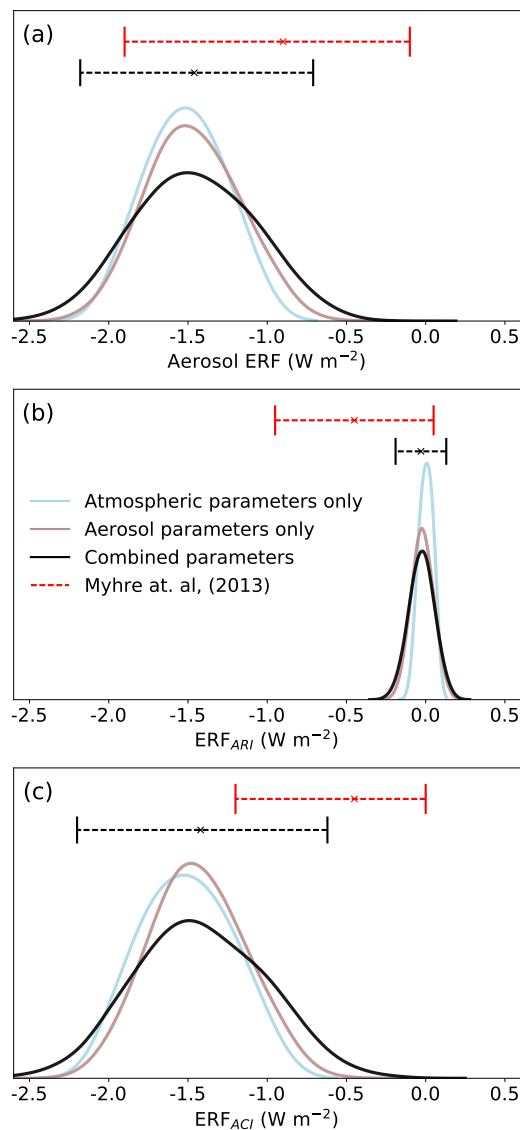
437

Figure 1. Probability density functions of 1850-2008 (a) aerosol ERF, (b) ERF_{ARI} and (c) ERF_{ACI}. Each sample contains 270000 emulator-derived model variants informed by the expert-elicited prior probability distributions of parameter values. Samples with aerosol and atmospheric parameter uncertainties neglected (Table A1) were obtained by setting each neglected parameter to its median value in the corresponding pdf. 90% credible intervals from (Myhre et al., 2013) are presented as red horizontal lines with best estimates marked using crosses. Our 95% credible intervals are presented in black and the sample median is presented using a cross.

The sample of aerosol ERFs in Fig. 1 has already been constrained by our choice of probability distributions for the uncertain parameters (Table A1). When we use uniform parameter distributions to sample parameter combinations (Section 2.3) the credible range (95%) of aerosol ERFs is -2.65 to -0.68 $\mathrm{W\,m^{-2}}$. By applying expert beliefs about parameter value likelihoods the aerosol ERF credible range is only -2.18 to -0.71 $\mathrm{W\,m^{-2}}$ (Fig. 1(a)). This implies that by applying the combined knowledge of experts with an understanding of the model processes and parametrisations we have effectively reduced the aerosol ERF credible range by around 25%.

The strongest aerosol ERFs in our distribution would lead to a negative forcing when combined with best estimates of changes in other forcing agents over the industrial period. A net negative forcing is incompatible with the observed increase in global mean surface temperatures over the industrial period (e.g. HadCRUT4, 2017). However, there is substantial uncertainty in the ERFs of multiple other forcing agents (Myhre et al., 2013; Fig. 8.16 and 8.18) so our most negative aerosol ERF values cannot be considered implausible using this criteria. Structural aspects of the model could account for the strongest forcings. For example, our model is missing marine sources of organic aerosols and related processes (Gantt et al., 2015) which, if included, would act as an important source of ice-nucleating particles (Vergara-Temprado et al., 2017) and pre-industrial aerosols (Gordon et al., 2017) which would weaken the aerosol forcing (Carslaw et al., 2013). However, our perturbed parameter ranges were to some extent intended to encompass the uncertainty caused by those structural deficiencies we were aware of. The values in the tails of the aerosol ERF pdf are likely to be the result of setting multiple parameters important for aerosol ERF to extreme values, which are also likely to cause extreme present-day ToA flux values and be considered implausible when compared to observations (Sections 3.5).

Figure 1 also shows the separate effects of the 18 combined aerosol parameters and the 9 combined physical atmosphere model uncertainties. Neglecting the uncertainty in aerosol parameters (by setting them to their median values in the all model variants) results in a 95% credible aerosol ERF interval of -1.98 to -1.04 $\mathrm{W\,m^{-2}}$, while neglecting uncertainty in atmospheric parameters results in a credible interval of -2.00 to -0.90 $\mathrm{W\,m^{-2}}$. Summary statistics of forcing from these samples are presented in Table A2. The distribution of aerosol ERF (as well as ERF_{ARI} and ERF_{ACI}) is wider and flatter (has a larger variance) in the combined sample than the distributions of atmosphere-only and aerosol-only sampled values. This suggests that important interactions between atmospheric and aerosol parameters cause the most extreme aerosol ERF values. The effects of the aerosol and physical model uncertainties do not have an additive effect on the aerosol ERF uncertainty because of compensating effects between the groups of parameters. These results show that both atmospheric and aerosol parameter perturbations are required to comprehensively sample model uncertainty. The main atmospheric and aerosol sources of aerosol ERF uncertainty are identified in Section 3.2.1.

3.1.1   Uncertainty in ERF$_{ACI}$

471   Maps of the means and standard deviations of ERF$_{ACI}$ resulting from perturbations to our 27 atmospheric and aerosol pa-
472   rameters are presented in Fig. 2. Forcings stronger than -3.5 W m^{-2} are concentrated over anthropogenic aerosol sources
473   (particularly Asia, America and Europe) and in marine stratocumulus regions (Atlantic Ocean, North Pacific Ocean and the
474   South Pacific Ocean off the South American coast). The standard deviation of ERF$_{ACI}$ is largest (up to 6 W m^{-2}) in the same
475   regions and is typically of the same order of magnitude as the mean regional value. The spatial distribution of mean ERF$_{ACI}$ is
476   very similar to the Atmospheric Chemistry and Climate Model Intercomparison Project (ACCMIP) multi-model mean pattern
477   (Shindell et al., 2013). However, the magnitudes of forcing differ, particularly over remote marine regions. For example, our
478   mean ERF$_{ACI}$ is stronger than -5 W m^2 over much of the North Pacific Ocean, whereas the ACCMIP mean aerosol ERF in the
479   Pacific is stronger than -3.5 W m^2 only in coastal regions near to anthropogenic sources. These strong remote marine ERF$_{ACI}$
480   values go some way to explaining the differences in global mean ERF$_{ACI}$ between our sample (around -1.4 W m^2) and the
481   ACCMIP multi-model mean (around -0.9 W m^2). In part, the magnitude of our ERF$_{ACI}$ values are caused by the above-cloud
482   aerosol adjustment (Ghan, 2013). Our model has a relatively weak cloud liquid water path response to aerosols (Ghan et al.,
483   2016; Malavelle et al., 2017), which suggests that our very negative marine forcing values are not caused by an overly strong
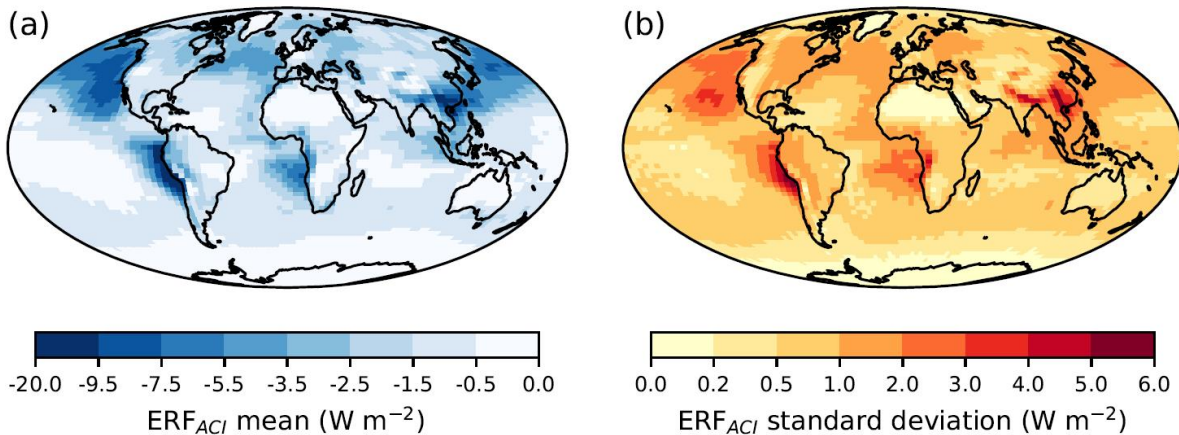484   aerosol second indirect effect.

485

Figure 2. (a) Mean and (b) standard deviation for 1850-2008 ERF$_{ACI}$ forcing. Values were calculated using output from 270000 emulator-derived model variants at the individual pixel level once degraded to N48 model resolution. These samples of model variants are informed by the expert-elicited parameter pdfs.

3.1.2 Uncertainty in ERF_{ARI}

487 Fig. 3 shows the spatial pattern of mean ERF_{ARI} and its standard deviation. Global mean ERF_{ARI} is near zero (95% credible
488 range -0.19 to 0.13 $W\,m^{-2}$; Fig. 1; Table A2). Although the possibility of a globally positive ERF_{ARI} has previously been con-
489 sidered unlikely (Boucher et al., 2013), it has important implications for our understanding of interactions between absorbing
490 aerosols, cloud-processes and boundary-layer dynamics. The near-zero global mean ERF_{ARI} results from the cancellation of
491 positive and negative regional forcings. Positive mean ERF_{ARI} values (up to 10 $W\,m^{-2}$) occur in regions where carbonaceous
492 aerosols often overlie relatively high-albedo clouds (continental Asia and off the west coasts of Africa and South America).
493 It is in these regions that the standard deviation of ERF_{ARI} is also largest (up to 5 $W\,m^{-2}$). Light-absorbing aerosols above
494 cloud heat the local atmosphere, which can suppress convection and affect cloud cover. This is important for calculating the
495 ERF_{ARI} from our simulations because we account for above-cloud scattering and absorption of aerosols in line with Ghan
496 (2013). Neglecting the effects of above-cloud aerosols in the ERF_{ARI} produces no positive values for this forcing component
497 (95% credible interval -0.69 to -0.24; Yoshioka et al., In prep.). Therefore, the magnitude of ERF_{ARI} over Asia, Africa and
498 South America (where it is positive and reduces cloud cover) determines the sign of global mean ERF_{ARI}.
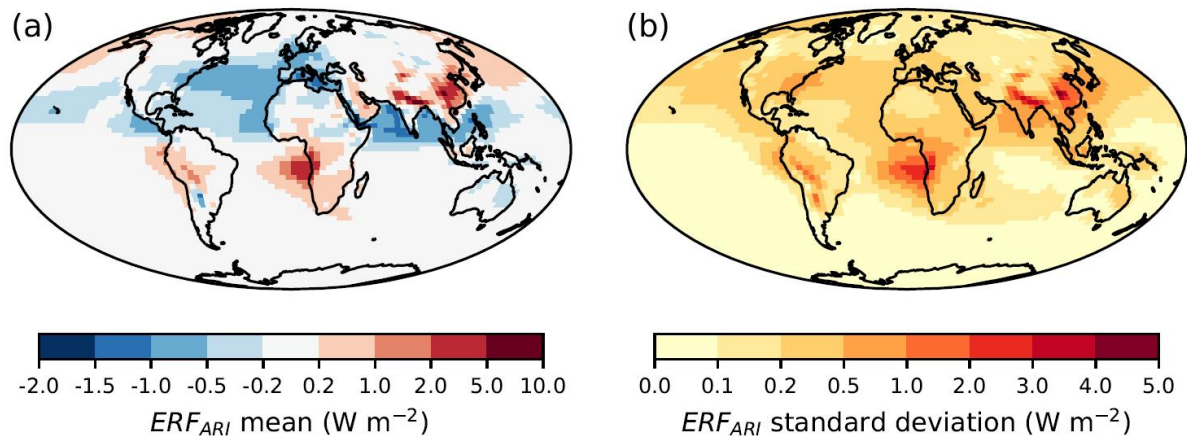499

Figure 3. (a) Mean and (b) standard deviation of 1850-2008 ERF_{ARI} forcing. Values were calculated using output from 270000 emulator-
derived model variants at the individual pixel level. These samples of model variants are informed by the expert-elicited parameter pdfs.

3.2 Sources of uncertainty in aerosol ERF and its components

3.2.1 Sources of uncertainty in global mean ERF_{ACI}

502 Fig. 4 summarises the causes of variance (sometimes referred to as the 'main effects') in global mean ERF_{ACI}, ERF_{ARI} and
503 aerosol ERF. Natural aerosol emissions (here, predominantly Sea_Spray, DMS and BB_Diam) persist as important sources of

504 industrial-period ERF_{ACI} uncertainty, as in previous studies of several climate models (Wilcox et al., 2015) and the aerosol-
505 only component of a global model (Carslaw et al., 2013). Here, natural aerosols are responsible for around 63% of the propor-
506 tion of ERF_{ACI} variance caused by aerosol parameters, compared to 45% of the variance in aerosol-cloud-albedo effect forcing
507 in the absence of rapid atmospheric adjustments (Carslaw et al., 2013). However, by far the largest source of uncertainty is
508 the Rad_Mcica_Sigma parameter. This cloud radiation parameter affects the spatial homogeneity of simulated clouds, altering
509 (amongst other things) reflected radiation, tropospheric temperature profiles and cloud amount (Section 3.3). Therefore, by
510 altering the radiative *state* of clouds in the pre-industrial and present-day atmospheres Rad_Mcica_Sigma affects uncertainty
511 in the simulated *change* in cloud radiative state (the ERF_{ACI}). Model process parameters Sig_W and C_R_Correl cause un-
512 certainty in ERF_{ACI} by altering the efficiency of the cloud droplet activation and deposition processes respectively. Other
513 parameters cause a small amount of the ERF_{ACI} uncertainty but only in individual months. Therefore, the six parameters
514 and associated processes identified here are the key to understanding the uncertainty in the global, annual mean ERF_{ACI} in
515 HadGEM.

3.2.2 Sources of uncertainty in global mean ERF_{ARI}

518 The sources of global mean ERF_{ARI} variance are summarised in Fig. 4(b). Parameters related to the emission and radiative
519 properties of carbonaceous absorbing aerosols (BC_RI, OC_RI and BB_Ems) are amongst the largest sources of ERF_{ARI}
520 variance in all months. However, the emission flux of carbonaceous aerosols (BB_Ems) and the radiative properties of organic
521 carbonaceous aerosols (OC_RI) cause much more of the ERF_{ARI} variance in high emission months (Jun - Aug) than they do in
522 the annual mean. In other months with lower concentrations of carbonaceous aerosols, uncertainty in anthropogenic emissions
523 (here, Anth_SO2) is the largest source of global mean ERF_{ARI} variance. Anthropogenic emissions affect the ERF_{ARI} by in-
524 fluencing aerosol properties in the present-day atmosphere. Other parameters (notably, Rad_Mcica_Sigma and Sig_W) affect
525 the balance between ERF_{ACI} and ERF_{ARI} by altering cloud radiative properties which are important for calculating above-
526 cloud aerosol effects (Ghan, 2013). Rad_Mcica_Sigma and Sig_W are the only parameters identified as important causes of
527 uncertainty in both ERF_{ACI} and ERF_{ARI}.

3.2.3 Sources of uncertainty in industrial-period global mean aerosol ERF

530 The aerosol ERF is the sum of the ERF_{ACI} and ERF_{ARI}. Therefore, the sources of aerosol ERF variance are also sources of
531 variance in the forcing components. The causes of aerosol ERF variance are summarised in Fig. 4(c). Aerosol ERF shares more
532 sources of variance with ERF_{ACI} than with ERF_{ARI} because ERF_{ACI} is the stronger and more uncertain forcing component
533 (Fig. 1). Natural aerosol emissions (Sea_Spray, DMS and BB_Diam) and model process parameters (Sig_W and C_R_Correl)
534 collectively cause over half of the aerosol ERF variance. Each of these key parameters causes a similar proportion of the
535 aerosol ERF and ERF_{ACI} variances. However, the cloud radiation parameter (Rad_Mcica_Sigma) causes more of the ERF_{ACI}
536 variance (around 35%) than aerosol ERF variance (less than 30%), despite also causing around 25% of the ERF_{ARI} variance.
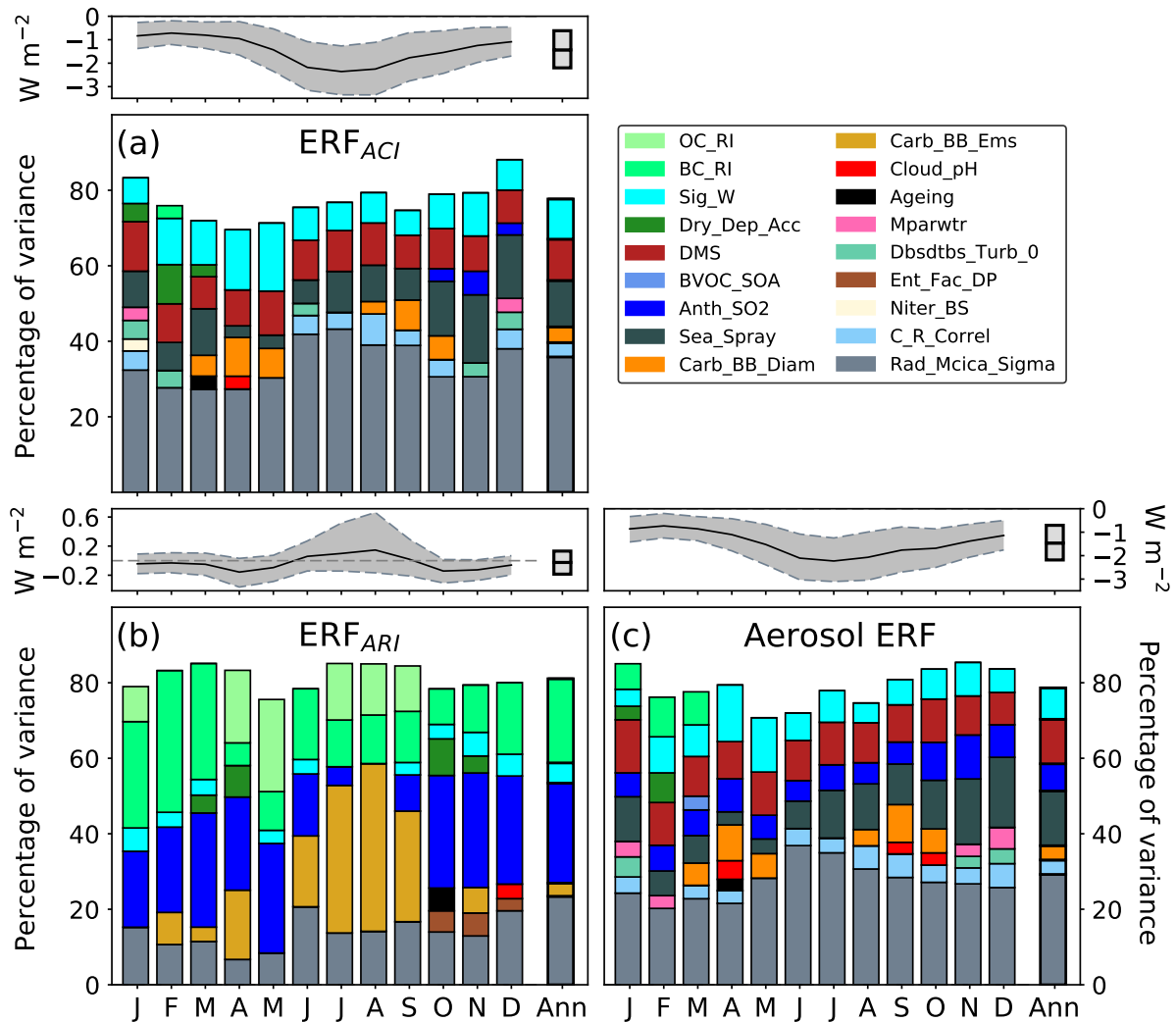
Figure 4. Percentage contributions to variance in global, monthly and annual mean 1850-2008 (a) ERF_{ACI}, (b) ERF_{ARI} and (c) aerosol ERF. Each bar contains only those parameters that cause at least 3% of the variance and interactions between parameters are neglected. Therefore, the percentage of variance accounted for is less than 100%. The monthly and annual median values and 95% credible intervals (from the 270000 model variants) are displayed in the top panel. The monthly median values are connected in bold and the credible intervals are shaded gray.

537   This suggests that the ERF_{ACI} and ERF_{ARI} responses to Rad_Mcica_Sigma are of opposite sign and thus partially cancel in

538   the aerosol ERF calculation. The other main difference between sources of aerosol ERF and ERF_{ACI} variance comes from

539   anthropogenic emissions. Anthropogenic emission uncertainty (Anth_SO2) causes up to 10% of the aerosol ERF variance in

540   all months. However, Anth_SO2 only causes a small percentage of the ERF_{ACI} variance in a few months. Therefore, this

541   parameter's contribution to aerosol ERF variance is predominantly through its influence on the ERF_{ARI} component of forcing.

542

3.2.4   Sources of uncertainty in multi-decadal aerosol ERF

544   The causes of aerosol radiative forcing uncertainty are known to depend on the anthropogenic emission period examined
545   (Carslaw et al., 2013; Regayre et al., 2014). A more detailed understanding of the causes of uncertainty in aerosol ERF re-
546   quires sensitivity analyses over multiple time periods. In this section, we examine the pattern of uncertainty in multi-decadal
547   (1978-2008) aerosol ERF, identify the main causes of uncertainty in multi-decadal aerosol ERF and discuss how these results
548   inform our understanding of aerosol ERF on longer time scales.

549

550   Fig. 5 shows the spatial pattern of mean aerosol ERF and its standard deviation over the 1978-2008 period. Global anthro-
551   pogenic sulphate emissions peaked in the late 1970s (Lamarque et al., 2010) then decreased in Europe and North America as
552   a result of clean air legislation, but increased significantly in Asia (Smith et al., 2011). Therefore, there are distinct regions
553   of positive and negative aerosol ERF in the 1978-2008 period. The cancellation of the regional aerosol ERFs of opposite sign
554   cause a near-zero global mean aerosol ERF (95% credible range of -0.6 to 0.8 $\mathrm{W\,m^{-2}}$). Over continental land masses, the
555   aerosol ERF standard deviation is largest (between 0.5 and 5 $\mathrm{W\,m^{-2}}$) in regions of substantial mean aerosol ERF (absolute
556   mean larger than around 1 $\mathrm{W\,m^{-2}}$). The aerosol ERF standard deviation is larger than around 0.3 $\mathrm{W\,m^{-2}}$ over most marine
557   regions and is largest over regions of persistent stratocumulus cloud, even when the mean forcing is near-zero (e.g. off the west
558   coast of South America). This suggests the sign of recent-decadal aerosol ERF forcing is uncertain over those regions.
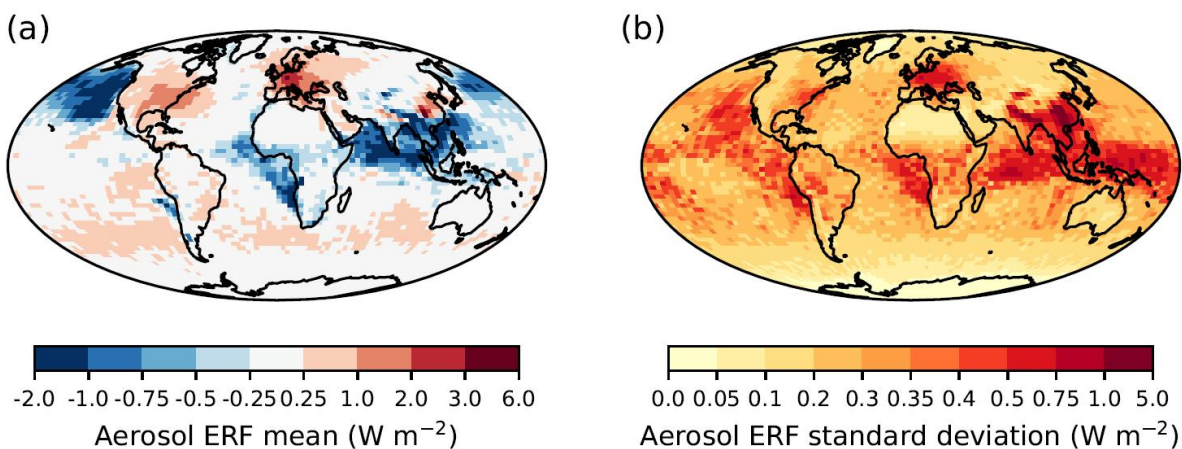
559

Figure 5. (a) Mean and (b) standard deviation of 1978-2008 aerosol ERF. Values were calculated using output from 270000 emulator-derived model variants at the individual pixel level. These samples of model variants are informed by the expert-elicited parameter pdfs.

560   The sources of variance in aerosol ERF and its components over the 1978 to 2008 period are summarised in Fig. 6. The
561   sign of the aerosol ERF over the 1978-2008 period is uncertain for much of the year and is only definitively negative in the
562   Northern Hemisphere summer. The cancellation of positive and negative regional aerosol ERFs has three main implications
563   for the global mean sensitivity analysis. Firstly, not all of the causes of regional aerosol ERF will be evident in the global mean
564   analysis (Regayre et al., 2015). Nevertheless, the causes of uncertainty in global mean 1978-2008 aerosol ERF will inform
565   our understanding. Secondly, the causes of global mean aerosol ERF uncertainty are seasonally dependent because changes in
566   the magnitude of incoming solar radiation determine the relative importance of regional uncertainties. Thirdly, the competing
567   regional effects cause the total variance accounted for by individual parameters to be much less than 100% (as low as 55% in
568   some months) with many parameters causing only a small amount (around 5%) of the variance. This suggests that important
569   interactions between multiple parameters in multiple regions are causing much of the global mean aerosol ERF variance in
570   recent decades.

571

572   There are multiple ways in which the causes of aerosol ERF uncertainty in the 1978-2008 period differ from those in the
573   1850-2008 period. Firstly, natural aerosol emission parameters have little influence on recent-decadal aerosol ERF uncertainty
574   because the global mean 1978-2008 aerosol ERF depends more linearly on changing anthropogenic emissions than the 1850-
575   2008 aerosol ERF (Carslaw et al., 2013). Secondly, the cloud radiation parameter Rad_Mcica_Sigma causes very little (less
576   than 3%) of the 1978-2008 aerosol ERF variance. The reduced importance of this parameter as a cause in aerosol ERF un-
577   certainty results from the cancellation of regional aerosol ERFs of opposite sign, which also depends on the linearity of the
578   multi-decadal aerosol ERF response to anthropogenic emission changes. Thirdly, in the 1978-2008 period anthropogenic and
579   model process parameters are a larger source of aerosol forcing uncertainty, as in previous analysis of this period (Regayre
580   et al., 2014). Here, uncertainty in the deposition rates of aerosols and aerosol precursor gases account for most (around 20%
581   each) of the multi-decadal aerosol ERF variance. The aerosol process parameter Cloud_pH causes another 10% of the 1978-
582   2008 aerosol ERF variance. The anthropogenic emission parameter Anth_SO2 and other model process parameters (Sig_W,
583   Rain_Frac, and BC_RI) each cause only a small amount (around 3%) of the variance.

584

585   **3.3   Sources of uncertainty in ToA radiative flux**

586   Identifying the sources of ToA reflected shortwave radiation (RSR) uncertainty will inform our understanding of how radiative
587   flux measurements can help to constrain the aerosol ERF uncertainty (Lohmann and Ferrachat, 2010) because the aerosol ERF
588   is essentially the aerosol-forced change in RSR between the pre-industrial (or 1978) and present-day atmospheres (plus addi-
589   tional small changes in outgoing long-wave radiation). The causes of present-day ToA RSR variance are summarised in Fig. 7
590   and are very similar in the pre-industrial and 1978 atmospheres (not shown).

591

592   The dominant source of ToA RSR uncertainty is the cloud radiation parameter Rad_Mcica_Sigma, which was also the
593   dominant parameter for the pre-industrial to present-day aerosol ERF. Uncertainty in this parameter alone causes over 60% of
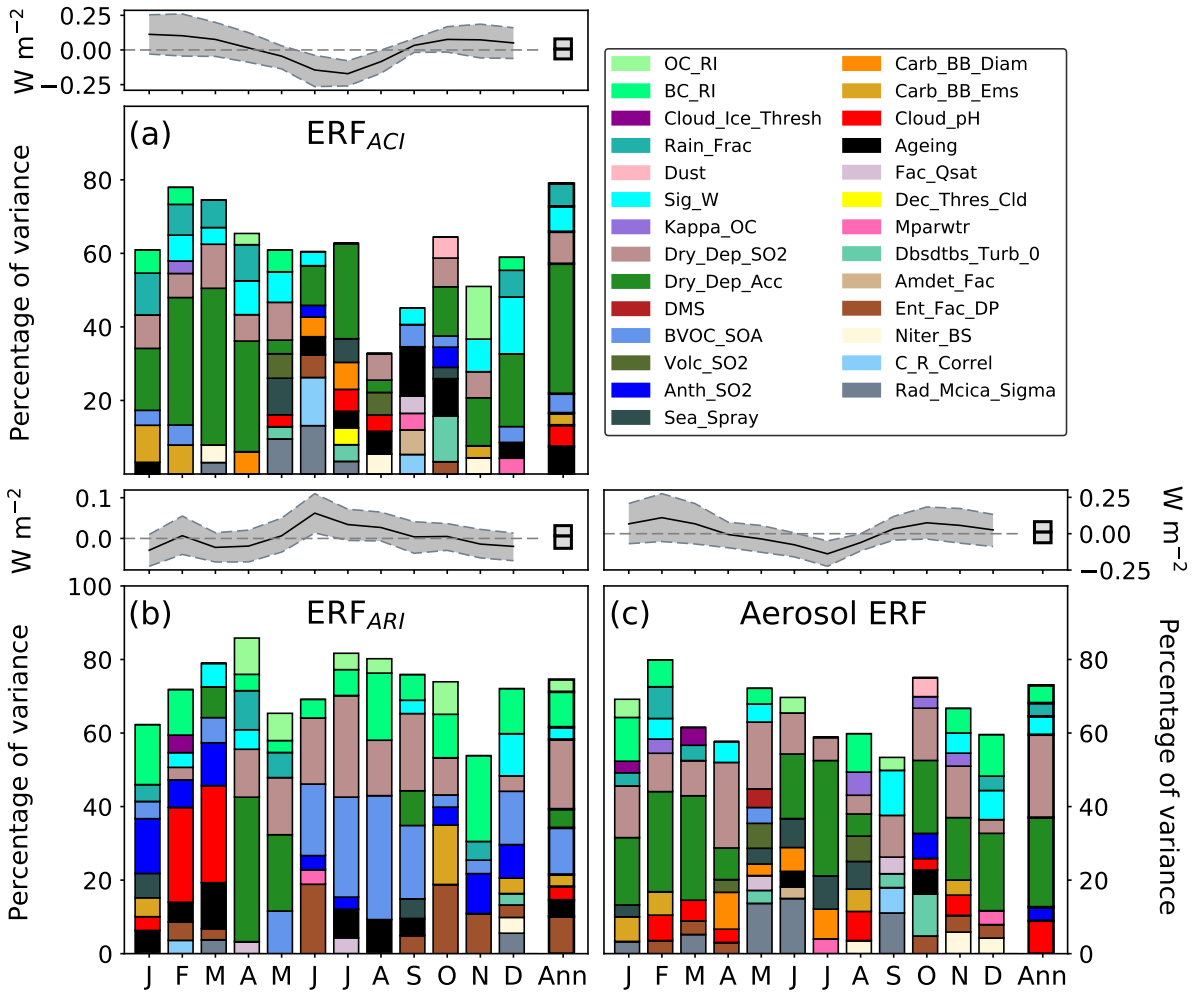
Figure 6. Percentage contributions to variance in 1978-2008 global, monthly and annual mean (a) ERF_{ACI}, (b) ERF_{ARI} and (c) aerosol ERF. Figure features are identical to Fig. 4.

594 the RSR variance by altering the total cloud albedo. The dominant role of this cloud radiative parameter in causing uncertainty

595 in the ToA radiative flux and aerosol ERF suggests that constraining this parameter to a very narrow range should constrain the

596 uncertainty in radiative fluxes (Haerter et al., 2009; Lohmann and Ferrachat, 2010) and consequentially in aerosol ERF (Lee

597 et al., 2016). But of course, there are a number of other parameters (Dbsdtbs_Turb_0, Ent_Fac_DP, Sig_W and C_R_Correl)

598 that cause ToA RSR uncertainty by altering the amount and/or albedo of clouds in the model. The mechanisms for altering

599 cloudiness and therefore the ToA radiative flux are different for each parameter. The Dbsdtbs_Turb_0 parameter causes around

600 10% of the ToA RSR variance by altering the mixing rate of clean and cloudy air masses. Increasing the proportion of dry

601 air in clouds has a dramatic effect on the amount of low-altitude cloud simulated in the model, making Dbsdtbs_Turb_0 the
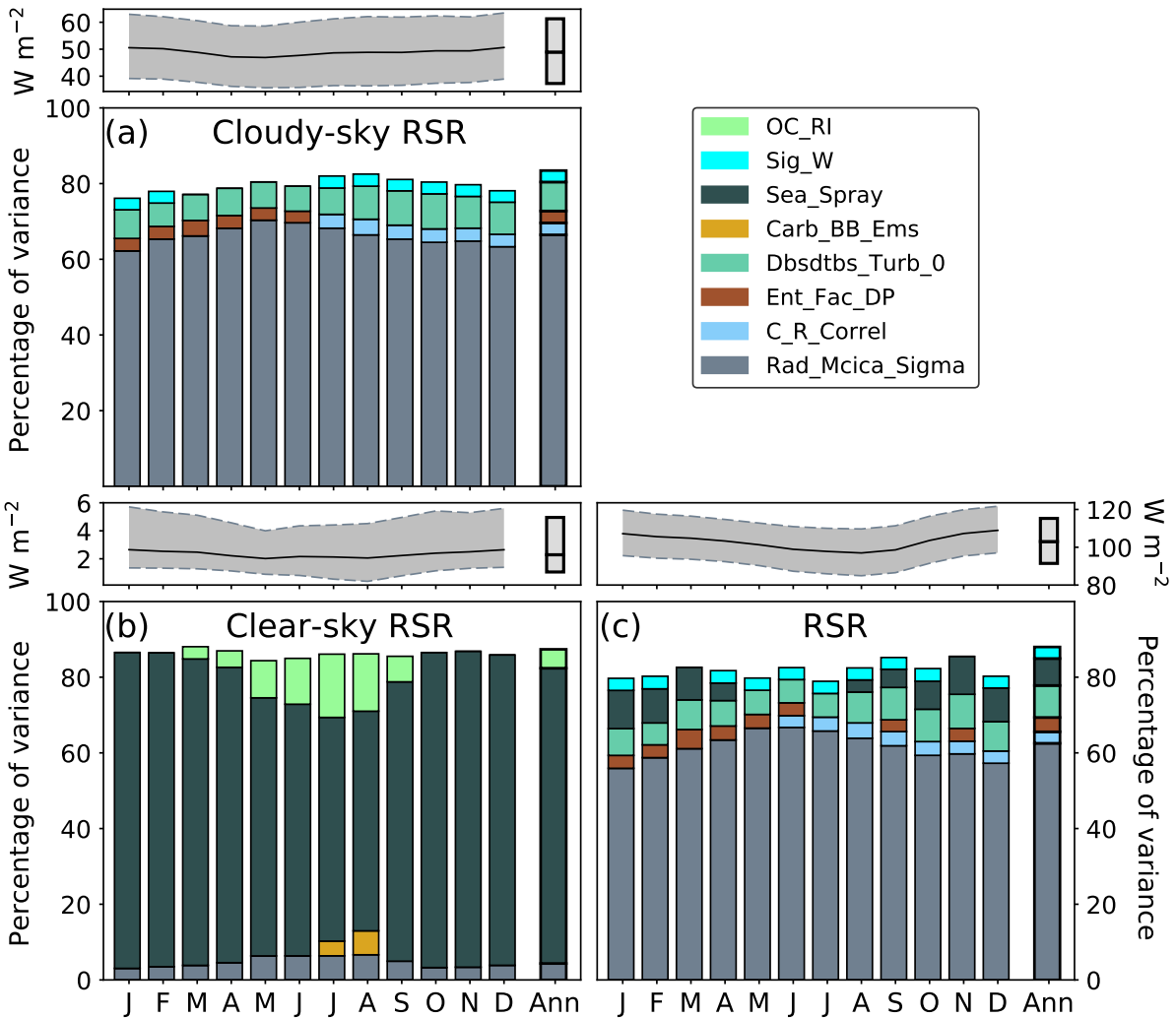
Figure 7. Percentage contributions to variance in present-day (2008) global, monthly and annual mean ToA (a) cloudy-sky RSR, (b) clear-sky RSR and (c) RSR. Figure features are identical to Fig. 4.

602   dominant cause of uncertainty in low-altitude cloud-fraction (Fig. 8). The Ent_Fac_Dp, Sig_W and C_R_Correl parameters

603   each cause around 5% of the RSR variance. The Ent_Fac_Dp parameter affects the strength of convection which also alters

604   precipitation rates and the vertical distribution of simulated clouds. Sig_W controls the activation of cloud condensation nuclei

605   into cloud droplets (affecting droplet effective radius and cloud albedo) and C_R_Correl alters the rate of cloud droplet accre-

606   tion by precipitating rain drops. The only parameter to cause ToA RSR variance (around 10%) by directly altering atmospheric
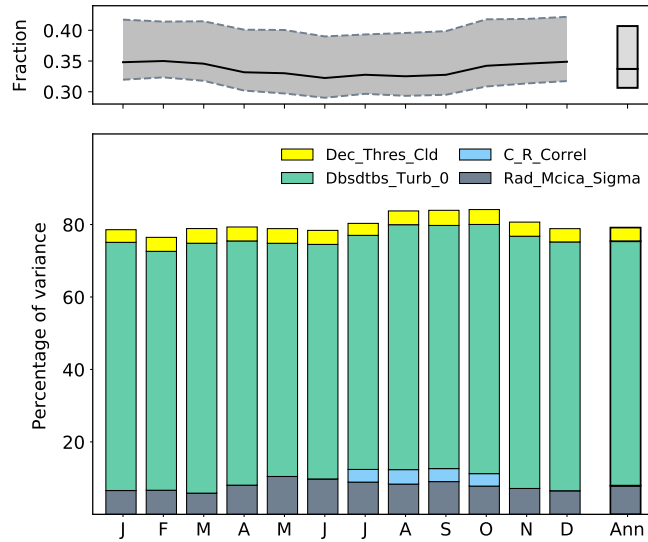
607   aerosol concentrations is Sea_Spray.

608

Figure 8. Percentage contributions to variance in present-day (2008) global, monthly and annual mean low altitude cloud amount. Figure features are identical to Fig. 4.

Figure 9 summarises the relative contributions of atmospheric and aerosol parameters to uncertainty in global mean values of present-day ToA RSR (from Fig. 7) and aerosol ERFs over the periods 1978-2008 (Fig. 6) and 1850-2008 (Fig. 4). Atmospheric parameters cause the majority (around 80%) of the variance in present-day ToA radiative flux, but only around 30% of the variance in 1850-PD aerosol ERF, and less than 10% of the 1978-PD aerosol ERF variance. The rest of the uncertainty is attributable to the aerosol model. This disparity arises because contributions to variance in aerosol ERF depend on how parameters influence the atmosphere's response to the *change* in anthropogenic emissions, while RSR variance depends on how they influence the *state* of the atmosphere.
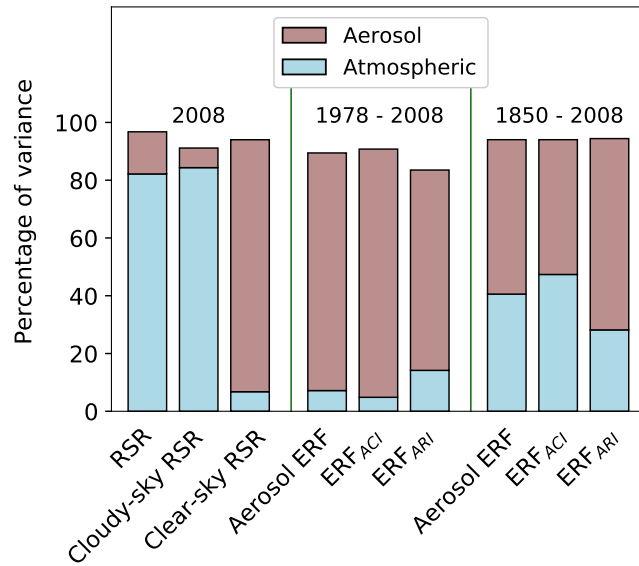
Figure 9. The relative contributions from atmospheric and aerosol parameters to variance in ToA radiative fluxes and aerosol effective radiative forcing over the 1978-2008 and 1850-2008 periods.

3.4 Identifying the sources of uncertainty at the regional level

3.4.1 Regional sources of uncertainty

Regional forcings can be important drivers of global and regional climate change (Chalmers et al., 2012; Booth et al., 2012; Bollasina et al., 2013; Shindell et al., 2013; Kirtman et al., 2013; Villarini and Vecchi, 2013; Allen et al., 2014). Furthermore, important sources of aerosol forcing uncertainty may be overlooked if regional sensitivity analysis results are neglected (Regayre et al., 2015). Examining how these sources of regional forcing uncertainty combine to cause uncertainty in global mean forcing uncertainty will inform our understanding of how to best observationally constrain the uncertainty. We identified regions of substantial aerosol ERF (ensemble mean stronger than around -2.5 $W\,m^{-2}$) for more in-depth analysis (Table A3 and Fig. 10). Emulators of regional-mean aerosol ERFs and its components were created so that the key causes of variance in each region could be identified (Fig. 11).
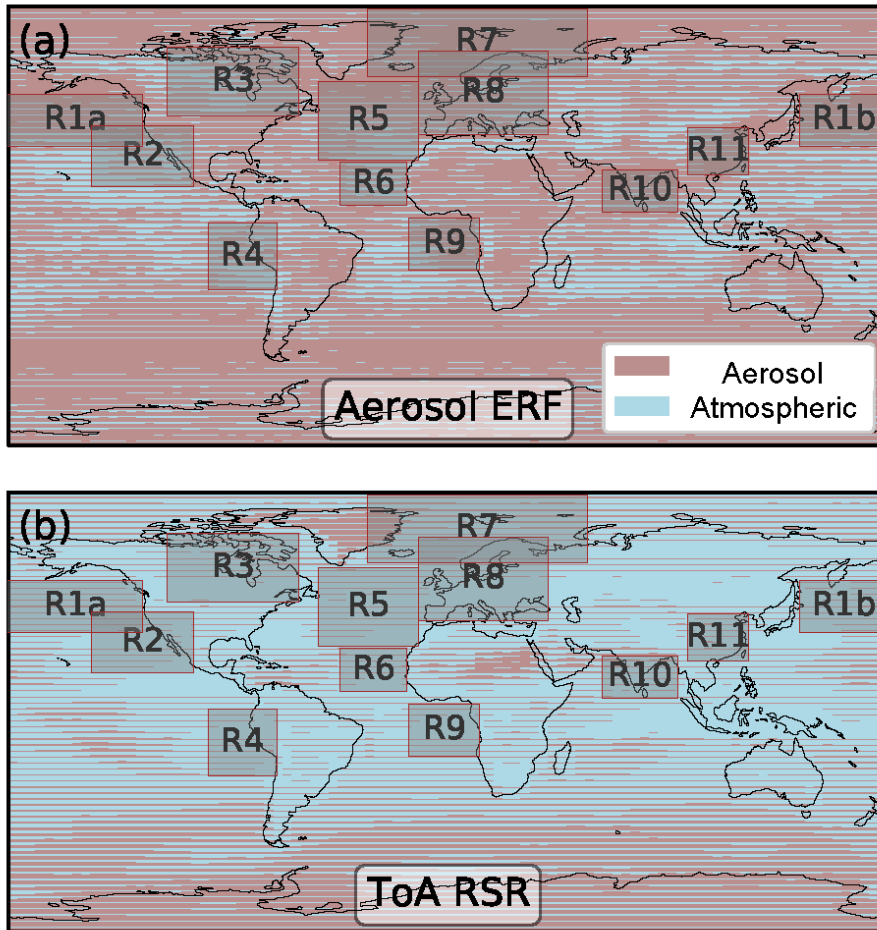
Figure 10. Maps of contributions to variance in (a) 1850-2008 aerosol ERF and (b) present-day (2008) ToA RSR from atmospheric and aerosol parameters. Each pixel contains a box that is shaded in proportion to the amount of variance caused by each source of uncertainty.
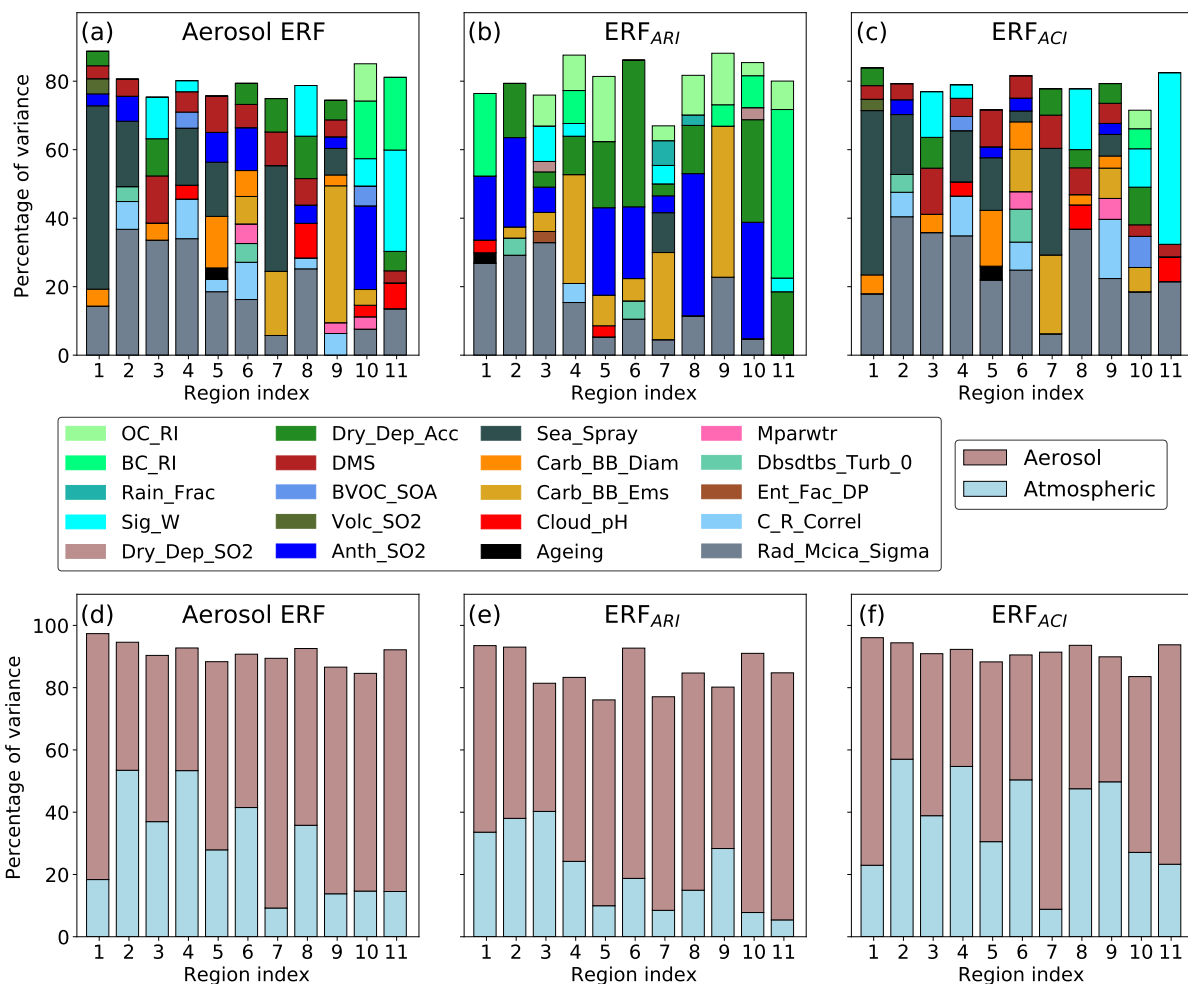
Figure 11. Sources of variance ((a), (b) and (c)) and grouped atmospheric and aerosol contributions to variance ((d), (e) and (f)) for 1850-2008 annual mean (a),(d) aerosol ERF, (b),(e) ERF$_{ARI}$ and (c),(f) ERF$_{ACI}$ for the 11 regions defined in table A3 and highlighted in Fig. 10.

628   The main causes of regional aerosol ERF uncertainty are often those parameters that cause global mean uncertainty. How-
629 ever, there are substantial differences between regions. Some parameters are important causes of global mean aerosol ERF
630 uncertainty because they cause a small amount (at least 5%) of the uncertainty in nearly all regions. For example, the DMS
631 parameter causes around 5% of the aerosol ERF variance in most regions and consequentially causes around 15% of the global
632 mean variance. The cloud radiation parameter Rad_Mcica_Sigma (which causes nearly 30% of the industrial-period aerosol
633 ERF variance) also causes aerosol ERF variance in most regions. But, the amount of regional aerosol ERF variance accounted
634 for by this parameter ranges from less than 3% (R9) to around 35% (R2, R3, R4).

635

636   Other parameters are important causes of global mean aerosol ERF uncertainty despite being important causes of uncertainty

637   in only around half of the regions examined. For example, the Sea_Spray parameter (which causes nearly 20% of the global

638   mean aerosol ERF variance) is by far the largest source (around 60%) of aerosol ERF variance in the North Pacific (R1) and

639   causes between 10 and 30% of the variance in several other marine regions. However, in tropical marine regions (R6 and R10)

640   and regions containing continental land mass (R3, R8 and R11) Sea_Spray causes less than 3% of the aerosol ERF variance.

641   The land-based regions (R3, R8, R11) are also where the cloud updraft parameter Sig_W causes aerosol ERF variance. The

642   importance of Sig_W over continents suggests cloud albedo is most sensitive to uncertainty in updraft velocity in the most-

643   polluted regions where cloud droplet concentrations are updraft-limited (Reutter et al., 2009; Sullivan et al., 2016).

644

645   Anth_SO2 makes its greatest contribution to aerosol ERF uncertainty in tropical marine regions (R6 and R10) by causing

646   uncertainty in ERF_{ARI}. The Anth_SO2 parameter also causes up to 40% of the ERF_{ARI} variance near anthropogenic sources

647   (R3 and R8) and up to 30% in outflow regions (R1, R2, R5). However, these substantial causes of ERF_{ARI} variance translate

648   into small (less than 10%) causes of aerosol ERF variance in most regions. The aerosol deposition parameter (Dry_Dep_Acc)

649   also causes more of the regional ERF_{ARI} variance (up to 45%) than regional aerosol ERF variance (less than 15%). However,

650   despite being an important cause of 1850-2008 aerosol ERF uncertainty in several regions, the dry deposition parameter is not

651   an important cause of global mean aerosol ERF uncertainty over this period (Fig. 4(c)).

652

653   The importance of carbonaceous aerosol parameters (Carb_BB_Ems, Carb_BB_Diam, BC_RI and OC_RI) as causes of

654   aerosol ERF uncertainty are highly region dependent. Uncertainty in the emission flux of carbonaceous aerosols Carb_BB_Ems

655   causes between 25 and 45% of the ERF_{ARI} variance in and near biomass burning regions (R4, R7 and R9). However, this only

656   translates into a cause of aerosol ERF uncertainty in regions R7 and R9 where the Carb_BB_Ems parameter also causes uncer-

657   tainty in ERF_{ACI} . Uncertainty in the size of emitted carbonaceous absorbing aerosols (Carb_BB_Diam) is more important as

658   a cause of uncertainty in ERF_{ACI} than in ERF_{ARI} because it determines the capacity for carbonaceous aerosols to act as cloud

659   condensation nuclei. Therefore, Carb_BB_Diam predominantly causes aerosol ERF variance (up to 15%) in the cloudiest

660   regions (R1, R5, R6 and R9). Uncertainty in the radiative properties of carbonaceous aerosols (BC_RI and OC_RI) collec-

661   tively cause ERF_{ARI} variance in almost all regions. However, uncertainty in aerosol ERF is affected by these parameters only

662   over China (R11) and near to India (R10). Over China the anthropogenic emission parameter (Anth_SO2) is surpassed by the

663   BC_RI and OC_RI parameters as causes of ERF_{ARI} and aerosol ERF uncertainty, despite carbonaceous aerosols making up

664   a relatively small proportion of aerosol emissions in these regions (Granier et al., 2011). The BC_RI parameter causes around

665   50% of the ERF_{ARI} variance and around 25% of the variance in aerosol ERF in China. However, anthropogenic emissions

666   do cause uncertainty in ERF_{ARI} and aerosol ERF in the Pacific (an outflow region for Chinese emissions). Near India, uncer-

667   tainty in BC_RI and OC_RI cause around 30% and 10% of the aerosol ERF variance respectively and cause a smaller amount

668   (between 5 and 10%) of variance in each of the forcing components. Despite being important sources of forcing uncertainty at

669   the regional level, Carb_BB_Diam is the only parameter related to carbonaceous aerosols which causes uncertainty in global,

670   annual mean aerosol ERF.

671

672   Figure 11 (d)-(f) shows that atmospheric parameters combined can cause up to around 50% of the regional aerosol ERF vari-
673   ance despite causing only around 30% of the global mean aerosol ERF variance. However, there are multiple regions where
674   uncertainty in the physical atmosphere parameters causes less than 20% of the aerosol ERF variance. Where atmospheric pa-
675   rameters are an important source of regional aerosol ERF uncertainty, the Rad_Mcica_Sigma parameter is almost always the
676   most important. On its own uncertainty in Rad_Mcica_Sigma causes over 20% of the aerosol ERF variance in coastal Pacific
677   regions (R2 and R4) as well as continental regions (R3 and R8). The atmospheric parameter controlling the accretion rate
678   of aerosols by rain drops (C_R_Correl) causes around 10% of the aerosol ERF variance in several tropical or sub-tropical
679   regions off the western coast of continents (R2, R4, R6 and R9). These are all regions of persistent stratocumulus cloud where
680   cloud albedo is highly susceptible to changes in aerosol concentrations and size distributions. The clear- and cloudy- air mix-
681   ing parameter Dbsdtbs_Turb_0 causes between 5 to 10% of the variance in aerosol ERF and its components in the Northern
682   Hemisphere regions of persistent stratocumulus cloud (R2 and R6) but not in Southern Hemisphere regions (R4 and R9). This
683   suggests that the relatively polluted Northern Hemisphere stratocumulus clouds are more sensitive to the sub-grid mixing of
684   clear- and cloudy air masses. In tropical regions (R6, R9 and R10) the convective parameter Mparwtr causes a small amount
685   (3 to 5%) of the aerosol ERF variance. This parameter alters the timing of precipitation and therefore affects cloud and aerosol
686   amount, and the ERF_{ACI} near the equator where convective instability and precipitation are greatest. The regions where phys-
687   ical atmosphere parameters cause the least aerosol ERF variance are either near to anthropogenic emission sources (R9, R10
688   and R11) or downwind of them (R1 and R7).

689

690   These results show that the relative importance of individual parameters as sources of uncertainty differ between regions.
691   However, the most important causes of global mean aerosol ERF uncertainty also cause uncertainty at the regional level.

692

693   **3.5   Observational constraint of the aerosol ERF uncertainty**

694   **3.5.1   Effect of ToA RSR constraint on aerosol ERF uncertainty**

695   We now explore the extent to which present-day measurements of global mean ToA RSR could in principle help to constrain
696   the change in flux between two time periods (the aerosol ERF), which was previously explored by Lohmann and Ferrachat
697   (2010) who perturbed four physical atmosphere parameters. We expect some constraint of aerosol ERF uncertainty based on
698   the common causes of uncertainty in ToA RSR and aerosol ERF. Observational constraint of a model output variable can lead
699   to constraint of the uncertain parameters. Therefore, when two model output variables share common causes of uncertainty
700   we can expect that constraint of one output will lead to constraint of the other. Our approach of drawing large samples of one
701   million parameter combinations from model emulators (using uniform pdfs for each parameter; Section 2.3) enables this link
702   through the uncertain parameters to be understood, which is not possible just from a perturbed parameter ensemble alone (e.g.

703 Lohmann and Ferrachat, 2010).

704

705   Our analysis reveals substantial overlap in the combinations of parameters causing uncertainty in 1850-2008 aerosol ERF
706 and present-day ToA RSR. The parameters Rad_Mcica_Sigma, Sea_Spray, C_R_Correl and Sig_W account for about 60%
707 of the aerosol ERF uncertainty and about 80% of the ToA flux uncertainty. It is important to note that it is irrelevant for
708 the observational constraint process that the ToA flux is much larger than the aerosol ERF. The important factor is that their
709 uncertainties are caused by common uncertain parameters, so constraint of one of them will constrain the other through the
710 constraint of the plausible parameter ranges and relationships.

711

712   Figure 12 shows the effect of constraining the modelled present-day global, annual mean RSR to within $\pm 0.25 \mathrm{W m^{-2}}$ of
713 98.3 $\mathrm{W m^{-2}}$, the multi-year average of observations from the Clouds and the Earth's Radiant Energy System (CERES; Loeb
714 et al., 2009). The $\pm 0.25 \mathrm{W m^{-2}}$ represents within-CERES product uncertainty (Loeb et al., 2012) and neglects multiple other
715 sources of satellite observational uncertainty (Loeb et al., 2009; Hartmann et al., 2013). We also neglect uncertainty caused by
716 unknown model structural errors (Goldstein and Rougier, 2004; Sexton et al., 2012; Stier et al., 2013), observation represen-
717 tativeness errors (Schutgens et al., 2017) and the emulators themselves (Oakley and O'Hagan, 2004) which are of the same
718 order of magnitude as the observational uncertainty. Therefore, our RSR observational constraint provides an upper bound on
719 the potential reduction in aerosol ERF uncertainty. This tight constraint eliminates 97% of the model variants and the obser-
720 vationally constrained RSR range is less than 2% of the original unconstrained range. Consequently, the smaller set of model
721 variants also predicts reasonably constrained 1978 and 1850 RSR ranges (Fig. 12(a)). However, despite reducing the plausible
722 parameter space by 97% and the RSR range by 98% the impact on the aerosol ERF uncertainty is more modest (Fig. 12(b) and
723 (c)). The effect of applying the RSR observational constraint is to rule out 1850-2008 aerosol ERF values lower than around
724 -2.4 $\mathrm{W m^{-2}}$, which represents around 15% of the original aerosol ERF range (-2.7, -0.7 $\mathrm{W m^{-2}}$). However, the 95% credible
725 range is only reduced by around 10% because the distribution of aerosol ERFs in the constrained sample is skewed towards
726 weaker forcings and the upper bound of the credible interval (-0.6 $\mathrm{W m^{-2}}$) is larger (Table A4). This reduction in aerosol ERF
727 range is much less than the 56% reduction found by Lohmann and Ferrachat (2010) based on a set of 169 perturbed parameter
728 simulations (compared to our one million model variants). We discuss the reasons for this modest reduction in aerosol ERF
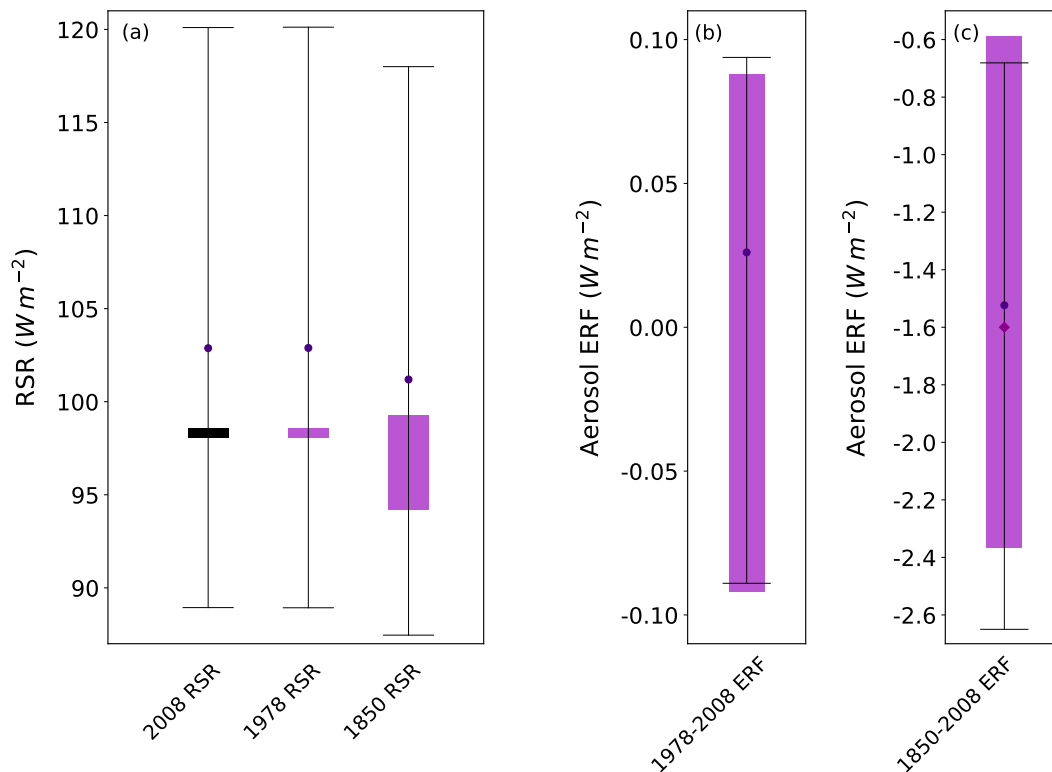729 uncertainty in sections 3.5.2 and 3.5.3.

730

Figure 12. (a) Observationally constrained present-day ToA RSR and the values of 1978 and 1850 ToA RSR and (b) 1978-2008 and (c) 1850-2008 aerosol ERF values from matching model variants. For each output variable the black lines show 95% credible intervals of the unconstrained one million member sample of model variants. The black box contains all model variants within $\pm 0.25 \mathrm{W\,m^{-2}}$ of the CERES-observed global annual mean present-day ToA RSR value. Purple boxes represent the 95% credible intervals of values obtained using model variants (parameter combinations) in the observationally constrained sample. The middle and right-hand axes are for 1978-2008 and 1850-2008 aerosol ERF respectively. Output from the simulation with all parameters set to their median values are shown as dots. The median 1850-2008 aerosol ERF from the observationally constrained sample is displayed as a diamond.

3.5.2 Constraining the relationships between the aerosol ERF and uncertain parameters

Fig. 13 shows how aerosol ERF is related to the values of the four main causes of aerosol ERF uncertainty before and after applying the observational constraint. There are clear relationships between the aerosol ERF and the individual parameters, but they are highly uncertain (even in the constrained sample) because there are many compensating errors among the other parameters (i.e., many ways to combine the parameters to get the same ToA RSR but very different aerosol ERF; Fig. 12). This diversity of credible model variants would be overlooked had we perturbed parameters individually, as is the case with one-at-a-time perturbation experiments (e.g. Gettleman, 2015).
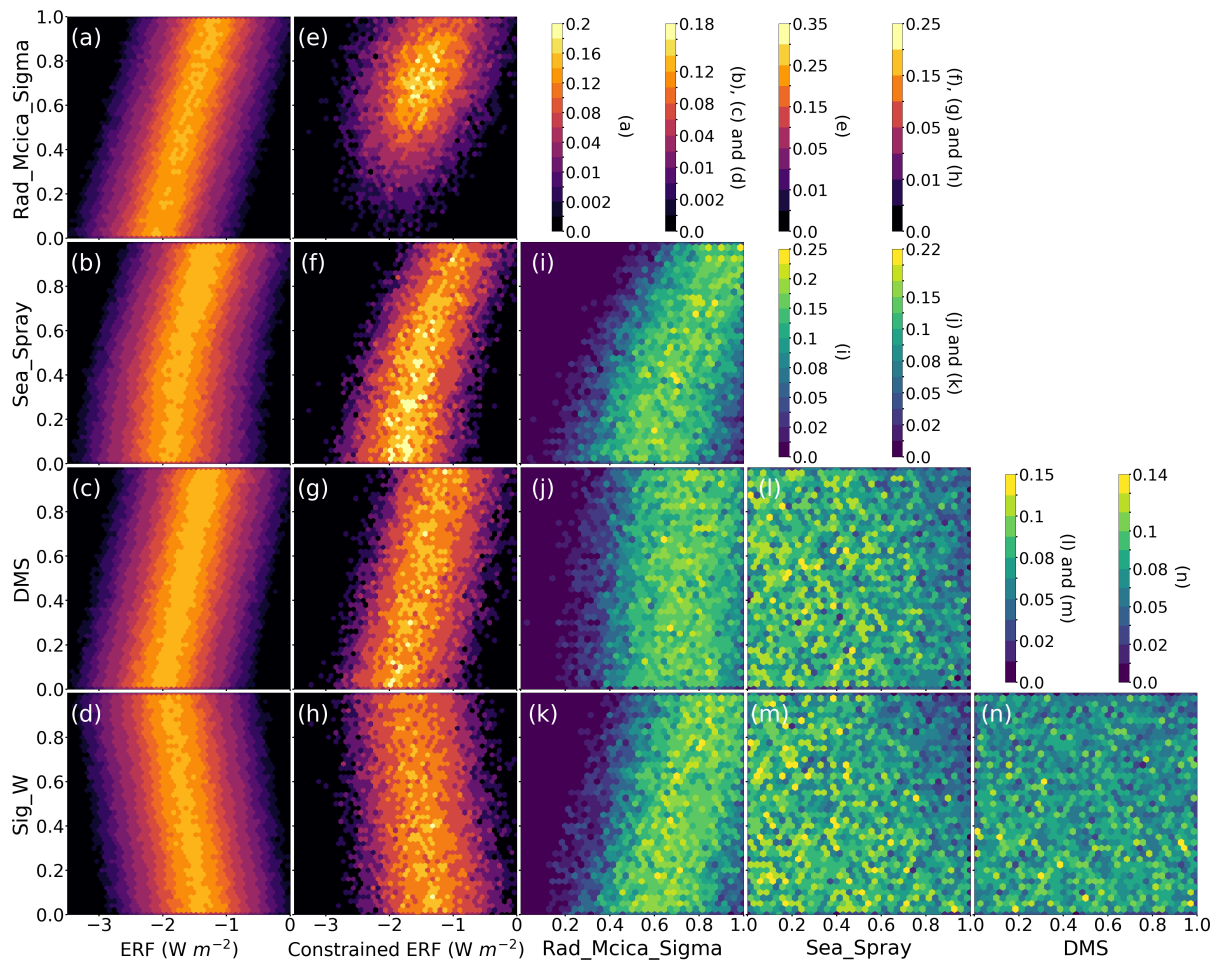
31

Figure 13. Probability density distributions of aerosol ERF and the parameters Rad_Mcica_Sigma, Sea_Spray, DMS, Sig_W in the uncon-strained sample (first column; (a)-(d)) and in the sample constrained to match the observed global annual mean RSR (second column; (e)-(h)). Probability density distributions of parameter values are shown for the constrained sample ((i)-(n)). Colour bars labelled (a)-(n) correspond with the sub-figures and show the percentage of each sample within each pixel. Some colour bars apply to multiple panels.

739   For each of the one million model variants in our unconstrained sample individual parameter values were drawn from uni-
740   form distributions with ranges defined by the expert elicited pdfs. Therefore, prior to applying the observational constraint the
741   model variants were evenly dispersed across every two-dimensional parameter subspace. We are therefore able to quantify the
742   effect of the observational constraint on the plausibility of individual and combined parameter values.

743

744   The cloud radiation parameter Rad_Mcica_Sigma is negatively correlated with the ToA radiative flux and this leads to a pos-
745   itive correlation with aerosol ERF: Increasing its value decreases the simulated cloud albedo and hence the ToA RSR. But, ToA
746   RSR is more sensitive to Rad_Mcica_Sigma in the present-day atmosphere than in the pre-industrial (because higher aerosol

32

747 concentrations increase the cloud albedo), so increasing the parameter value weakens the aerosol ERF. Figure 13 shows that
748 low values of Rad_Mcica_Sigma (less than around 0.4 in the scaled range 0 to 1) are inconsistent with the observed RSR. The
749 proportion of model variants with Rad_Mcica_Sigma values less than 0.4 drops from 40% in the unconstrained sample to just
750 8% in the constrained case. In other words, the observational constraint suggests the plausible lower limit of this parameter is
751 higher than we assumed in our expert elicitation. We can therefore state that the strongest aerosol ERFs are also implausible
752 (as shown in Fig. 12) because they are associated with low values of Rad_Mcica_Sigma.
753
754   Figure 13 also shows that the aerosol ERF is weaker for larger Sea_Spray and DMS values. An abundance of natural
755 aerosols increases background (pre-industrial) atmospheric aerosol concentrations and limits the influence of anthropogenic
756 aerosol emissions on clouds and radiation (Carslaw et al., 2013). Figure 13 shows that the observed ToA radiative flux is more
757 consistent with low emissions of natural aerosols (the density of Sea_Spray values larger than 0.5 decreases from 50% to
758 44% after constraint of the ToA flux). The decreased likelihood of higher natural aerosol emissions in the constrained sample
759 suggests that the weakest aerosol ERF values are less congruent with observed ToA RSR. However, there remain many obser-
760 vationally plausible model variants with high natural aerosol emissions.
761
762   The largest values of the cloud updraft parameter (Sig_W) are also less plausible in the constrained sample (Fig. 13; 27%
763 of the sample are larger than 0.7, instead of 30%). This suggests that present-day RSR observations are more consistent with
764 lower vertical velocities, but the largest values cannot be ruled out completely because of the way that other compensating
765 parameters affect RSR. Lower values of Sig_W weaken the aerosol ERF by reducing cloud droplet concentrations primarily
766 in the present-day polluted atmosphere, because cloud droplet activation is more sensitive to Sig_W in the present-day atmo-
767 sphere than in the aerosol-limited pre-industrial atmosphere. Therefore, observational constraint of ToA radiative flux reduces
768 the likelihood of weak aerosol ERFs through a constraint of the distribution of Sig_W values.
769

3.5.3   Constraining the relationships between uncertain parameters

771 Fig. 13 also shows the important parameter inter-dependencies revealed by observationally constraining the ToA radiative flux.
772 The Rad_Mcica_Sigma and Sea_Spray parameters are positively correlated in the observationally constrained sample. For
773 example, a modelled ToA RSR consistent with observations can be achieved using high values of Rad_Mcica_Sigma (which
774 decreases cloud albedo) and relatively high values of Sea_Spray (which increases cloud albedo). In other words, these param-
775 eters have compensating effects on the ToA radiative flux. The same compensation applies to the aerosol ERF: the weakest
776 ERFs in our pdf (larger than around -1 $\mathrm{W\,m^{-2}}$) are associated with high Rad_Mcica_Sigma and high Sea_Spray values. How-
777 ever, the RSR and aerosol ERF depend on these two parameters in quite different ways. Higher Rad_Mcica_Sigma values
778 *weaken* the aerosol ERF by *reducing* the present-day ToA RSR, whilst higher Sea_Spray values *weaken* the aerosol ERF by
779 *increasing* present-day RSR. Hence, constraining the relationship between the two largest sources of aerosol ERF uncertainty

780   using observations of present-day RSR has not drastically reduced the aerosol ERF uncertainty.

782   The cloud droplet activation parameter (Sig_W) is also positively correlated with Rad_Mcica_Sigma in the observationally
783   constrained sample (Fig. 13). As with sea spray emissions, higher values of Sig_W increase cloud albedo and compensate
784   for the effect of high Rad_Mcica_Sigma values on ToA RSR. These parameters both exert a greater influence on present-
785   day cloud radiative properties; in the case of Sig_W, cloud radiative properties are more susceptible to this parameter in the
786   present-day simulations because cloud droplet activation is more likely to be updraft-limited (rather than aerosol-limited) in
787   an anthropogenically-polluted atmosphere. Therefore, in contrast to the Sea_Spray and Rad_Mcica_Sigma relationship, the
788   Sig_W and Rad_Mcica_Sigma parameters have additive (not compensating) effects on aerosol ERF. Parameters with additive
789   effects on the aerosol ERF are more susceptible to the effects of model equifinality. Therefore, the relationship between aerosol
790   ERF and Sea_Spray is better constrained than the relationship between aerosol ERF and Sig_W.

792   The Sig_W and Sea_Spray parameters both act to counter the effect of Rad_Mcica_Sigma on cloud albedo in the con-
793   strained sample. Therefore, the density of model variants with simultaneously large (above around 0.6) Sig_W and Sea_Spray
794   values is lower in the constrained sample (down from 16% to 11%). No such restrictions apply to simultaneously small values
795   (less than 0.4) of these two parameters. In fact the proportion of simultaneously small Sig_W and Sea_Spray in the sample
796   increases from 16% to 19% after applying the constraint which rules out other parts of parameter space. This suggests that in
797   simulations with low natural aerosol emissions and low cloud droplet activation efficiency, there are multiple other contributing
798   factors keeping the ToA RSR in agreement with observations. For example, by limiting the mixing rates of clear and cloudy air
799   masses, a low value of the Dbsdtbs_Turb_0 parameter (an important source of ToA RSR uncertainty) can compensate for the
800   decrease in cloud droplet concentrations caused by a low value of the cloud droplet activation parameter. A replacement source
801   of aerosols large enough to act as cloud condensation nuclei is also required to compensate for low natural aerosol emissions.
802   There are multiple ways in which this could be achieved. For example, a low value of the dry deposition velocity parameter
803   Dry_Dep_Acc (known to be important for cloud active aerosol concentrations; Lee et al., 2013) increases the atmospheric
804   lifetime of aerosols, allowing them to grow in size and activate to form cloud droplets, even in a low activation efficiency
805   simulations.

807   The DMS parameter has no obvious relationships with the other main sources of aerosol ERF uncertainty in the constrained
808   sample. This is despite DMS affecting aerosol ERF in the same regions as other key parameters and causing aerosol ERF
809   uncertainty through a similar mechanism to Sea_Spray. In other words, higher values of DMS and Sea_Spray suppress the
810   aerosol ERF by increasing background (1850) aerosol concentrations. Therefore, the value of the DMS parameter is more
811   likely (54% of the time) to be small (lower than 0.5) when the value of Sea_Spray is high (above 0.8). In summary, model
812   variants with high values of both of the important natural aerosol emission parameters are less likely to be consistent with the
813   observed ToA RSR.

815 These results highlight the importance of understanding the potential causes of equifinality when interpreting results from
816 such a complex model (Beven and Freer, 2001). Reducing the remaining uncertainty in global mean aerosol ERF will require
817 observations which further constrain the relationships between aerosol ERF and the key sources of uncertainty.
818

3.5.4 Regional constraint of global mean aerosol ERF uncertainty

820 Our overall aim is to constrain the uncertainty in global annual mean aerosol ERF because the total ERF is commonly used to
821 quantify the multi-model diversity in historically forced changes to the climate (Myhre et al., 2013; pp 661). However, regional
822 variations in aerosol forcing can be important drivers of climate variability (Chalmers et al., 2012; Booth et al., 2012; Bollasina
823 et al., 2013; Shindell et al., 2013; Kirtman et al., 2013) and can contribute to global mean forcing uncertainty in complex
824 ways (Regayre et al., 2015). Therefore we now use satellite observations of the North Pacific (region R1; latitude 32N-54N;
825 longitude 125W-144E; the largest regional contribution to global mean aerosol ERF) ToA RSR from July to further constrain
826 annual, global mean aerosol ERF uncertainty.
827

828 The regionally averaged CERES observed ToA RSR is 162.8 $\mathrm{W\,m^{-2}}$ (CERES, 2017) with an estimated uncertainty of $\pm 2\%$
829 (Hartmann et al., 2013, 2.3.1, pp 181). The original sample of one million model variants is reduced to around 10% by apply-
830 ing the North Pacific July mean RSR constraint and to just 0.5% of the original sample by applying both the global mean and
831 North Pacific constraints together (Table A4). In combination with the global mean observation, the North Pacific RSR con-
832 straint has little additional effect on the credible forcing ranges (-2.30 to -0.56 $\mathrm{W\,m^{-2}}$ compared to -2.37 to -0.59 $\mathrm{W\,m^{-2}}$). The
833 range of plausible aerosol ERF values has been further reduced by only around 2%. This suggests that the regional observation
834 has provided little additional constraint on the relationships between aerosol ERF and the main sources of uncertainty (Fig. S1).
835

4 Conclusions

837 We sampled the uncertainty in 18 aerosol and 9 atmospheric parameters within a single global climate model, identified the
838 important causes of aerosol ERF uncertainty and constrained this uncertainty using ToA radiative flux measurements. The
839 credible range of aerosol ERF values in our original sample of one million model variants was -2.65 to -0.68 $\mathrm{W\,m^{-2}}$ when
840 we assume the parameter values have equal likelihood of being at any point in the elicited ranges. The aerosol ERF uncer-
841 tainty decreases when we constrain global mean ToA RSR (-2.37 to -0.59 $\mathrm{W\,m^{-2}}$) and when we constrain both North Pacific
842 and global RSR (-2.30 to -0.56 $\mathrm{W\,m^{-2}}$). These results suggest that additional constraint of aerosol ERF uncertainty could be
843 achieved using multiple regional ToA flux observations. However, a greater reduction (25%) in the aerosol ERF uncertainty
844 (95% credible range, -2.18 to -0.71 $\mathrm{W\,m^{-2}}$) can be achieved by applying probability distributions to the parameters based on
845 expert elicitation (Section 3.1). These results suggest that the strongest aerosol ERF values (about 20% of the unconstrained

35

846   range) can be considered implausible based on expert opinion and observational evidence.

847

848   Our results reveal that aerosol parameters take a dominant role over atmospheric parameters as the leading cause of aerosol

849   ERF uncertainty over the industrial period and in recent decades. Atmospheric parameters cause the majority (over 80%) of the

850   uncertainty in present-day ToA reflected short-wave radiation but only around 30% of the aerosol ERF variance. A handful of

851   the aerosol and atmospheric parameters that we have examined dominate the uncertainty in global mean aerosol ERF. A cloud

852   radiation parameter, natural aerosol emissions and model process parameters that affect cloud droplet formation and removal

853   are the key sources of global mean aerosol ERF uncertainty over the industrial period. The most important causes of 1978-2008

854   aerosol ERF uncertainty are model process parameters controlling the deposition rates of aerosols and aerosol precursor gases.

855   Our analysis shows that uncertainties in aerosol parameters are of secondary importance for determining present-day ToA

856   radiative flux, but they are a much more important source (over half) of the uncertainty in the change in atmospheric radiative

857   balance (the aerosol ERF) on multi-century and multi-decadal timescales.

858

859   Uncertainty in the ERF_{ARI} component of forcing (-0.19 to 0.13 W m^{-2}) is largely caused by parameters related to car-

860   bonaceous aerosols. However, these parameters contribute little to uncertainty in the total aerosol ERF, which is dominated by

861   uncertainty in the ERF_{ACI} component of forcing (-2.20 to 0.61 W m^{-2}) in our analyses. In our simulations light-absorbing

862   aerosols heat the local atmosphere above clouds, suppress convection and affect cloud cover. However, we do not represent

863   all of the processes that determine the magnitude of carbonaceous aerosol forcing. For example, we neglect the deposition

864   of absorbing-aerosols onto high-albedo land surfaces. Therefore, despite the large uncertainties in our carbonaceous aerosol

865   parameters, our global mean ERF_{ARI} uncertainty range does not span the range of values found by Bond et al. (2013).

866

867   At the regional level, uncertainty in aerosol ERF is predominantly caused by the same parameters that cause global mean

868   aerosol ERF uncertainty. Some parameters such as the cloud radiation parameter Rad_Mcica_Sigma and the natural aerosol

869   emission parameter DMS are important for global mean aerosol ERF uncertainty because they cause at least a small amount

870   (5%) of the uncertainty in nearly all regions. Other important causes of global mean aerosol ERF uncertainty (Sea_Spray,

871   Sig_W and Anth_SO2) are amongst the largest causes of the aerosol ERF uncertainty in some regions (marine, polluted and

872   polluted-marine regions respectively) but cause very little of the uncertainty elsewhere. We show that because carbonaceous

873   aerosols only cause aerosol ERF uncertainty in high-emission months and in regions close to emission sources, most of the

874   carbonaceous aerosol parameters (with the exception of Carb_BB_Diam) are not important for global, annual mean aerosol

875   ERF uncertainty.

876

877   One important source of ERF_{ACI} uncertainty we did not include in our study is the autoconversion rate of cloud drops into

878   rain drops (Michibata and Takemura, 2015; Malavelle et al., 2017; Toll et al., 2017). Were we to include the autoconversion rate

879   as an additional source of uncertainty the credible range of aerosol ERFs would be larger. If the autoconversion rate were an

880   important cause of uncertainty in both ToA flux and aerosol ERF, the constraint on ERF uncertainty would likely be stronger.

However, if autoconversion were to affect ToA flux and aerosol ERF in different ways or to different extents then including this additional source of uncertainty may amplify the equifinality problem by introducing another important degree of freedom. The additional uncertainty from autoconversion could be constrained to a large extent using collocated observations of changes in liquid water path, cloud fraction and aerosol concentrations. We expect such observations of cloud-aerosol relationships will be particularly useful for constraining a model's ability to represent transitions between cloud regimes and we plan to test their efficacy as constraints in the next phase of our research.

A well-constrained multi-decadal historical aerosol ERF would provide more policy-relevant information on near-term temperature change than industrial-period ERF which remains challenging to constrain (Hawkins et al., 2017). Constraining recent-decadal aerosol ERF uncertainty may prove to be an easier task than constraining uncertainty in industrial-period forcing because the multi-decadal uncertainty is caused by model process parameters that could be observed directly. Global mean aerosol ERF in recent decades depends more linearly on changing anthropogenic emissions than industrial-period aerosol ERF. Therefore, the causes of aerosol ERF uncertainty in recent decades (1978-2008) are model deposition rates (model process parameters) and anthropogenic emissions, whilst the 1850-2008 aerosol ERF is most sensitive to natural aerosol emissions (which collectively cause around 63% of the aerosol contribution to ERF_{ACI} variance). The magnitude of global mean aerosol forcing on the decadal timescale depends on the combination of uncertain positive and negative regional forcings (Regayre et al. 2015; Fig. 5). Hence, projects designed to improve our understanding of the state and behaviour of aerosol-cloud-radiation interactions on regional scales and within specific cloud regimes will aid efforts to constrain global mean forcing. In summary, reducing the uncertainty in aerosol ERF will require a much deeper understanding of how the uncertainties in state variables, model parameters and the relationships between them combine at the regional and global levels in complex global climate models. We develop our understanding of the potential to constrain regional aerosol ERF uncertainty using multiple observable quantities (e.g. aerosol optical depth and aerosol concentrations) in Johnson et al. (2018).

Climate models are routinely tuned to match present-day ToA radiative fluxes (in conjunction with multiple other observational metrics) so as to ensure accurate characterisation of the state of the atmosphere (Kay et al., 2012; Mauritsen et al., 2012; Flato et al., 2013; Hourdin et al., 2017). Our sensitivity analysis shows that the ToA radiative flux and the 1850-2008 aerosol ERF share common sources of uncertainty. Therefore, observational constraint of ToA flux representing just 0.5% of the model's prior range has reduced the 95th percent credible interval of our simulated global mean aerosol ERF by around 10%. These results counter the belief that observations of ToA reflected short-wave radiation should not constrain the aerosol ERF (because RSR values are two orders of magnitude larger than the aerosol ERF). However, comprehensively sampling model uncertainty provides a densely populated multi-dimensional parameter space which connects the observed value (RSR) to the model variable of interest (the aerosol ERF). The RSR observation constrains the parameter space and in doing so constrains the aerosol ERF uncertainty. However, we caution that the constraint will only be robust if all relevant parameters affecting RSR have been explored.

Our results show that the plausible ranges of individual parameters as well as the relationships between them are constrained by present-day observations, thereby substantially reducing the model parameter space that can be considered observationally plausible. We use RSR observations with a small observational uncertainty to demonstrate their potential use as a constraint on aerosol ERF uncertainty. However, despite a very large reduction in plausible parameter space, the effectiveness of the observational constraint is modest because it is hampered by compensating effects between multiple uncertain parameters, which results in multiple equally plausible solutions (sometimes referred to as 'equifinality'; Beven and Freer 2001; Lee et al. 2016). The challenge now is to find optimum combinations of constraints that overcome this problem using a more robust framework that accounts for all quantifiable sources of uncertainty (Sexton et al., 2012; Williamson et al., 2013). For aerosol ERF this means simultaneously constraining aerosols, clouds, and radiation *state* variables as well as the relationships between them so as to constrain uncertainty in the *change* of state on multiple timescales.

By highlighting how different parameters and processes control the change in planetary radiative balance in a single state of the art model, our results suggest that compensating effects between groups of uncertain parameters and associated processes are one important reason why uncertainty in aerosol ERF has persisted through several generations of climate model development. Given the huge range of interacting processes and uncertainties, it is highly unlikely that single observational constraints (as employed in so-called emergent constraint studies; e.g. Cherian et al. (2014)) will enable a robust reduction in aerosol ERF uncertainty. Our results, combined with those of other studies that have comprehensively sampled model uncertainties (Calisto et al., 2014; Lee et al., 2016; Ghan et al., 2016), suggest that reducing aerosol ERF uncertainty further will require the simultaneous application of a large number of observational constraints (Sanderson, 2010; Sexton et al., 2012; Collins et al., 2012; Reddington et al., 2017) covering polluted and pristine environments (Carslaw et al., 2013; Hamilton et al., 2014) and targeting the specific processes and relationships identified here.

5 Code availability

Code can be made available upon request from the corresponding author.

6 Data availability

Data can be made available upon request from the corresponding author. The authors welcome use of the perturbed parameter ensemble for advancing climate research.

946　and J. Johnson designed the experiments. All simulations were created by L. Regayre. M. Yoshioka advised on computational aspects of the

947　ensemble creation. The screening of atmospheric parameters was conducted by L. Regayre, D. Sexton and K. Carslaw. L. Regayre and J.

948　Johnson elicited probability density functions of all aerosol parameters and K. Carslaw, N. Bellouin, K. Pringle, M. Yoshioka and L. Lee

949　participated (alongside many other experts) in the formal elicitation process.

References

Allen, R. J., Norris, J. R., and Kovilakam, M.: Influence of anthropogenic aerosols and the Pacific Decadal Oscillation on tropical belt width, Nat. Geosci., 7, 270–274, doi:10.1038/NGE02091, 2014.

Andreae, M. O., Jones, C. D., and Cox, P. M.: Strong present-day aerosol cooling implies a hot future, Nat., 435, 1187–1190, doi:doi:10.1038/nature03671, 2005.

Andrianakis, I., Vernon, I., McCreesh, N., McKinley, T. J., Oakley, J. E., Nsubuga, R. N., Goldstein, M., and White, R. G.: History matching of a complex epidemiological model of human immunodeficiency virus transmission by using variance emulation, J. R. Stat. Soc. Ser. C Appl. Stat., 66, 717–740, doi:10.1111/rssc.12198, 2017.

Barker, H. W. and Räisänen, P.: Radiative sensitivities for cloud structural properties that are unresolved by conventional GCMs, Quart. J. Roy. Meteor. Soc., 131, 3103–3122, doi:10.125/qj.04.174, 2005.

Barrett, T. J., Brattström, S., Sharma, S., Worthy, D. E. J., and Novelli, P.: The role of scavenging in the seasonal transport of black carbon and sulfate to the Arctic, Geophys. Res. Lett., 38, doi:doi:10.1029/2011GL048221, 2011.

Bellucci, A., Mariotti, A., and Gualdi, S.: The role of forcings in the Twentieth-Century North Atlantic multidecadal variability: The 1940-1975 North Atlantic cooling case study, J. Cli., 30, 7317–7337, doi:10.1175/JCLI-D-16-0301.1, 2017.

Beven, K. and Freer, J.: Equifinality, data assimilation, and uncertainty estimation in mechanistic modelling of complex environmental systems using the GLUE methodology, J. Hydrol., 249, 11–29, doi:10.1016/S0022-1694(01)00421-8, 2001.

Bollasina, M. A., Ming, Y., and Ramaswamy, V.: Earlier onset of the Indian monsoon in the late twentieth century: The role of anthropogenic aerosols, Geophys. Res. Lett., 40, 3715–3720, doi:10.1002/grl.50719, 2013.

Bond, T. C., Doherty, S. J., Fahey, D. W., Forster, P. M., Berntsen, T., DeAngelo, B. J., Flanner, M. G., Ghan, S., Kärcher, B., Koch, D., Kinne, S., Kondo, Y., Quinn, P. K., Sarofim, M. C., Schultz, M. G., Schulz, M., Venkataraman, C., Zhang, H., Zhang, S., Bellouin, N., Guttikunda, S. K., Hopke, P. K., Jacobson, M. Z., Kaiser, J. W., Klimont, Z., Lohmann, U., Schwarz, J. P., Shindell, D., Storelvmo, T., Warren, S. G., and Zender, C. S.: Bounding the role of black carbon in the climate system: A scientific assessment, J. Geo. Res. Atmos., 118, 5380–5552, doi:10.1002/jgrd.50171, 2013.

Booth, B. B. B., Dunstone, N. J., Halloran, P. R., Andrews, T., and Bellouin, N.: Aerosols implicated as a prime driver of twentieth-century North Atlantic climate variability, Nat., 484, 228–232, doi:10.1038/nature10946, 2012.

Boucher, O., Randall, D., Artaxo, P., Bretherton, C., Feingold, G., Forster, P., Kerminen, V. M., Kondo, Y., Liao, H., Lohmann, U., Rasch, P., Satheesh, S. K., Sherwood, S., Stevens, B., and Zhang, X. Y.: Clouds and Aerosols, in: Climate Change 2013: The Physical Science Basis. Contribution of Working Group I to the Fifth Assessment Report of the Intergovernmental Panel on Climate Change, edited by Stocker, T. F., Qin, D., Plattner, G. K., Tignor, M., Allen, S. K., Boschung, J., Nauels, A., Xia, Y., Bex, V., and Midgley, P. M., Cambridge University Press, Cambridge, United Kingdom and New York, USA, 2013.

Boutle, I. A., Abel, S. J., Hill, P. G., and Morcrette, C. J.: Spatial variability of liquid cloud and rain: observations and microphysical effects, Quart. J. Roy. Meteor. Soc., 140, 585–594, doi:10.1002/qj.2140, 2014.

Browse, J., Carslaw, K. S., Arnold, S. R., Pringle, K. J., and Boucher, O.: The scavenging processes controlling the seasonal cycle in Arctic sulphate and black carbon aerosol, Atmos. Chem. Phys., 12, 6775–6798, doi:10.5194/acp-12-6775-2012, 2012.

Calisto, M., Folini, D., Wild, M., and Bengtsson, L.: Cloud radiative forcing intercomparison between fully coupled CMIP5 models and CERES satellite data, Ann. Geophys., 32, 793–807, doi:10.5194/angeo-32-793-2014, 2014.

997   Carslaw, K. S., Lee, L. A., Reddington, C. L., Pringle, K. J., Rap, A., Forster, P. M., Mann, G. W., Spracklen, D. V., Woodhouse, M., Regayre,

998   L. A., and Pierce, J. R.: Large contribution of natural aerosols to uncertainty in indirect forcing, Nat., 503, 67–71, doi:10.1038/nature12674,

999   2013.

1000   Carslaw, K. S., Gordon, H., Hamilton, D. S., Johnson, J. S., Regayre, L. A., and Yoshioka, M.: Aerosols in the pre-industrial atmosphere,

1001   Curr. Clim. Change Rep., 3, 1–15, doi:10.101007/s40641-017-0061-2, 2017.

1002   Carslaw, K. S., Johnson, J. S., Regayre, L. A., and Lee, L. A.: All models are uncertain, but we can do something about it, EOS, TBC, TBC,

1003   doi:TBC, 2018.

1004   CERES: Clouds and the Earth's Radiant Energy System. **https://ceres.larc.nasa.gov/order_data.php**. Accessed: August 2017, https://ceres.

1005   larc.nasa.gov/order_data.php, 2017.

1006   Chalmers, N., Highwood, E. J., Hawkins, E., Sutton, R., and Wilcox, L. J.: Aerosol contribution to the rapid warming of near-term climate

1007   under RCP 2.6, Geophys. Res. Lett., 39, L18709, doi:10.1029/2012GL052848, 2012.

1008   Cherian, R., Quass, J., Salzmann, M., and Wild, M.: Pollution trends over Europe constrain global aerosol forcing as simulated by climate

1009   models, Geophys. Res. Lett., 41, 2176–2181, doi:10.1002/2013GL058715, 2014.

1010   Collins, M., Booth, B. B. B., Bhaskaran, B., Harris, G. R., Murphy, J. M., Sexton, D. M. H., and Webb, M. J.: Climate model errors, feedbacks

1011   and forcings: a comparison of perturbed physics and multi-model ensembles, Clim. Dyn., 36, 1737–1766, 2010.

1012   Collins, M., Chandler, R. E., Cox, P. M., Huthnance, J. M., Rougier, J., and Stephenson, D. B.: Quantifying future climate change, Nat. Clim.

1013   Ch., 2, 403–409, 2012.

1014   Collins, M., Knutti, R., Arblaster, J., Dufresne, J. L., Fichefet, D., Friedlingstein, P., Gao, X., Gutowski, W. J., Johns, T., Krinner, G.,

1015   Shongwe, M., Tebaldi, C., Weaver, A. J., and Wehner, M.: Long-term Climate Change: Projections Commitments and Irreversibility, in:

1016   Climate Change 2013: The Physical Science Basis. Contribution of Working Group I to the Fifth Assessment Report of the Intergovern-

1017   mental Panel on Climate Change, edited by Stocker, T. F., Qin, D., Plattner, G. K., Tignor, M., Allen, S. K., Boschung, J., Nauels, A., Xia,

1018   Y., Bex, V., and Midgley, P. M., Cambridge University Press, Cambridge, United Kingdom and New York, NY, USA, 2013.

1019   Croft, B., Pierce, J. R., Martin, R. V., Hoose, C., and Lohmann, U.: Uncertainty associated with convective wet removal of entrained aerosols

1020   in a global climate model, Atmos. Chem. Phys., 12, 10 725–10 748, 2012.

1021   Dunstone, N. J., Smith, D. M., Booth, B. B. B., Hermanson, L., and Eade, R.: Anthropogenic aerosol forcing of Atlantic tropical storms, Nat.

1022   Geosci., 6, 534–539, doi:10.1038/ngeo1854, 2013.

1023   Flato, G., Marotzke, J., Abiodun, B., Braconnot, P., Chou, S. C., Collins, W., Cox, P., Driouech, F., Emori, S., Eyring, V., Forest, C., Glecker,

1024   P., Guilyardi, E., Jacob, C., Kattsov, V., Reason, C., and Rumukainen, M.: Evaluation of Climate Models, in: Climate Change 2013: The

1025   Physical Science Basis. Contribution of Working Group I to the Fifth Assessment Report of the Intergovernmental Panel on Climate

1026   Change, edited by Stocker, T. F., Qin, D., Plattner, G. K., Tignor, M., Allen, S. K., Boschung, J., Nauels, A., Xia, Y., Bex, V., and Midgley,

1027   P. M., Cambridge University Press, Cambridge, United Kingdom and New York, USA, 2013.

1028   Gantt, B., Johnson, M. S., Crippa, M., Prévôt, A. S. H., and Meskhidze, N.: Implementing marine organic aerosols into the GEOS-Chem

1029   model, Geosci. Mod. Dev., 8, 619–629, doi:10.5194/gmd-8-619-2015, 2015.

1030   Gettleman, A.: Putting the clouds back in aerosol–cloud interactions, Atmos. Chem. Phys., 15, 12 397–12 411, doi:10.5194/acp-15-12397-

1031   2015, 2015.

1032   Gettleman, A., Kay, J. E., and Fasullo, J. T.: Spatial decomposition of climate feedbacks in the Community Earth System Model, J. Cli., 26,

1033   3544–3561, doi:10.1175/JCLI-D-12-00497.1, 2013.

41

Ghan, S. J.: Technical Note: Estimating aerosol effects on cloud radiative forcing, Atmos. Chem. Phys., 13, 9971–9974, doi:10.5194/acp-13-9971-2013, 2013.

Ghan, S. J., Wang, M., Zhang, S., Ferrachat, S., Gettleman, A., Griesfeller, J., Kipling, Z., Lohmann, U., Morrison, H., Neubauer, D., Partridge, D. G., Stier, P., Takemura, T., Wang, H., and Zhang, K.: Challenges in constraining anthropogenic aerosol effects on cloud radiative forcing using present-day spatiotemporal variability, Proc. Natl. Acad. Sci., 113, 5804–5811, doi:10.1073/pnas.1514036113, 2016.

Gnanadesikan, A., Scott, A. A., Pradal, M. A., and Seviour, W. J. M.: Regional responses to black carbon aerosols: The importance of air-sea interaction, J. Geo. Res. Atmos., 122, 12 982–12 999, doi:10.1002/2017JD027589, 2017.

Golaz, J. C., Horowitz, L. W., and II, H. L.: Cloud tuning in a coupled climate model: impact on 20th century warming, Geophys. Res. Lett., pp. 1–20, 2013.

Goldstein, M. and Rougier, J.: Probabilistic formulations for transferring inferences from mathematical models to physical systems, siam, 26, 467–487, doi:10.1137/S106482750342670X, 2004.

Gordon, H., Kirkby, J., Baltensperger, U., Bianchi, F., Breitenlechner, M., Curtius, J., Dias, A., Dommen, J., Donahue, N. M., Dunne, E. M., Duplissy, J., Ehrhart, S., Flagan, R. C., Frege, C., Fuchs, C., Hansel, A., Hoyle, C. R., Kulmala, M., Kurten, A., Lehtipalo, K., Makhmutov, V., Molteni, U., Rissanen, M. P., Stozhkov, Y., Trostl, J., Tsagkogeorgas, G., Wagner, R., Williamson, C., Wimmer, D., Winkler, P. M., Yan, C., and Carslaw, K. S.: Causes and importance of new particle formation in the present-day and preindustrial atmospheres, J. Geo. Res. Atmos., 122, 8739–8760, doi:10.1002/2017JD026844, 2017.

Granier, C., Bessagnet, B., Bond, T., D'Angiola, A., van der Gon, H. D., Frost, G. J., Heli, A., Kaiser, J. W., Kinne, S., Kilmont, Z., Kloster, S., Lamarque, J. F., Liousse, C., Masui, T., Meleux, F., Mieville, A., Ohara, T., Raut, J. C., Riahi, K., Schultz, M. G., Smith, S. J., Thompson, A., van Aardenne, J., van der Werf, G. R., and van Vuuren, D. P.: Evolution of anthropogenic and biomass burning emissions of air pollutants at global and regional scales during the 1980-2010 period, Climatic Change, 109, 163–190, doi:10.1007/s10584-011-0154-1, 2011.

Gryspeerdt, E., Quaas, J., Ferrachat, S., Gettelman, A., Ghan, S., Lohmann, U., Morrison, H., Neubauer, D., Partridge, D. G., Stier, P., Takemura, T., Wang, H., Wang, M., and Zhang, K.: Constraining the instantaneous aerosol influence on cloud albedo, Proc. Natl. Acad. Sci., 114, 4899–4904, doi:10.1073/pnas.1617765114, 2017.

Guo, L., Highwood, E. J., Shaffrey, L. C., and Turner, A. G.: The effect of regional changes in anthropogenic aerosols on rainfall of the East Asian Sumer Monsoon, Atmos. Chem. Phys., 13, 1521–1534, doi:10.5194/acp-13-1521-2013, 2013.

HadCRUT4: Met Office Hadley Centre observations dataset, HadCRUT4. **https://www.metoffice.gov.uk/hadobs/hadcrut4**. Accessed: October 2017, 2017.

HadGEM3: Met Office climate prediction model: HadGEM3 family. **http://www.metoffice.gov.uk/research/modelling–systems/unified–model/climate–models/hadgem3**. Accessed: March 2017, 2017.

Haerter, J. O., Roeckner, E., Tomassini, L., and von Storch, J. S.: Parametric uncertainty effects on aerosol radiative forcing, Geophys. Res. Lett., 36, L15707, doi:10.1029/2009GL039050, 2009.

Hamilton, D. S., Lee, L. A., Pringle, K. J., Reddington, C. L. S., Spracklen, D. V., and Carslaw, K. S.: Occurrence of pristine aerosol on a polluted planet, Proc. Natl. Acad. Sci., 111, 18 466–18 471, doi:10.1073/pnas.1415440111, 2014.

Hartmann, D. L., A. M. G. Klein T., Rusticucci, M., Alexander, L. V., Brönnimann, S., Charabi, Y., Dentener, F. J., Dlugokencky, E. J., Easterling, D. R., Kaplan, A., Soden, B. J., Thorne, P. W., Wild, M., and Zhai, P. M.: Observations: Atmosphere and Surface, in: Climate Change 2013: The Physical Science Basis. Contribution of Working Group I to the Fifth Assessment Report of the Intergovernmental

Panel on Climate Change, edited by Stocker, T. F., Qin, D., Plattner, G. K., Tignor, M., Allen, S. K., Boschung, J., Nauels, A., Xia, Y., Bex, V., and Midgley, P. M., Cambridge University Press, Cambridge, United Kingdom and New York, NY, USA, 2013.

Hawkins, E., Ortega, P., Suckling, E., Schurer, A., Hergl, G., Jones, P., Joshi, M., Osborne, T., Masson-Delmotte, V., Mignot, J., Thorne, P., and Jan van Oldenborgh, G.: Estimating changes in global temperature since the preindustrial period, Bull. Amer. Meteor. Soc., pp. 1841–1856, doi:10.1175/BAMS-D-16-0007.1, 2017.

Hetzel, J.: Package 'Trapezoid', https://cran.r-project.org/web/packages/trapezoid/trapezoid.pdf, 2012.

Hourdin, F., Mauritsen, T., Gettleman, A., Golaz, J., Balaji, V., Duan, Q., Folini, D., Klocke, D. J. D., Qian, Y., Rauser, F., Rio, C., Tomassini, L., Watanabe, M., and Williamson, D.: The art and science of climate model tuning, Bull. Amer. Meteorol. Soc., 98, 589–602, doi:10.1175/BAMS-D-15-00135.1, 2017.

Johnson, J. S., Cui, Z., Lee, L. A., Gosling, J. P., Blyth, A. M., and Carslaw, K. S.: Evaluating uncertainty in convective cloud microphysics using statistical emulation, J. Adv. Model. Earth Syst., 7, 162–187, doi:10.1002/2014NS000383, 2015.

Johnson, J. S., Regayre, L. A., Yoshioka, M., Pringle, K. J., Lee, L. A., Sexton, D., Rostron, J., Booth, B. B. B., and Carslaw, K. S.: The importance of comprehensive parameter sampling and multiple observations for robust constraint of aerosol radiative forcing, Atmos. Chem. Phys., 18, TBC, doi:TBC, 2018.

Karydis, V. A., Tsimpidi, A. P., Bracer, S., Pozzer, A., Nenes, A., and Lelieveld, J.: Global impact of mineral dust on cloud droplet number concentration, Atmos. Chem. Phys., 17, 5601–5621, doi:10.5194/acp-17-5601-2017, 2017.

Kasoar, M., Voulgarakis, A., Lamarque, J.-F., Shindell, D. T., Bellouin, N., Collins, W. J., Faluvego, G., and Tsigaridis, K.: Regional and global temperature response to anthropogenic SO_2 emissions from China in three climate models, Atmos. Chem. Phys., 16, 9785–9804, doi:10.5194/acp-16-9785-2016, 2016.

Kay, J. E., Hillman, B. R., Klein, S. A., Zhang, Y., Medeiros, B., Pincus, R., Gettleman, A., Eaton, B., Boyle, J., Marchand, R., and Ackerman, T. P.: Exposing Global Cloud Biases in the Community Atmosphere Model (CAM) Using Satellite Observations and Their Corresponding Instrument Simulators, J. Cli., 25, 5190–5207, doi:10.1175/JCLI-D-11-00469.1, 2012.

Khain, A. P., Ovtchinnikov, M., Pinsky, M., Potrovsky, A., and Krugliak, H.: Notes on state-of-the-art numerical modeling of cloud micro-physics, Atmos. Res., 55, 159–224, doi:10.1016/S0169-8095(00)00064-8, 2000.

Kim, D., Chin, M., Yu, H. B., Diehl, T., Tan, Q., Kahn, R. A., Tsigaridis, K., Bauer, S. E., Takemura, T., Pozzoli, L., Bellouin, N., Schulz, M., Peyridieu, S., Chedin, A., and Koffi, B.: Sources, sinks and transatlantic transport of North African dust aerosol: A multimodel analysis and comparison with remote sensing data, J. Geo. Res. Atmos., 119, 6259–6277, doi:10.1002/2013JD021099, 2014.

Kipling, Z., Stier, P., Johnson, C. E., Mann, G. W., Bellouin, N., Bauer, S. E., Bergman, T., Chin, M., Diehl, T., Ghan, S. J., Iversen, T., Kirkevag, A., Kokkola, H., Liu, X. H., Luo, G., von Noije, T., Pringle, K. J., von Salzen, K., Schulz, M., Seland, O., Skeie, R. B., Takemura, T., Tsigaridis, K., and Zhang, K.: What controls the vertical distribution of aerosol? Relationships between process sensitivity in HadGEM3-UKCA and inter-model variation from AeroCom Phase II, Atmos. Chem. Phys., 16, 2221–2241, doi:10.5194/acp-16-2221-2016, 2016.

Kirtman, B., Power, S. B., Adedoyin, J. A., Boer, G. J., Bojariu, R., Camilloni, I., Doblas-Reyes, F. J., Fiore, A. M., Kimoto, M., Meehl, G. A., Prather, M., Sarr, A., Schär, C., Sutton, R., van Oldenborgh, G. J., Vecchi, G., and Wang, H. J.: Near-term Climate Change: Projections and Predictability, in: Climate Change 2013: The Physical Science Basis. Contribution of Working Group I to the Fifth Assessment Report of the Intergovernmental Panel on Climate Change, edited by Stocker, T. F., Qin, D., Plattner, G. K., Tignor, M., Allen, S. K., Boschung, J., Nauels, A., Xia, Y., Bex, V., and Midgley, P. M., Cambridge University Press, Cambridge, United Kingdom and New York, NY, USA, 2013.

Knutti, R., Krähenmann, S., Frame, D. J., and Allen, M. R.: Comment on "Heat capacity, time constant, and sensitivity of earth's climate system" by SE Schwartz.", J. Geo. Res. Atmos., 113, 1984–2012, doi:10.1029/2007JD009473, 2008.

Knutti, R., Masson, D., and Gettleman, A.: Climate model genealogy: Generation CMIP5 and how we got there, Geophys. Res. Lett., 40, 1194–1199, doi:10.1002/grl.50256, 2013.

Koffi, B., Schulz, M., Breon, F. M., Dentener, F., Steensen, B. M., Griesfeller, J., Winker, D., Balkanski, Y., Bauer, S. E., Bellouin, N., Berntsen, T., Bian, H. S., Chin, M., Diehl, T., Easter, R., Ghan, S., Hauglustaine, D. A., Iversen, T., Kirkevag, A., Liu, X. H., Lohmann, U., Myhre, G., Rasch, P., Seland, O., Skeie, R. B., Steenrod, S. D., Stier, P., Tackett, J., Takemura, T., Tsigaridis, K., Vuolo, M. R., Yoon, J., and Zhang, K.: Evaluation of the aerosol vertical distribution in global aerosol models through comparison against CALIOP measurements: AeroCom phase II results, J. Geo. Res. Atmos., 121, 7254–7283, doi:10.1002/2015JD024639, 2016.

Kooperman, G. J., Pritchard, M. S., Ghan, S. J., Wang, M., Somerville, R. C. J., and Russell, L. M.: Constraining the influence of natural variability to improve estimates of global aerosol indirect effects in a nudged version of the Community Atmosphere Model 5, J. Geo. Res., 117, 1–16, doi:10.1029/2012JD018588, 2012.

Korhonen, H., Carslaw, K. S., Spracklen, D. V., Mann, G. W., and Woodhouse, M. T.: Influence of oceanic dimethyl sulfide emissions on cloud condensation nuclei concentrations and seasonality over the remote Southern Hemisphere oceans: A global model study, J. Geo. Res., 113, 16, 2008.

Kretzschmar, J., Salzmann, M., Mülmenstädt, J., Boucher, O., and Quass, J.: Comment on "Rethinking the Lower Bound on Aerosol Radiative Forcing, J. Cli., 30, 6579–6584, doi:10.1175/JCLI-D-16-0668.1, 2017.

Lacagnina, C., Hasekamp, O. P., Huisheng, B., Curci, G., Myhre, G., van Noije, T., Schulz, M., Skeie, R. B., Takemura, T., and Zhang, K.: Aerosol single-scattering albedo over the global oceans: Comapring PARASOL retrievals with AERONET, OMI, and AeroCom models estiamtes, J. Geo. Res. Atmos., 120, 9814–9836, doi:10.1002/2015JD023501, 2015.

Lamarque, J. F., Bond, T. C., Eyring, V., Granier, C., Heli, A., Kilmont, Z., Lee, D., Liousse, C., Mieville, A., Owen, B., Schultz, M. G., Shindell, D., Smith, S. J., Stehfest, E., Van Aardenne, J., Cooper, O. R., Kainuma, M., Mahowald, N., McConnell, J. R., Naik, V., Riahi, K., and van Vuuren, D. P.: Historical (1850-2000) gridded anthropogenic and biomass burning emissions of reactive gases and aerosols: methodology and application, Atmos. Chem. Phys., 10, 7017–7039, doi:10.5194/acp-10-7017-2010, 2010.

Lebo, Z. J. and Feingold, G.: On the relationship between responses in cloud water and precipitation to changes in aerosol, Atmos. Chem. Phys., 14, 11 817–11 831, doi:10.5194/acp-14-11817-2014, 2014.

Lee, L. A., Carslaw, K. S., Pringle, K. J., Mann, G. W., and Spracklen, D. V.: Emulation of a complex global aerosol model to quantify sensitivity to uncertain parameters, Atmos. Chem. Phys., 11, 12 253–12 273, doi:10.5194/acp-11-12253-2011, 2011.

Lee, L. A., Carslaw, K. S., Pringle, K. J., and Mann, G. W.: Mapping the uncertainty in global CCN using emulation, Atmos. Chem. Phys., 12, 9739–9751, doi:10.5194/acp-12-9739-2012, 2012.

Lee, L. A., Pringle, K. J., Reddington, C. L., Mann, G. W., Stier, P., Spracklen, D. V., Pierce, J., and Carslaw, K. S.: The magnitude and causes of uncertainty in global model simulations of cloud condensation nuclei, Atmos. Chem. Phys., 13, 8879–8914, doi:10.5194/acp-13-8879-2013, 2013.

Lee, L. A., Reddington, C. L., and Carslaw, K. S.: On the relationship between aerosol model uncertainty and radiative forcing uncertainty, Proc. Natl. Acad. Sci., 113, 5820–5827, doi:10.1073/pnas.1507050113, 2016.

Liu, X. H. and Wang, J. A.: How important is organic aerosol hygroscopicity to aerosol indirect effect?, Environ. Res. Lett., 5, 044 010, doi:10.1088/1748-9326/5/4/044010, 2010.

1147 Liu, Y. and Gupta, H. V.: Uncertainties in hydrologic modeling: Toward an integrated data assimilation framework, Water Resour. Res., 43,
1148   1–17, doi:10.1029/2006WR005756, 2007.

1149 Loeb, N. G., Wielicki, B. A., Doelling, D. R., Smith, G. L., Keyes, D. F., Kato, S., Manalo-Smith, N., and Wong, T.: Toward Optimal Closure
1150   of the Earth's Top-of-Atmosphere Radiation Budget, J. Climate., 22, 748–766, doi:10.1175/2008JCLI2637.1, 2009.

1151 Loeb, N. G., Kato, S., Su, W., Wong, T., Rose, F. G., Doelling, D. R., Norris, J. R., and Huang, X.: Advances in Understanding Top-of-
1152   Atmosphere Radiation Variability from Satellite Observations, Surv. Geophys., 33, 359–385, doi:10.1007/s10712-012-9175-1, 2012.

1153 Lohmann, U.: Why does knowledge of past aerosol forcing matter for future climate change?, J. Geo. Res. Atmos., 122, 5021–5023,
1154   doi:10.1002/2017JD026962, 2017.

1155 Lohmann, U. and Ferrachat, S.: Impact of parametric uncertainties on the present-day climate and on the anthropogenic aerosol effect, Atmos.
1156   Chem. Phys., 10, 11 373–11 383, 2010.

1157 Malavelle, F. F., Haywood, J. M., Ones, A. J., Gettleman, A., Larisse, L. C., Bauduin, S., Allan, R. P., Karset, I. H. H., Kristjansson, J. E.,
1158   Oreopoulos, L., Ho, N. C., Lee, D., Bellouin, N., Boucher, O., Grosvenor, D. P., Carslaw, K. S., Dhomse, S., Mann, G. W., Schmidt, A.,
1159   andf M. E. Hartley, H. C., Dalvi, M., Hill, A. A., Johnson, B. T., Jphnson, C. E., Knight, J. R., Jeff, R., O'Connor, F. M., Partridge, D. G.,
1160   Stier, P., Myhre, G., Platnick, S., Stephens, G. L., Takahashi, H., and Thordarson, T.: Strong constraints on aerosol-cloud interactions from
1161   volcanic eruptions, Nat., 543, 485–491, doi:10.1038/nature22974, 2017.

1162 Manktelow, P. T., Carslaw, K. S., Mann, G. W., and Spracklen, D. V.: The impact of dust on sulfate aerosol, CN and CCN during an East
1163   Asian dust storm, Atmos. Chem. Phys., 10, doi:10.5194/acp-10-365-2010, 2010.

1164 Mann, G. W., Carslaw, K. S., Spracklen, D. V., Ridley, D. A., Manktelow, P. T., Chipperfield, M. P., Pickering, S. J., and Johnson, C. E.:
1165   Description and evaluation of GLOMAP-mode aerosol microphysics model for the UKCA composition-climate model, Geosci. Mod.
1166   Dev., 3, 519–551, doi:10.5194/gmd-3-519-2010, 2010.

1167 Mann, G. W., Carslaw, K. S., Reddington, C. L., Pringle, K. J., Schulz, M., Asmi, A., Spracklen, D. V., Ridley, D. A., Woodhouse, M. T., Lee,
1168   L. A., Zhang, K., Ghan, S. J., Easter, R. C., Liu, X., Stier, P., Lee, Y. H., Adams, P. J., Tost, H., andS. E. Bauer, J. L., Tsigaridis, K., van
1169   Noije, T. P. C., Strunk, A., Vignati, E., Bellouin, N., Dalvi, M., Johnson, C. E., Bergman, T., Kokkola, H., von Salzen, K., Yu, F., Luo, G.,
1170   Petzold, A., Heitzenberg, J., Clarke, A., Ogren, A., Gras, J., Baltensperger, U., Kaminski, U., Jennings, S. G., O'Dowd, C. D., Harrison,
1171   R. M., Beddows, D. C. S., Kulmala, M., Viisanen, Y., Ulevicius, V., Mihalopoulos, N., Zdimal, V., Fiebig, M., Hansson, H., Swietlicki,
1172   E., and Henzing, J. S.: Intercomparison and evaluation of global aerosol microphysical properties among AeroCom models of a range of
1173   complexity, Atmos. Chem. Phys., 14, 4679–4713, doi:10.5194/acp-14-4679-2014, 2014.

1174 Mauritsen, T., Stevens, B., Roeckner, E., Crueger, T., Esch, M., Giorgetta, M., Haak, H., Jungclaus, J., Klocke, D., Matei, D., Mikolajewicz,
1175   U., Notz, D., Pincus, R., Schmidt, H., and Tomassini, L.: Tuning the climate of a global model, J. Adv. Model. Earth Syst., 4, M00A01,
1176   doi:10.1029/2012MS000154, 2012.

1177 Metzger, A., Verheggen, B., Dommen, J., Duplissy, J., Prevot, A. S. H., Weingartner, E., Riipinen, I., Kulmala, M., Spracklen, D. V., Carslaw,
1178   K. S., and Baltensperger, U.: Evidence for the role of organics in aerosol particle formation under atmospheric conditions, Proc. Natl. Acad.
1179   Sci., 107, 6646–6651, doi:10.1073/pnas.0911330107, 2010.

1180 Michibata, T. and Takemura, T.: Evaluation of autoconversion schemes in a single model framework with satellite observations, J. Geo. Res.
1181   Atmos., 120, 1–21, doi:10.1002/2015JD023818-T, 2015.

1182 Morgan, M. G., Adams, P. J., and Keith, D. W.: Elicitation of expert judgements about aerosol forcing, Clim. Change., 75, 195–214,
1183   doi:10.1007/s10584-005-9025-y, 2006.

1184 Myhre, G., Shindell, D., Bréon, F. M., Collins, W., Fuglestvedt, J., Huang, J., Koch, D., Lamarque, J. F., Lee, D., Mendoza, B., Nakajima,
1185   T., Robock, A., Stephens, G., Takemura, T., and Zhang, H.: Anthropogenic and Natural Radiative Forcing, in: Climate Change 2013:
1186   The Physical Science Basis. Contribution of Working Group I to the Fifth Assessment Report of the Intergovernmental Panel on Climate
1187   Change, edited by Stocker, T. F., Qin, D., Plattner, G. K., Tignor, M., Allen, S. K., Boschung, J., Nauels, A., Xia, Y., Bex, V., and Midgley,
1188   P. M., Cambridge University Press, Cambridge, United Kingdom and New York, NY, USA, 2013.

1189 Nam, C., Bony, S., Dufresne, J. L., and Chepfer, H.: The 'too few, too bright' tropical low-cloud problem in CMIP5 models, Geophys. Res.
1190   Lett., 39, L21 801, doi:10.1029/2012GL053421, 2012.

1191 Neubauer, D., Lohmann, U., Hoose, C., and Frontoso, M. G.: Impact of the representation of marine stratocumulus clouds on the anthro-
1192   pogenic aerosol effect, Atmos. Chem. Phys., 14, 11 997–12 022, doi:10.5194/acp-14-11997-2014, 2014.

1193 Oakley, J. E. and O'Hagan, A.: Probabilistic sensitivity analysis of complex models: a Bayesian approach, JRSSB, 66, 751–769, 2004.

1194 Pan, X., Chin, M., Gautam, R., Bian, H., Kim, D., Colarco, P. R., Diehl, T. L., Takemura, T., Pozzoli, L., Tsigaridis, K., Bauer, S., and
1195   Bellouin, N.: A multi-model evaluation of aerosols over South Asia: common problems and possible causes, Atmos. Chem. Phys., 15,
1196   5903–5928, doi:10.5194/acp-15-5903-2015, 2015.

1197 Pennell, C. and Reichler, T.: On the effective number of climate models, J. Cli., 24, 2358–2367, 2010.

1198 Petters, M. D. and Kreidenweis, S. M.: A single parameter representation of hygroscopic growth and cloud condensation nucleus activity,
1199   Atmos. Chem. Phys., 7, 1961–1971, doi:10.5194/acp-7-1961-2007, 2007.

1200 Pianosi, F., Beven, K., Freer, J., Hall, J. W., Rougier, J., Stephenson, D. B., and Wagener, T.: Sensitivity analysis of environmental models:
1201   A systematic review of practical workflow, Environ. Mod. Soft., 79, 214–232, doi:10.1016/j.envsoft.2016.02.008, 2016.

1202 Pringle, K. J., Carslaw, K. S., Fan, T., Mann, G. W., Hill, A., Stier, P., Zhang, K., and Tost, H.: A multi-model assessment of the impact of
1203   sea spray geoengineering on cloud droplet number, Atmos. Chem. Phys., 12, 11 647–11 663, 2012.

1204 Qian, Y., Yan, H., Zhangshuan, H., Gardar, J., Klein, S., Lucas, D., Neale, R., Rasch, P., Swiller, L., Tannahill, J., Wang, H., Wang, M., and
1205   Zhao, C.: Parametric sensitivity analysis of precipitation at global and local scales in the Comunity Atmosphere Model CAM5, J. Adv.
1206   Model. Earth Syst., 7, 382–411, doi:10.1002/2014MS000354, 2015.

1207 Räisänen, P., Barker, H. W., Khairoutdinov, M. F., Li, J., and Randall, D. A.: Stochastic generation of subgrid-scale cloudy columns for
1208   large-scale models, Quart. J. Roy. Meteor. Soc., 130, 2047–2067, doi:10.125/qj.03.99, 2004.

1209 Randles, C. A., Kinne, S., Myhre, G., Schulz, M., Stier, P., Fisher, J., Doppler, L., Highwood, E., Ryder, C., Harris, B., Huttunen, J., Ma,
1210   Y., Pinker, R. T., Mayer, B., Neubauer, D., Hitzenberger, R., Oreopoulos, L., Lee, D., Pitari, G., Di Genova, G., Quaas, J., Rose, F. G.,
1211   Kato, S., Rumbold, S. T., Vardavas, I., Hatzianastassiou, N., Matsoukas, C., Yu, H., Zhang, F., Zhang, H., and Lu, P.: Intercomparison
1212   of shortwave radiative transfer schemes in global aerosol modeling: results from the AeroCom Radiative Transfer Experiment, Atmos.
1213   Chem. Phys., 13, 2347–2379, doi:10.5194/acp-13-2347-2013, 2013.

1214 Reddington, C. L., Carslaw, K., Spracklen, D., Frontoso, M., Collins, L., Merikanto, J., Minikin, A., Hamburger, T., Coe, H., Kulmala,
1215   M., Aalto, P., Flentje, H., Plass-Dulmer, C., Birmili, W., Wiedensolher, A., Wehner, B., Tuch, T., Sonntag, A., O'Dowd, C., Jennings,
1216   S., Dupuy, R., Baltensperger, U., Weingartner, E., Hansson, H., Turnved, P., Laj, P., Skellegri, K., Boulton, J., Putaud, J., Gruening, C.,
1217   Swietlicki, E., Roldin, P., Henzing, J., Moerman, M., Mihalopoulos, N., Kouvarakis, G., Zdimal, V., Zikova, N., Marinoni, A., Bosasoni,
1218   P., and Duchi, R.: Primary versus secondary contributions to particle number concentrations in the European boundary layer, Atmos.
1219   Chem. Phys., 11, 12 007–12 036, 2011.

1220 Reddington, C. L., Carslaw, K. S., Stier, P., Schutgens, N., Coe, H., Liu, D., Allan, J., Browse, J., Pringle, K., Lee, L., Yoshioka, M., Johnson,
1221   J., Regayre, L., Spracklen, D., Mann, G., Clarke, A., Hermann, M., Henning, S., Wex, H., Kristensen, T., Leaitch, W., Poeschl, U., Rose,

1222   D., Andreae, M., Schmale, J., Kondo, Y., Oshima, N., Schwarz, J., Nenes, A., Andreson, B., Roberts, G., Snider, J., Leck, C., Quinn, P.,

1223   Chi, X., Ding, A., Jimenez, J., and Zhang, Q.: The Global Aerosol Synthesis and Science Project (GASSP), Bull. Amer. Meteorol. Soc.,

1224   In Press, doi:10.1175/BAMS-D-15-00317.1, 2017.

1225   Regayre, L. A., Pringle, K. J., Booth, B. B. B., Lee, L. A., Mann, G. W., Browse, J., Woodhouse, M. T., Rap, A., Reddington, C. L. S., and

1226   Carslaw, K. S.: Uncertainty in the magnitude of aerosol-cloud radiative forcing over recent decades, Geophys. Res. Lett., 41, 9040–9049,

1227   doi:10.1002/2014GL062029, 2014.

1228   Regayre, L. A., Pringle, K. J., Lee, L. A., Booth, B. B. B., Rap, A., Browse, J., Mann, G. W., Woodhouse, M. T., Reddington, C. L. S., and

1229   Carslaw, K. S.: The climatic importance of uncertainties in regional aerosol-cloud radiative forcings over recent decades, J. Climate., 28,

1230   6589–6607, doi:10.1175/JCLI-D-15-0127.1, 2015.

1231   Reutter, P., Su, H., Trentmann, J., Simmel, M., Rose, D., Gunthe, S. S., Wernli, H., Andreae, M. O., and Pöschl, U.: Aerosol- and updraft-

1232   limitedregimes of cloud dropletformation: influence of particle number, size and hygroscopicity on the activation of cloud condensation

1233   nuclei CCN, Atmos. Chem. Phys., 9, 7067–7080, doi:10.5194/acp-9-7067-2009, 2009.

1234   Rodrigues, L. F. S., Vernon, I., and Bower, R.: Constraints on galaxy formation models from the galaxy stellar mass function and its evolution,

1235   Mon. Not. R. Astron. Soc., 466, 2418–2435, doi:10.1093/mnras/stw3269, 2017.

1236   Rougier, J.: Ensemble averaging and mean squared error, J. Cli., 29, 8865–8870, doi:10.1175/JCLI-D-16-0012.1, 2016.

1237   Saltelli, A., Tarantola, S., and Chan, K. P. S.: A quantitative model-independent method for global sensitivity analysis of model output,

1238   Technometrics, 41, 39–56, doi:10.2307/1270993, 1999.

1239   Saltelli, A., Chan, K., and Scott, E. M.: Sensitivity Analysis, Wiley, Oxford, U.K., 2000.

1240   Samset, B. H., Myhre, G., Herber, A., Kondo, Y., Li, S. M., Moteki, N., Koike, M., Oshima, N., Schwarz, J. P., Balkanski, Y., Bauer, S. E.,

1241   Bellouin, N., Berntsen, T. K., Bian, H., Chin, M., Diehl, T., Easter, R. C., Ghan, S. J., Iversen, T., Kirkevag, A., Lamarque, J. F., Lin, G.,

1242   Liu, X., Penner, J. E., Schulz, M., Seland, O., Skeie, R. B., Stier, P., Takemura, T., and Zhang, K. T. K.: Modelled black carbon radiative

1243   forcing and atmospheric lifetime in AeroCom Phase II constrained by aircraft observations, Atmos. Chem. Phys., 14, 12 465–12 477,

1244   doi:10.5194/acp-14-12465-2014, 2014.

1245   Sanderson, B. M.: A multimodel study of parametric uncertainty in predictions of climate response to rising greenhouse gas concentrations.,

1246   J. Climate., 24, 1362–1377, doi:10.1175/2010JCLI3498.1, 2010.

1247   Schmidt, A., Ostro, B., Carslaw, K. S., Wilson, M., Thordarson, T., Mann, G. W., and Simmons, A. J.: Excess mortality in Europe following

1248   a future Laki-style Icelandic eruption, Proc. Natl. Acad. Sci., 108, 15 710–15 715, 2011.

1249   Schulz, M., Textor, C., Kinne, S., Balkanski, Y., Bauer, S., Berntsen, T., Berglen, T., Boucher, O., Dentener, F., Guibert, S., Isaksen, I. S. A.,

1250   Iversen, T., Koch, D., Kirkevag, A., Liu, X., Montanaro, V., Myhre, G., Penner, J. E., Pitari, G., Reddy, S., Seland, O., Stier, P., and

1251   Takemura, T.: Radiative forcing by aerosols as derived from the AeroCom present-day and pre-industrial simulations, Atmos. Chem.

1252   Phys., 6, 5225–5246, 2006.

1253   Schutgens, N., Tsyro, S., Gryspeerdt, E., Goto, D., Weigum, N., Schulz, M., and Stier, P.: On the spatio-temporal representativeness of

1254   observations, Atmos. Chem. Phys., 17, 9761–9780, doi:10.5194/acp-17-9761-2017, 2017.

1255   Seinfeld, J. H., Bretherton, C., Carslaw, K. S., Coe, H., DeMott, P. J., Dunlea, E. J., Feingold, G., Ghan, S., Guenther, A. B., Kahn, R.,

1256   Kraucunas, I., Kreidenweis, S. M., Molina, M. J., Nenes, A., Penner, J. E., Prather, K. A., Ramanathan, V., Ramaswamy, V., Rasch, P. J.,

1257   Ravishankara, A. R., Rosenfeld, D., Stephens, G., and Wood, R.: Improving our fundamental understanding of the role of aerosol-cloud

1258   interactions in the climate system, Proc. Natl. Acad. Sci., 113, 5781–5790, doi:10.1073/pnas.1514043113, 2016.

Sexton, D. M. H., Murphy, J. M., Collins, M., and Webb, M. J.: Multivariate probabilistic projections using imperfect climate models Part I: outline of methodology, Clim. Dyn., 38, 2513–2542, 2012.

Sexton, D. M. H., Karmalkar, A., Murphy, J., and Booth, B. B. B.: The elicitation of distributions of parameters in HadGEM3 versions GA4 and GA7 for use in perturbed parameter ensembles, Hadley Centre technical note 101, Met Office, U.K., 2018.

Shindell, D. T., Lamarque, J. F., Schulz, M., Flaner, M., Jiao, C., Chin, M., Young, P., Lee, Y., Rotstayn, L., Mahowald, N., Milly, G., Faluvegi, G., Balkanski, Y., Collins, W. J., Conley, A. J., Dalsoren, S., Easter, R., Ghan, S., Horowitz, L., Liu, X., Myhre, G., Nagashima, T., Naik, V., Rumbold, S. T., Skeie, R., Sudo, K., Szopa, S., Takemura, T., Voulgarakis, A., Yoon, J. H., and Lo, F.: Radiative forcing in the ACCMIP historical and future climate simulations, Atmos. Chem. Phys., 13, 2939–2974, doi:10.5194/acp-13-2939-2013, 2013.

Shiogama, H., Watanabe, M., Yoshimori, M., Yokohata, T., Ogura, T., Annan, J. D., Hargreaves, J. C., Abe, M., Kamae, Y., O'ishi, R., Nobui, R., Emori, S., Nozawa, T., Abe-Ouchi, A., and Kimoto, M.: Perturbed physics ensemble using the MIROC5 coupled atmosphere-ocean GCM without flux corrections: experimental design and results, Clim. Dyn., 39, 3041–3056, doi:10.1007/s00382-012-1441-x, 2012.

Shrivastava, M., Zhao, C., Easter, R. C., Qian, Y., Zelenyuk, A., Fast, J. D., Liu, Y., Zhang, Q., and Guenther, A.: Sensitivity analysis of simulated SOA loadings using a variance-based statistical approach, J. Adv. Model. Earth Syst., 8, 499–519, doi:10.1002/2015MS000554, 2016.

Smith, S. J., van Aardenne, J., Klimont, Z., Andres, R. J., Volke, A., and Arias, S. D.: Anthropogenic sulfur dioxide emissions: 1850 to 2005, Atmos. Chem. Phys., 11, 1101–1116, doi:10.5194/acp-11-1101-2011, 2011.

Snedecor, G. W. and Cochran, W. G.: Statistical methods, Iowa State University Press, 8th edn., 1989.

Spracklen, D. V., Pringle, K. J., Carslaw, K. S., Chipperfield, M. P., and Mann, G. W.: A global off-line model of size-resolved aerosol microphysics: I. Model development and prediction of aerosol properties, Atmos. Chem. Phys., 5, 2227–2252, doi:10.5194/acp-5-2227-2005, 2005.

Spracklen, D. V., Carslaw, K. S., Merikanto, J., Mann, G. W., Reddington, C. L., Pickering, S., Ogren, J. A., Andrews, E., Baltensperger, U., Weingartner, E., Boy, M., Kulmala, M., Laakso, L., Lihavainen, H., Kivekas, N., Komppula, M., Mihalopoulos, N., Kouvarakis, G., Jennings, S., O'Dowd, C., Birmili, W., Wiedensolher, A., Weller, R., Gras, J., Laj, P., Sellegri, K., Bonn, B., Krejci, R., Laaksonen, A., Hamed, A., Minikin, A., Harrison, R. M., Talbot, R., and Sun, J.: Explaining global surface aerosol number concentrations in terms of primary emissions and particle formation, Atmos. Chem. Phys., 10, 4775–4793, 2010.

Spracklen, D. V., Carslaw, K. S., Pöschl, U., Rap, A., and Forster, P.: Global cloud condensation nuclei influenced by carbonaceous combustion aerosol, Atmos. Chem. Phys., 11, 9067–9087, doi:10.5194/acp-11-9067-2011, 2011a.

Spracklen, D. V., Jimenez, J. L., Carslaw, K. S., Worsnop, D. R., Evans, M. J., Mann, G. W., Zhang, Q., Canagaratna, M. R., Allan, J., Coe, H., McFiggans, G., Rap, A., and Forster, P.: Aerosol mass spectrometer contraint on the global secondary organic aerosol budget, Atmos. Chem. Phys., 11, 12 109–12 136, doi:10.5194/acp-11-12109-2011, 2011b.

Stevens, B.: Rethinking the Lower Bound on Aerosol Radiative Forcing, J. Cli., 28, 4794–4819, doi:10.1175/JCLI-D-14-00656.1, 2015.

Stevens, B. and Feingold, G.: Untangling aerosol effects on clouds and precipitation in a buffered system, Nat., 461, 607–613, 2009.

Stier, P., Schutgens, N. A. J., Bian, H., Boucher, O., Chin, M., Ghan, S., Huneeus, N., Kinne, S., Lin, G., Myhre, G., Penner, J. E., Randles, C., Samset, B., Schulz, M., Yu, H., and Zhou, C.: Host model uncertainties in aerosol radiative forcing estimates: results from the AeroCom prescribed intercomparison study, Atmos. Chem. Phys., 13, 3245–3270, doi:10.5194/acp-13-3245-2013, 2013.

Storelvmo, T., Lohmann, U., and Bennartz, R.: What governs the spread in shortwave forcings in the transient IPCC AR4 models?, Geophys. Res. Lett., 36, doi:10.1029/2008GL036069, 2009.

Sullivan, S. C., Lee, D., Oreopoulos, L., and Nenes, A.: Role of updraft velocity in temporal variability of global cloud hydrometeor number, Proc. Natl. Acad. Sci., 113, 5791–5796, doi:10.1073/pnas.1514039113, 2016.

Taylor, K. E., Stouffer, R. J., and Meehl, G. A.: An Overview of CMIP5 and the Experiment Design, Bull. Amer. Meteor. Soc., 93, 485–498, doi:10.1175/BAMS-D-11-00094.1, 2012.

Telford, P. J., Braesicke, P., Morgenstern, O., and Pyle, J. A.: Technical Note: Description and assessment of a nudged version of the new dynamics Unified Model, Atmos. Chem. Phys., 8, 1701–1712, doi:10.5194/acp-8-1701-2008, 2008.

Tett, S. F. B., Rowlands, D. J., Mineter, M. J., and Cartis, C.: Can Top-Of-Atmosphere Radiation Measurements Constrain Climate Predictions? Part II: Climate Sensitivity, J. Climate., 26, 9367–9383, doi:10.1175/JCLI-D-12-00596.1, 2013.

Textor, C., Schulz, M., Guibert, S., Kinne, S., Balkanski, Y., Bauer, S., Berntsen, T., Berglen, T., Boucher, O., Chin, M., Dentener, F., Diehl, T., Easter, R., Feichter, H., Fillmore, D., Ghan, S., Ginoux, P., Gong, S., Grini, A., Hendricks, J., Horowitz, L., Huang, P., Isaksen, I., Iversen, I., Kloster, S., Koch, D., Kirkevåg, A., Kristjansson, J. E., Krol, M., Lauer, A., Lamarque, J. F., Liu, X., Montanaro, V., Myhre, G., Penner, J., Pitari, G., Reddy, S., Seland, O., Stier, P., Takemura, T., and Tie, X.: Analysis and quantification of the diversities of aerosol life cycles within AeroCom, Atmos. Chem. Phys., 6, 1777–1813, doi:10.5194/acp-6-1777-2006, 2006.

Textor, C., Schulz, M., Guibert, S., Kinne, S., Balkanski, Y., Bauer, S., Berntsen, T., Berglen, T., Boucher, O., Chin, M., Dentener, F., Diehl, T., Feichter, J., Fillmore, D., Ginoux, P., Gong, S., Grini, A., Hendricks, J., Horowitz, L., Huang, P., Isaksen, I. S. A., Iversen, T., Kloster, S., Koch, D., Kirkevåg, A., Kristjansson, J. E., Kro, M., Lauer, A., Lamarque, J. F., Liu, X., Montanaro, V., Myhre, G., Penner, J. E., Pitari, G., Reddy, M. S., Seland, O., Stier, P., Takemura, T., and Tie, X.: The effect of harmonized emissions on aerosol properties in global models - an AeroCom experiment, Atmos. Chem. Phys., 7, 4489–4501, doi:10.5194/acp-7-4489-2007, 2007.

Toll, V., Christensen, M., Gassó, S., and Bellouin, N.: Volcano and ship tracks indicate excessive aerosol-induced cloud water increases in a climate model, Geophys. Res. Lett., 44, 12 492–12 500, doi:10.1002/2017GL075280, 2017.

Tost, H., Lawrence, M. G., Brühl, C., and Jöckel, P.: Uncertainties in atmospheric chemistry modelling due to convection parameterisations and subsequent scavenging, Atmos. Chem. Phys., 10, 1931–1951, 2010.

Tsigaridis, K., Daskalakis, N., Kanakidou, M., Adams, P. J., Artaxo, P., Bahadur, R., Balkanski, Y., Bauer, S. E., Bellouin, N., Benedetti, A., Bergman, T., Berntsen, T. K., Beukes, J. P., Bian, H., Carslaw, K. S., Chin, M., Curci, G., Diehl, T., Easter, R. C., Ghan, S. J., Gong, S. L., Hodzic, A., Hoyle, C. R., Iversen, T., Jathar, S., Jimenez, J. L., Kaiser, J. W., Kirkevåg, A., Koch, D., Kokkola, H., Lee, Y. H., Lin, G., Liu, X., Luo, G., Ma, X., Mann, G. W., Mihalapoulos, N., J.-J.Morcrette, J.-F.Müller, Myhre, G., Myriokefalitakis, S., Ng, N. L., O'Donnell, D., Penner, J. E., Pozzoli, L., Pringle, K. J., Russell, L. M., Schulz, M., Sciare, J., Seland, O., Shindell, D. T., Sillman, S., Skeie, R. B., Spracklen, D., Stavrakou, T., Steenrod, S. D., Takemura, T., Titta, P., Tilmes, S., Tost, H., van Noije, T., van Zyl, P. G., von Salzen, K., Yu, F., Wang, Z., Wang, Z., Zaveri, R. A., Zhang, H., Zhang, K., Zhang, Q., and Zhang, X.: The AeroCom evaluation and intercomparison of organic aerosol in global models, Atmos. Chem. Phys., 14, 10 845–10 895, doi:10.5194/acp-14-10845-2014, 2014.

van der Werf, G. R., Randerson, J. T., Giglio, L., Collatz, G. J., Mu, M., Kasibhatla, P. S., Norton, D. C., DeFries, R. S., Jin, Y., and van Leeuwen, T. T.: Global fire emissions and the contribution of deforestation, savanna, forest, agricultural, and peat fires (1997-2009), Atmos. Chem. Phys., 10, 11 707–11 735, doi:10.5194/acp-10-11707-2010, 2010.

Vehkamäki, H., Kulmala, M., Napari, I., Lehtinen, K. E. J., Timmreck, C., Noppel, M., and Laaksonen, A.: An improved parameterization for sulfuric acid-water nucleation rates for tropospheric and stratospheric conditions, J. Geo. Res., 107, doi:10.1029/2002JD002184, 2002.

Vergara-Temprado, J., Murray, B. J., Wilson, T. W., O'Sullivan, D., Browse, J., Pringle, K. J., Ardon-Dryer, K., Bertram, A. K., Burrows, S. M., Ceburnis, D., DeMott, P. J., Mason, R. H., O'Dowd, C., Rinaldi, M., and Carslaw, K. S.: Contribution of feldspar and marine organic aerosols to global ice nucleating particle concentrations, Atmos. Chem. Phys., 17, 3637–3658, doi:10.5194/acp-17-3637-2017, 2017.

1334 Villarini, G. and Vecchi, G. A.: Projected increases in North Atlantic tropical cyclone intensity from CMIP5 models, J. Cli., 26, 3231–3240,
1335   doi:10.1175/JCLI-D-12-00441.1, 2013.

1336 Welch, B. L.: The generalization of 'Student's' problem when several different population variances are involved, Biometrika, 34, 28–35,
1337   doi:10.1093/biomet/34.1-2.28, 1947.

1338 West, R. E. L., Stier, P., Jones, A., Johnson, C. E., Mann, G. W., Bellouin, N., Partridge, D. G., and Kipling, Z.: The importance of vertical
1339   velocity variability for estimates of the indircet aerosol effects, Atmos. Chem. Phys., 14, 6369–6393, doi:10.5194/acp-14-6369-2014,
1340   2014.

1341 Wilcox, L. J., Highwood, E. J., Booth, B. B. B., and Carslaw, K. S.: Quantifying sources of inter-model diversity in the cloud albedo effect,
1342   Geophys. Res. Lett., 42, 1568–1575, doi:10.1002/2015GL063301, 2015.

1343 Williamson, D., Goldstein, M., Allison, L., Blaker, A., Challenor, P., Jackson, L., and Yamazaki, K.: History matching for exploring
1344   and reducing climate model parameter space using observations and a large perturbed physics ensemble, Clim. Dyn., 41, 1703–1729,
1345   doi:10.1007/s00382-013-1896-4, 2013.

1346 Yoshioka, M., Regayre, L. A., Pringle, K. J., Johnson, J. S., Mann, G. W., Partridge, D., Stier, P., Kipling, Z., Bellouin, N., Sexton, D. M. H.,
1347   Lister, G. M. S., Browse, J., Booth, B. B. B., Johnson, C. E., Johnson, B., Mollard, J. D. P., and Carslaw, K. S.: Ensembles of global
1348   climate model variants for the quantification and constraint of uncertainty in aerosols and their radiative forcing, J. Adv. Model. Earth
1349   Syst., TBC, TBC, In prep.

1350 Zhang, S., Wang, M., Ghan, S., Ding, A., Wang, H., Zhang, K., Neubauer, D., Lohmann, U., Ferrachat, S., Takeamura, T., Gettleman, A.,
1351   Morrison, H., Lee, Y. H., Shindell, D. T., Partridge, D. G., Stier, P., Kipling, Z., and Fu, C.: On the characteristics of aerosol indirect effect
1352   based on dynamic regimes in climate models, Atmos. Chem. Phys. Discuss., 15, 23 683–23 729, doi:10.5194/acpd-15-23683-2015, 2015.

1353 Zhou, C., Liu, X., Qian, Y., Yoon, J., Hou, Z., Lin, G., McFarlane, S., Wang, H., Yang, B., L.Ma, P., Yan, H., and Bao, J.: A sensitivity study
1354   of radiative fluxes at the top of the atmosphere to cloud-microphysics and aerosol parameters in the community atmosphere model CAM5,
1355   Atmos. Chem. Phys., 13, 10 969–10 987, doi:10.5194/acp-13-10969-2013, 2013.

Table A1. Descriptions of the perturbed parameters. Parameters are grouped according to their source within the model as either 'Atm' for atmospheric or 'Aer' for aerosol parameters.

Name	Source	Description	PDF
Rad_Mcica_Sigma	Atm	Fractional standard deviation of sub-grid condensate seen by radiation	Trapezoid (0.1,0.4,1.5,2.2,2,2)
C_R_Correl	Atm	Cloud and rain sub-grid horizontal spatial correlation	Trapezoid (0.0, 0.6, 0.9, 1.0, 1.8, 1. 1, 1.5)
Niter_BS	Atm	Number of microphysics iteration sub-steps	Uniform (5, 20)
Ent_Fac_Dp	Atm	Entrainment amplitude scale factor	Trapezoid (0, 0.5, 2, 4, 2, 2)
Amdet_Fac	Atm	Mixing detrainment rate scale factor	Trapezoid (0, 0.5, 10.0, 15.0, 2, 2)
Dbsdtbs_Turb_0	Atm	Cloud erosion rate (s^{-1})	Trapezoid (0, 1e-04, 5e-04, 1e-03, 2, 2)
Mparwtr	Atm	Maximum value of function controlling convective parcel maximum condensate	Trapezoid (1e-3, 1e-3, 1.5e-3, 2e-3, 2, 2)
Dec_Thres_Cld	Atm	Threshold for cloudy boundary layer decoupling	Trapezoid (0.01, 0.011, 0.1, 0.8, 2, 4, 4)
Fac_Qsat	Atm	Rate of change in convective parcel maximum condensate	Uniform (0.25, 1)
Ageing	Aer	Ageing of hygrophobic aerosols (no. of monolayers of organic material)	Trapezoid (0.3, 1, 5, 10, 2, 2)
Cloud_pH	Aer	pH of cloud droplets	Trapezoid (4.6, 5.3, 6.3, 7, 4, 2)
Carb_BB_Ems	Aer	Carbonaceous biomass burning emission scale factor	Trapezoid (0.25,0.8,2.2,4,2,2)
Carb_BB_Diam	Aer	Carbonaceous biomass burning emission diameter (nm)	Trapezoid (90, 160, 240, 300, 2, 2)
Sea_Spray	Aer	Sea spray aerosol emission scale factor	Trapezoid (0.125, 0.6, 3, 8, 4, 3)
Anth_SO2	Aer	Anthropogenic SO_2 emission scale factor	Trapezoid (0.6, 0.81, 1.09, 1.5, 2, 2)
Volc_SO2	Aer	Volcanic SO_2 emission scale factor	Trapezoid (0.71, 0.99, 1.7, 2.38, 4, 1.1)
BVOC_SOA	Aer	Biogenic secondary aerosol formation from volatile organic compounds scale factor	Trapezoid (0.81, 1.08, 3.5, 5.4, 3, 3)
DMS	Aer	Dimethylsulphide surface ocean SO_2 concentration scale factor	Trapezoid (0.5, 1.26, 1.82, 2, 2, 3)
Dry_Dep_Acc	Aer	Accumulation mode dry deposition velocity scale factor	Trapezoid (0.1, 0.32, 3.16, 10, 2, 2)
Dry_Dep_SO2	Aer	SO_2 dry deposition velocity scale factor	Trapezoid (0.2, 0.56, 1.78, 5, 2, 2)
Kappa_OC	Aer	Köhler coefficient of organic carbon	Trapezoid (0.1, 0.14, 0.25, 0.6, 4, 4)
Sig_W	Aer	Updraft vertical velocity standard deviation	Trapezoid (0.1, 0.36, 0.44, 0.7, 2, 2)
Dust	Aer	Dust emission scale factor	Trapezoid (0.5, 0.7, 1.4, 2, 2, 2)
Rain_Frac	Aer	Fraction of cloud covered area in large-scale clouds where scavenging occurs	Trapezoid (0.3, 0.31, 0.55, 0.7, 2, 3)
Cloud_Ice_Thresh	Aer	Threshold of cloud ice fraction above which nucleation scavenging is suppressed	Trapezoid (0.1, 0.105, 0.35, 0.5, 2, 3)
BC_RI	Aer	Imaginary part of the black carbon refractive index	Trapezoid (0.2, 0.352, 0.616, 0.8, 4, 2)
OC_RI	Aer	Imaginary part of the organic carbon refractive index	Trapezoid (0, 0, 0.05, 0.1, 2, 6)

Table A2. Summary statistics for the pdfs of 1850-2008 aerosol ERF, ERF_{ARI} and ERF_{ACI} presented in Fig. 1. Perturbations to atmospheric and/or aerosol parameters cause the uncertainty in model output in each case. All values are in $W\,m^{-2}$. For all samples the null hypotheses of equivalent means or standard deviations are rejected at the 99% confidence level using Welch's t (Welch, 1947) and Bartlett (Snedecor and Cochran, 1989) tests respectively.

Sample	Perturbations	Mean	Standard deviation	95% Credible interval	Credible range
ERF	Atmosphere and aerosol	-1.46	0.38	(-2.18, -0.71)	1.46
	Atmosphere only	-1.51	0.25	(-1.98, -1.04)	0.94
	Aerosol only	-1.47	0.29	(-2.01, -0.90)	1.11
ERF_{ARI}	Atmosphere and aerosol	-0.03	0.08	(-0.19, 0.13)	0.31
	Atmosphere only	0.00	0.04	(-0.08, 0.08)	0.16
	Aerosol only	-0.02	0.07	(-0.16, 0.11)	0.27
ERF_{ACI}	Atmosphere and aerosol	-1.42	0.41	(-2.20, -0.61)	1.59
	Atmosphere only	-1.51	0.29	(-2.04, -0.96)	1.08
	Aerosol only	-1.43	0.30	(-1.99, -0.85)	1.14

Table A3. Latitude and longitude boundaries for regions R1-R11. Some regional averages are filtered to include only marine or non-marine data.

Region	Description	Filter	Latitudes	Longitudes
R1	North Pacific	Marine	32.5 to 54	144 to -125
R2	East Pacific Stratocumulus Deck	Marine	16 to 41	-146 to -104
R3	Canada	All	45 to 73	-115 to -61
R4	South-east Pacific Stratocumulus deck	Marine	-26 to 1	-98 to -70
R5	North Atlantic	Marine	27 to 59	-53 to -12
R6	South-east North Atlantic	Marine	8.5 to 26	-44 to -17
R7	Arctic	Marine	61 to 89	-33 to 57
R8	Europe	All	37.5 to 71.5	-12 to 41
R9	South-east Atlantic Stratocumulus deck	Marine	-18 to 3	-16 to 13
R10	North Indian Ocean	Marine	5.5 to 23	63 to 94
R11	China	Land	21 to 40	98 to 123

Table A4. Present-day ToA RSR constraints and the resulting 95% credible intervals of 1850 RSR and 1850-2008 aerosol ERF $(\mathrm{W\,m^{-2}})$ for the unconstrained and constrained samples.

Constraint	Sample size	2008 RSR	1850 RSR	1850-2008 ERF	1850-2008 ERF credible range
Unconstrained	1000000	(88.9, 120.1)	(87.5, 118.0)	(-2.65, -0.68)	1.97
CERES $(98.3 \pm 0.25\ \mathrm{W\,m^{-2}})$	20127	(98.05, 98.55)	(94.2, 99.3)	(-2.37, -0.59)	1.78
CERES North Pacific $(162.8 \pm 3.3\ \mathrm{W\,m^{-2}})$	108493	(89.6, 106.8)	(88.0, 105.1)	(-2.25, -0.53)	1.72
Combined constraint	4699	(98.1, 98.5)	(95.7, 97.8)	(-2.30, -0.56)	1.74